Iterative solvers for poromechanics

Iterative solvers for poromechanics

Manuel Antonio Borregales Reverón

Thesis for the degree of Philosophiae Doctor (PhD)
University of Bergen, Norway
2019

UNIVERSITY OF BERGEN

Iterative solvers for poromechanics

Iterative solvers for poromechanics

Manuel Antonio Borregales Reverón

Thesis for the degree of Philosophiae Doctor (PhD)
at the University of Bergen

Date of defense: 22.11.2019

Year: 2019

Title: Iterative solvers for poromechanics

Name: Manuel Antonio Borregales Reverón

Print: Skipnes Kommunikasjon / University of Bergen

Preface

This dissertation is submitted as a partial fulfillment of the requirements for the degree of Doctor of Philosophy (PhD) at the University of Bergen. The advisory committee has consisted of Florin Adrian Radu (University of Bergen), Kundan Kumar (Karlstad University) and Jan Martin Nordbotten (University of Bergen).

The PhD project has been financially supported by the University of Bergen in cooperation with the FME-SUCCESS center (grant 193825/S60) funded by the Research Council of Norway.

Abstract

This thesis concerns iterative solvers for poromechanics problems. The problems in the studies have involved linear poromechanics, non-linear poromechanics, and poromechanics under large deformation. We included high order discretizations, applied linearization techniques and splitting methods to develop new solvers. We studied the robustness and convergence of these solvers.

By studying the fixed stress method as an iterative solver for poromechanics, we developed an optimized version of it. Furthermore, by extending the convergence analysis in the time domain, we developed a new version of the fixed stress method that is partially parallelized. This splitting method was combined with linearization techniques to develop solvers for non-linear poromechanics. By studying the convergence of the linearisation schemes, we developed new solvers and extended the applicability to more complex phenomena, for instance poromechanics with large deformation.

Outline

This thesis is organized in two parts. The first part gives an overview of scientific theory and mathematical methods that are relevant to the thesis. The second part contains papers that are either published or submitted for publication in scientific journals.

Part I is structured as follows: In Chapter 1 the main topic covered in the dissertation, i.e. numerical solvers for poromechanics problems, is introduced. The mathematical modelling is presented in Chapter 2, which includes the governing equations for poromechanics. In Chapter 3 we present the numerical framework used in the included papers. Finally, the papers are presented and discussed in Chapter 4.

Part II contains the scientific results, which are grouped as main and related works. The main contribution consists of the following four scientific articles:

Paper A M. Borregales, F.A. Radu, K. Kumar, and J.M. Nordbotten. Robust iterative schemes for non-linear poromechanics. *Computational Geosciences*, 22(4):1021–1038, 2018.

Paper B M. Borregales and F.A. Radu. Higher Order Space-Time Elements for a Non-linear Biot Model. *Numerical Mathematics and Advanced Applications ENUMATH 2017, Lecture Notes in Computational Science and Engineering* 126 541-549, 2018.

Paper C M. Borregales, K. Kumar, J.M. Nordbotten and F.A. Radu. Iterative solvers for Biot model under small and large deformation. arXiv:1905.12996[math.NA], 2019.

Paper D M. Borregales, K. Kumar, F.A. Radu, C. Rodrigo and F.J. Gaspar. A parallel-in-time fixed-stress splitting method for Biots consolidation model. *Computers and Mathematics with Applications*, 77(6):1466–1478, 2019.

Also, the following two supplementary articles, on related work, are included:

Paper E J.W. Both, M. Borregales, J.M. Nordbotten, K. Kumar, and J.M. Nordbotten. Robust fixed stress splitting for Biots equations in heterogeneous media. *Applied Mathematics Letters*, 68 101–108, 2017.

Paper F F.A. Radu, M. Borregales, F.J. Gaspar, K. Kumar and C. Rodrigo. L-scheme and Newton based solvers for a nonlinear Biot model. *Proceedings: 6th European Conference on Computational Mechanics (Solids, Structures and Coupled Problems), 7th European Conference on Computational Fluid Dynamics*, ISBN: 978-84-947311-6-7 3505–3518, 2018.

Acknowledgements

Words fall short for expressing gratitude. It was a great experience, Florin. I want to express profound gratitude to you, for all the advice and opportunities you gave me to develop as a mathematician. I sincerely thank Kundan Kumar for his always positive attitude, and his helpful insight. Thanks to Jan Martin Nordbotten for his contagious passion for doing exciting research.

I want to thank the FME-SUCCESS project and Sarah Gasda and all the support I have received from them. Thanks to professor Markus Bause and especially to Uwe Koecher for being unbelievably helpful throughout this thesis. Thanks to professors Francisco Gaspar and Carmen Rodrigo for all the collaboration.

Victor, Davide and especially David, I'm happy to have been sharing an office with you guys. I like that our days at the office always started with a: "Priviet," "Buongiorno," or "Buenos dias, marico."

I want to thank the porous media group, including professors, postdocs, and all the Ph.D. students. I thank, with special mention to the people that were always there, bringing light and joy throughout this journey: Wietse, David Seus, Michael, Jakub, Ana, Max, Ingeborg, Alessio, Maria, Nazanin, and Valentin; I love you guys.

Quiero enviar un especial agradecimiento a mi familia, por todos los valores que me ensearon, a mi mamá Olga, a mi papá Manuel (que dios lo tenga en su gloria), a mi tío Edgar, a mi Abuela Carmen y ta Jeanette (que me miran las dos desde el cielo). Gracias a mis hermanos José, Yuruari y Yurubí por soportarme y motivarme a seguir cada vez más hacia adelante.

Quiero agradecer a mis amigos Abraham y Diana por su cario y motivación a salir adelante; a Luber por el tiempo compartido cuando llegue a Bergen; a Leire por su alegría y a Ruben por las aventuras que hemos estado compartiendo desde aquel proyecto en Matlab con Renom. A todos los compaeros del antiguo laboratorio de conversión de energía mecánica en especial Jesus, Milan y Andrea. Gracias a Miguel,

mi tutor de maestría, que puso en mi la idea de hacer un doctorado y me dio muchos consejos de “loro viejo”: gracias maestro.

Thanks to the people in Flåm Port for the fantastic opportunity they gave me this summer.

Gudny, receive my highest gratitude. You are part of this thesis, I couldnt have done it without your patience and support. I’m profoundly grateful and fortunate to be with you. Thanks to you, to your beautiful family: Gunnbjørg, Gunnhild, Lars, Guttorm, Beatrice, Geir and especially to Gustav for all the good values you all teach me every day.

It was a great journey, and I hope the words here expressed bring you a hint of all the gratitude I have for you.

Contents

Preface iii

Abstract v

Outline vii

Acknowledgements ix

I Scientific Background 1

1 Motivation 3
1.1 Main results . . . 4

2 Mathematical modelling of poromechanics problems 7
2.1 Porous medium . . . 7
2.2 Deformation . . . 8
2.3 Conservation laws . . . 9
2.3.1 Conservation of momentum . . . 9
2.3.2 Conservation of mass . . . 9
2.4 Constitutive relations . . . 9
2.4.1 Darcy's law . . . 9
2.4.2 Hooke's law . . . 10
2.5 Piola transformation . . . 10
2.6 Poromechanics . . . 11
2.6.1 Poromechanics under small deformation . . . 12

3 Numerical framework 15
3.1 Space-time discretization . . . 15
3.1.1 Semi-Discretization in time: continuous Galerkin cG(r) . . . 16
3.1.2 Semi-Discretization in time: discontinuous Galerkin dG(r) . . . 17
3.1.3 Discretization in space: cG(p+1)-MFEM(p) . . . 18
3.1.4 Lower order space-time discretization dG(0)-cG(1)-MFEM(0) 20
3.2 Solvers for coupled problems . . . 21

3.2.1 Monolithic scheme . . . 21
3.2.2 Splitting scheme . . . 22
3.3 Linearizations schemes . . . 23
3.3.1 Newton's method . . . 23
3.3.2 L-scheme . . . 24

4 Introduction to the papers 25
4.1 Main results . . . 25
4.1.1 Paper A: Robust iterative schemes for non-linear poromechanics 25
4.1.2 Paper B: Higher order space-time elements for a non-linear Biot model . . . 26
4.1.3 Paper C: Iterative solvers for Biot model under small and large deformation . . . 27
4.1.4 Paper D: A parallel-in-time fixed-stress splitting method for Biot's consolidation model . . . 27
4.2 Related work . . . 28
4.2.1 Paper E: Robust fixed stress splitting for Biots equations in heterogeneous media . . . 28
4.2.2 Paper F: L-scheme and Newton based solvers for a nonlinear Biot model . . . 29
4.3 Conclusions and outlook . . . 29

Bibliography 31

II Included papers 43

A Robust iterative schemes for non-linear poromechanics

B Higher Order Space-Time Elements for a Non-linear Biot Model

C Iterative solvers for Biot model under small and large deformation

D A parallel-in-time fixed-stress splitting method for Biot's consolidation model

E Robust fixed stress splitting for Biots equations in heterogeneous media

F L-scheme and Newton based solvers for a nonlinear Biot model

Part I

Scientific Background

Chapter 1

Motivation

This dissertation presents a contribution in the context of solvers for poromechanics. The term "poromechanics" refers to a coupled process between fluid flow and mechanical deformation of a porous medium, and it plays a crucial role in many societally relevant applications such as geothermal energy extraction, energy storage in the subsurface, reservoir simulations, CO_2 sequestration and the mechanics of biological tissues. We will discuss two examples of these in more detail: CO_2 sequestration and the mechanics of biological tissues. These applications enhance the need for improved mathematical models and robust numerical solvers for poromechanics.

CO_2 storage security: CO_2 storage is one of the most promising approaches for a large scale reduction of anthropogenic gas emissions in the atmosphere. It consists of injecting CO_2 e.g. in deep saline aquifers or depleted oil reservoirs. Accurate prediction of the behavior of the injected CO_2 is important for the long term success of the sequestration, because even a low rate leakage over long time periods can undo the positive outcomes of net CO_2 sequestered [88, 89].

A significant issue for storage security is the geomechanical response of the reservoir. Geomechanical deformation can be induced by CO_2 injection, and this could create or reactivate fracture networks in the sealing caprocks, providing a pathway for CO_2 leakage [121]. Hence, accurate predictions of the possible reservoir deformation, migration of the injected CO_2 and assurance of the storage security, require poromechanics models.

Fully coupled numerical schemes for poromechanics guarantee that the numerical solution is formally consistent with the underlying continuous differential equations. Nevertheless, due to the complexities associated with monolithic solvers, what is used as industry standard continues to be the so-called weakly- or iteratively-coupled approaches [90, 108]. Weakly coupled schemes, wherein the iterations are not continued until convergence, have been questioned [50, 90, 96]. Therefore, in order to ensure the robustness and accuracy of the resulting computations, it is essential to understand the efficiency, stability, and convergence of iterative splitting schemes.

Poromechanics of biological tissues: Unlike many geomechanics applications, which usually assume small deformations in the porous medium, biological poromechanics models often experience large deformations and require more complicated non-linear poromechanics theory [16], for porous media such as soft tissues, membranes and bones. For instance, the brain is contained by the rigid skull, and it is susceptible to volume changes that can immediately translate to pressure changes inside the skull [51]. Various congenital conditions and conditions of the elderly are manifestations of this pressure imbalance, that causes life-altering morphological changes in the central nervous system. The development of biological modelling that includes poromechanics is essential in the understanding of these illnesses.

Another example of poromechanics in biological tissues is the coupling between fluid flow in coronary vessels with the mechanical deformation of heart tissue. In this case, the mechanical deformation is a central feature of cardiac physiology and can be accounted for by using a poromechanics model of coronary perfusion [63]. This coupling has been shown to exist in the large epicardial coronary vessels where flow is impeded and even reversed during contraction. This complicated interplay between the dynamics of vessel compression with resistance and pressure gradients motivates to incorporate elastodynamics [81, 129] and hyperelasticity [16, 44] in the poromechanics models.

1.1 Main results

The main contribution of this thesis is proposing new solvers for poromechanics problems and the rigorous convergence analysis for some of these. These solvers are robust and efficient, and can be used for both linear and non-linear poromechanics problems.

1. **Rigorous convergence analysis for linearization schemes for non-linear poromechanics.** We propose and analyse linearization schemes such as the L-scheme (in Papers A, B, and E) and Newton's method (in Paper C) combined with monolithic and splitting schemes for solving non-linear poromechanics problems.

2. **Developing solvers for poromechanics under large deformation.** Robust iterative schemes are proposed for solving poromechanics problems that follow the Saint Venant-Kirchoff constitutive law (in Paper C). The solver is written in a Lagrangian frame of reference. The applicability, robustness, and convergence of the schemes is shown by illustrative numerical examples.

3. **Optimizing existing solver for linear poromechanics.** We propose a new, optimized tuning parameter for the splitting solver fixed-stress method. Additionally, we prove global, linear convergence in energy norms of the method for heterogeneous media (in Paper E).

4. **Development a new parallel fixed stress splitting scheme.** We developed and analysed a parallel-in-time iterative solver for poromechanics (in Paper D). The main benefit of the new solver is that the mechanics sub-problem can be solved in a parallel-in-time manner. The new parallel fixed-stress scheme is very efficient; it requires around 20% computational cost of fixed-stress.

Chapter 2

Mathematical modelling of poromechanics problems

In order to model fluid flow in a deformable porous medium, it is required to satisfy the conservation of momentum and the conservation of mass. The resulting system has typically more unknowns than equations. Thus, constitutive laws are needed to close the poromechanics system. In this chapter, we will introduce the partial differential equations needed to model poromechanics.

2.1 Porous medium

A porous medium is a material that contains pores. These pores are void spaces with a length scale that goes from nanometers to micrometers [113]. The fluid that fills the pores may flow between the interconnection of these pores. Predictions for fluid flow in porous media are relevant for many applications. Reservoir simulations for CO_2 sequestration is an example of these. However, a reservoir has length scales from meters to kilometers. Therefore, it is computationally impractical to model fluid flow in porous media in a complete reservoir with the complete pore-scale geometry. In this regard, small volumes called representative elementary volumes (REVs) [15] are considered. In a REV, the actual route of the fluid flow through the pore medium is unknown. However, the average mass flux flowing through a part of the porous domain can be obtained.

A porous medium is characterized by its porosity $\phi \in [0, 1]$. The ratio between the volume of the pores filled by fluid, and the total volume within a REV, defines the effective porosity of the medium.

$$\phi := \frac{\text{Volume of voids}}{\text{Volume of REV}}.$$

We denote the density of the fluid ρ_f, and we can use porosity to define the actual fluid density $\phi\rho_f$ inside a REV.

A fluid is called compressible if any change in normal pressure (or tension) generates a density change [15]. If density remains constant, the fluid is called incompressible. In a deformable porous medium with constant temperature, the isothermal compressibility constant of the fluid is defined by

$$c_f := \frac{1}{\rho_f}\frac{d\rho_f}{dp}.$$

Under isothermal conditions, a closed non-linear relation between the density ρ_f and the pressure p can be obtained if c_f is independent of the pressure [15]. This relation can be expressed as follows

$$\rho_f = \rho_{f_0} e^{c_f (p - p_0)},$$

where ρ_{f_0} is the fluid density at a reference pressure p_0.

2.2 Deformation

We will consider a poroelastic domain $\Omega \subset \mathbb{R}^d$ for $d = \{2,\ 3\}$ with boundary $\partial\Omega$. A deformation field is an assignment of displacement vectors for all points in domain Ω to a current (or deformed) domain Ω_t at time t. We use bold letters for variables, functions or spaces that represent vectors or tensors, and the identity tensor will be denoted by $\mathbf{I}$. Let Φ be the deformation map that is continuously differentiable and invertible: $\boldsymbol{\Phi} := \{\mathbf{X} \in \Omega \to \mathbf{x}\ = \boldsymbol{\Phi}(\mathbf{X}) \in \Omega_t\}$. Mathematically, the deformation field is denoted by

$$\mathbf{u}(\mathbf{X}) := \mathbf{x}\ - \mathbf{X}\ = \boldsymbol{\Phi}(\mathbf{X}) - \mathbf{X}.$$

It is also important to mention that a deformation field may introduce a volumetric change [115]. Given the gradient of the transformation

$$\mathbf{F} := \nabla_{\mathbf{X}} \boldsymbol{\Phi} = \nabla_{\mathbf{X}} (\mathbf{X} + \mathbf{u}(\mathbf{X})) = \mathbf{I} + \nabla_{\mathbf{X}} \mathbf{u}$$

at the reference domain Ω, we can obtain the volumetric change of the transformation by

$$J := \det(\mathbf{F}).$$

In order to exclude deformation due to rigid-body motions, we introduce the concept of strain. Strain is a description of deformation in terms of relative deformation in Ω. Strain measures how much a given deformation differs locally from a rigid-body deformation. There is no unique way to define strain mathematically [115]. Hence, we will use the Green-Lagrangian strain tensor $\mathbf{E}$ defined by

$$\mathbf{E}(\mathbf{u}) := \frac{1}{2}(\mathbf{C} - \mathbf{I}) = \frac{1}{2}\left(\nabla_{\mathbf{X}} \mathbf{u} + (\nabla_{\mathbf{X}} \mathbf{u})^{\top} + (\nabla_{\mathbf{X}} \mathbf{u})^{\top} \nabla_{\mathbf{X}} \mathbf{u}\right), \tag{2.1}$$

which measures the difference between the right Cauchy-Green deformation tensor $\mathbf{C} := \mathbf{F}^{\top}\mathbf{F}$ and $\mathbf{I}$. This Green-Lagrangian strain tensor is non-linear, and can be linearised in case of infinitesimal deformation as follows,

$$\boldsymbol{\varepsilon}(\mathbf{u}) := \frac{1}{2}\left(\nabla_{\mathbf{X}} \mathbf{u} + (\nabla_{\mathbf{X}} \mathbf{u})^{\top}\right). \tag{2.2}$$

2.3 Conservation laws

We consider mass and momentum as the quantities to be conserved during the coupled process between fluid flow and mechanic deformation in a porous medium.

2.3.1 Conservation of momentum

The law of conservation of momentum says that the rate of change of the linear momentum $\mathbf{p} := \int_\omega \rho_b \mathbf{v}\, d\mathbf{x}$ is equal to the force $\mathbf{f}_\sigma$ applied to ω and the corresponding reaction force generated due to internal stress $\boldsymbol{\sigma}$ inside ω ([115])

$$\frac{d}{dt}\int_\omega \rho_b \mathbf{v}\; d\mathbf{x} = \int_\omega \left(\nabla_\mathbf{x}\cdot\boldsymbol{\sigma} + \mathbf{f}_\sigma\right)\; d\mathbf{x}. \tag{2.3}$$

The left hand side can be neglected since we are not interested in the rigid body dynamic of the porous material. Then, the differential version of the conservation of momentum can be written for any domain ω as follows

$$-\nabla_\mathbf{x}\cdot\boldsymbol{\sigma} = \mathbf{f}_\sigma. \tag{2.4}$$

2.3.2 Conservation of mass

The law of conservation of mass says that the rate of change of the fluid mass over time $m_f := \int_\omega \phi\rho_f\; d\mathbf{x}$ is equal to the fluxes $\mathbf{q}$ across the boundary and the contribution of any source or sink term f_m [15]. This law can be expressed mathematically for any domain ω as follows

$$\frac{d}{dt}\int_\omega \phi\rho_f\; d\mathbf{x} = -\int_{\partial\omega} \mathbf{q}\cdot\mathbf{n}\; d\mathbf{x} + \int_\omega f_m\; d\mathbf{x}, \tag{2.5}$$

where $\mathbf{n}$ is the outward normal vector to $\partial\omega$, with unit length. We can obtain the differential equation associated to the conservation of mass using the Divergence theorem over the flux term as follows

$$\frac{\partial}{\partial t}\left(\phi\rho_f\right) + \nabla_\mathbf{x}\cdot\mathbf{q} = f_m. \tag{2.6}$$

2.4 Constitutive relations

We will consider two constitutive equations to relate: fluid flow with pressure gradient in porous media and stress tensor with mechanical deformation.

2.4.1 Darcy's law

The proportionality relation between the volumetric flux $\mathbf{q}_v$ and the pressure gradient in Ω_t is given by Darcy's law

$$\mathbf{q}_v = -\mathbf{k}\left(\nabla_{\mathbf{x}} p - \rho_f \mathbf{g}\right). \tag{2.7}$$

The proportionality parameter $\mathbf{k}$ is a second-rank tensor that represents the resistance of the fluid to flow in each direction. The fluid flow, or volumetric flux, is denoted by $\mathbf{q}_v$. There are mainly two properties related to $\mathbf{k}$, permeability and viscosity. Permeability is a property of the porous medium, it is independent of the fluid and it measures the ability of a porous material to allow fluids to pass through it [15]. Viscosity, on the other hand, is a property of the fluid that measure its internal friction [75]. The parameter $\mathbf{k}$ is directly proportional to the permeability of the porous domain and inverse proportional to the viscosity and density of the fluid [15]. The relation between the mass flux $\mathbf{q}$ and the volumetric flux is given by $\mathbf{q} = \rho_f \mathbf{q}_v$. The gravitational acceleration is denoted by $\mathbf{g}$.

2.4.2 Hooke's law

A general relation between the stress and the strain tensor is given by

$$\boldsymbol{\sigma} = \beta_0 \mathbf{I} + \beta_1 \boldsymbol{\varepsilon} + \beta_2 \boldsymbol{\varepsilon}^2, \tag{2.8}$$

where the coefficients β_0, β_1 and β_2 are functions of the invariants

$$\begin{aligned} \varepsilon_I &= \mathrm{tr}(\boldsymbol{\varepsilon}), \\ \varepsilon_{II} &= \frac{1}{2}\left(\mathrm{tr}(\boldsymbol{\varepsilon})^2 - \mathrm{tr}(\varepsilon^2)\right), \\ \varepsilon_{III} &= \det(\boldsymbol{\varepsilon}). \end{aligned}$$

The trace of a second-rank tensor and its determinant is denoted by $\mathrm{tr}(\cdot)$ and $\det(\cdot)$, respectively. It has been proven by Ciarlet in [43] that every constitutive law can be written in this way (Eq. (2.8)). However, under the assumption of small deformations, Hooke's law can be applied. Similar to Darcy's law, Hooke's law offer a proportionality relation between the strain tensor $\boldsymbol{\varepsilon}$ and the stress tensor $\boldsymbol{\sigma}$,

$$\boldsymbol{\sigma} = \mathbb{C} : \boldsymbol{\varepsilon}, \tag{2.9}$$

where the proportionality constant $\mathbb{C}$ is a fourth-rank tensor that depends on the properties of the porous material. Hooke's law can be simplified for isotropic porous materials as follows

$$\boldsymbol{\sigma} = 2\mu\boldsymbol{\varepsilon} + \lambda \mathrm{tr}(\boldsymbol{\varepsilon}), \tag{2.10}$$

where μ and λ are the Lamé parameters.

2.5 Piola transformation

Since the transformation Φ is unknown and Ω_t is not available, we must write Eqs. (2.4) and (2.6) into a Lagrangian frame of reference. Here, we use the Piola transformation to map variables from Ω_t to Ω.

The conservation of momentum Eq. (2.4) in the Lagrangian frame of reference would read as follows

$$-\nabla_{\mathbf{X}} \cdot \mathbf{\Pi} = \rho_0 \mathbf{g}, \tag{2.11}$$

where $\mathbf{\Pi}$ is the Piola transformation of $\boldsymbol{\sigma}$ also known as the first Piola-Kirchhoff stress tensor $\mathbf{\Pi} = J\mathbf{F}^{-\top}\boldsymbol{\sigma}$. We now introduce the second Piola-Kirchhoff stress tensor $\mathbf{\Sigma} = \mathbf{F}^{-1}\Pi$, since all constitutive laws are obtained for $\mathbf{\Sigma}$ (Ciarlet [43])

$$\mathbf{\Sigma} = \beta_0 \mathbf{I} + \beta_1 \mathbf{C} + \beta_2 \mathbf{C}^2, \tag{2.12}$$

where β_0, β_1 and β_2 are functions of the invariants C_I, C_{II} and C_{III}

$$\begin{aligned} C_I &= \operatorname{tr}(\mathbf{C}), \\ C_{II} &= \frac{1}{2}\left(\operatorname{tr}(\mathbf{C})^2 - \operatorname{tr}\left(\mathbf{C}^2\right)\right), \\ C_{III} &= \det(\mathbf{C}). \end{aligned}$$

By considering isotropic material, using Eq. (2.1) (see e.g [115]) and choosing $\beta_0 = \lambda \mathfrak{c}(C_I) - \mu - 1$, $\beta_1 = \mu$ and $\beta_2 = 0$, we get from Eq. (2.12)

$$\mathbf{\Sigma} = 2\mu \mathbf{E} + \mathfrak{c}(\operatorname{tr}(\mathbf{E}))\mathbf{I}, \tag{2.13}$$

where $\mathfrak{c}(\cdot)$ represents a non-linear function of the volumetric strain.

The Lagrangian formulation and conservation of mass is given by

$$\frac{\partial}{\partial t}\left(J\rho_f \phi\right) + \nabla_{\mathbf{X}} \cdot \mathbf{Q} = f_m, \tag{2.14}$$

where $\mathbf{Q}$ corresponds to the Piola transformation of the flux variable $\mathbf{q}$, $\mathbf{Q} = J\mathbf{F}^{-1}\mathbf{q}$. This Lagrangian $\mathbf{Q}$ can be obtained by the Lagrangian formulation of Darcy's law as follows

$$\mathbf{Q} = -\mathbf{K}\left(\nabla_{\mathbf{X}} p - \rho_f \mathbf{g}_0\right), \tag{2.15}$$

where $\mathbf{K} = J\mathbf{F}^{-1}\mathbf{k}\mathbf{F}^{-\top}$ is the corresponding transformation of the mobility tensor $\mathbf{k}$ in Ω_t and $\mathbf{g}_0 = \mathbf{F}^{\top}\mathbf{g}$.

2.6 Poromechanics

Poromechanics refers to coupled processes between fluid flow and mechanical deformation in a porous medium. This coupled model was first introduced by Biot and it relates changes in the total stress and fluid pressure with changes in strain and fluid mass, respectively [18, 19, 46, 116]. This relation is defined mathematically by the second Piola-Kirchhoff poroelastic stress tensor $\mathbf{\Sigma}$, which is composed by the effective mechanical stress $\mathbf{\Sigma}^{eff}$ and the pore pressure p by the following relation

$$\mathbf{\Sigma} = \mathbf{\Sigma}^{eff} - J\mathbf{F}^{-1}\mathbf{F}^{\top} p. \tag{2.16}$$

The term $J\mathbf{F}^{-1}\mathbf{F}^{\top}$ ensures that pressure p exerts an isotropic stress in Ω_t.

In addition, changes in the Lagrangian fluid mass term are proportional to changes in fluid pressure and volume [67]. This relation can be written mathematically by

$$\frac{\partial}{\partial t}\left(J\rho_f\phi\right) = c_M\frac{\partial p}{\partial t} + c_\alpha\frac{\partial J}{\partial t}, \tag{2.17}$$

where $c_M = \frac{1}{M} + c_f\phi_0$ and $c_\alpha = J\frac{\partial\phi}{\partial J} + \phi_0$ given by the Biot modulus M.

We therefore include the poroelastic relationships (2.16)-(2.17) to the conservations laws, and we obtain the following poromechanics problem:
Find $(\mathbf{u}, \mathbf{q}, p)$ such that

$$\begin{aligned} -\nabla_{\mathbf{X}}\cdot(\mathbf{F}\boldsymbol{\Sigma}) &= \rho_{b0}\mathbf{g}, \\ \boldsymbol{\Sigma} &= \boldsymbol{\Sigma}^{eff} - J\mathbf{F}^{-1}\mathbf{F}^{\top}p, \\ \mathbf{Q} &= -\mathbf{K}\left(\nabla_{\mathbf{X}}p - \rho_f\mathbf{g}_0\right), \\ \frac{\partial}{\partial t}\left(c_M p + c_\alpha J\right) + \nabla_{\mathbf{X}}\cdot\mathbf{Q} &= S_{f0}. \end{aligned} \tag{2.18}$$

To complete the model, we consider homogeneous Dirichlet boundary conditions and initial conditions given by $(\mathbf{u}_0, p_0)$, such that $\Gamma(\mathbf{u}_0, p_0) = \Gamma_0$, and $\boldsymbol{\Pi}(\mathbf{u}_0, p_0) = \boldsymbol{\Pi}_0$ at time $t = 0$. The functions Γ_0 and $\boldsymbol{\Pi}_0$ are given and sufficiently regular. Additionally, the initial data $\mathbf{u}_0$ and p_0 are not independent, and can be obtained in practice by solving the flow problem for p_0, and then solving the mechanics problem for $\mathbf{u}_0$.

2.6.1 Poromechanics under small deformation

In case of infinitesimal deformations and rotations, the distinction between Ω and Ω_t may be ignored. Therefore, $\boldsymbol{\sigma}$ can be identified with $\boldsymbol{\Pi}$, and $J \approx 1$, $\mathbf{F} \approx \mathbf{I}$. Furthermore, the Lagrangian strain tensor can be approximated by $\mathbf{E} \approx \boldsymbol{\varepsilon}$ where $\boldsymbol{\varepsilon} = \frac{1}{2}\left(\nabla_{\mathbf{x}}\mathbf{u}^{\top} + \nabla_{\mathbf{x}}\mathbf{u}\right)$ is the linearized strain tensor. Then, the poroelastic Cauchy stress tensor $\boldsymbol{\sigma}$ can be written in terms of the fluid pressure p and the displacement $\mathbf{u}$ as

$$\boldsymbol{\sigma}(\mathbf{u}, p) = \boldsymbol{\sigma}^{eff}(\mathbf{u}) - \alpha p\mathbf{I}, \tag{2.19}$$

where α is the dimensionless Biot coefficient, and $\boldsymbol{\sigma}^{eff}(\mathbf{u})$ the effective stress tensor, given by

$$\boldsymbol{\sigma}^{eff}(\mathbf{u}) = 2\mu\boldsymbol{\varepsilon}(\mathbf{u}) + \lambda\mathrm{tr}(\boldsymbol{\varepsilon}(\mathbf{u}))\mathbf{I}. \tag{2.20}$$

see e.g. [18, 19, 45, 49]. The change in time of the volumetric change can still influence the fluid pressure. This effect can be written mathematically as $\frac{\partial J}{\partial t} = \frac{\partial}{\partial t}\nabla_{\mathbf{x}}\cdot\mathbf{u}$ [79].

Then, the quasi-static linear Biot model reads as follows: Find $(\mathbf{u}, \mathbf{q}, p)$ such that

$$\begin{aligned} -\nabla_{\mathbf{x}}\cdot\left[2\mu\boldsymbol{\varepsilon}(\mathbf{u}) + \lambda\mathrm{tr}(\boldsymbol{\varepsilon}(\mathbf{u}))\right] + \alpha\nabla_{\mathbf{x}}\cdot(pI) &= \mathbf{f}_\sigma, \\ \mathbf{q} &= -\mathbf{k}\left(\nabla_{\mathbf{x}}p - \rho_{f,ref}\mathbf{g}\right), \\ \frac{\partial}{\partial t}\left(c_M p + \alpha\nabla_{\mathbf{x}}\cdot\mathbf{u}\right) + \nabla\cdot\mathbf{q} &= f_m. \end{aligned} \tag{2.21}$$

To complete the model, we consider homogeneous Dirichlet boundary conditions (BC) and initial conditions given by $\mathbf{u} = \mathbf{u}_0$ and $p = p_0$ at time $t = 0$. The functions $\mathbf{u}_0$, p_0 are given and are sufficiently regular.

Problem (2.21) is well posed [110]. Furthermore, extensions of the linear Biot equations include well-posedness for the dynamic poro-elasticity [81], thermo-poro-elasticity with non-linear, thermal convection [33], poro-visco-elasticity with a purely visco-elastic strain [20, 110], thermo-poro-visco-elasticity [30] and linear poro-elasticity with a deformation-dependent, non-linear permeability [20].

Chapter 3

Numerical framework

Finding closed form solutions for poroelastic problems is very difficult and normally based on various simplifications. We therefore resort to numerical approximations. Here we will describe some of the numerical techniques we used to obtain and approximate solutions for poromechanics problems. First, we will describe a space-time discretization of the Eqs. (2.21). Second, we will show two linearization techniques: Newton's method and the L-scheme. Third, we will describe a monolithic and a splitting approach for solving coupled problems.

3.1 Space-time discretization

The quasi-static Biot model (2.21) can be understood as the limit of the fully dynamic Biot-Allard model [81]. The quasi-static characteristic of the Biot model comes from neglecting the acceleration of the solid skeleton in the conservation of momentum equation (2.4). This approximation does not allow the application of the Biot model (2.21) to problems with higher dynamics in the solid's deformation. Here, the Biot model (2.21) would be studied as a prototype model. We believe that the discretization that is presented below can also be generalized to more dynamic poroelasticity.

We start by defining the function space $L^2(\Omega)$ of Lebesgue measurable and square integrable functions on Ω, and let $H^m(\Omega)$ (with $m \geq 1$) be the space of L^2-functions having weak derivatives up to order m in $L^2(\Omega)$. Again, we use bold letters to denote vector or tensor variables and vector or tensor spaces. We denote the inner product by $\langle \cdot, \cdot \rangle$ and norm in $L^2(\Omega)$ by $\|\cdot\|$. For rank 2 tensors $\mathbf{A}$, $\mathbf{B} \in \mathbb{R}^{d,d}$, the internal product is defined by $\langle \mathbf{A} : \mathbf{B} \rangle := \int_\Omega \sum_{i,j=1}^{d} A_{ij} B_{ij} d\mathbf{x}$. Further, we consider the spaces

$$\mathbf{H}_0^1(\Omega) := \{\mathbf{u} \in \mathbf{H}^1(\Omega) |\ \mathbf{u} = 0 \text{ on } \partial\Omega\},$$

$$\mathbf{H}(\mathrm{div}; \Omega) := \{\mathbf{q} \in \mathbf{L}^2(\Omega) \mid \nabla \cdot \mathbf{q} \in L^2(\Omega)\}.$$

Let $X_0 \subset X \subset X_1$ be three reflexive Banach spaces with continuous embeddings and let $I = (0,T)$ be the time interval. Following [13, 14] we consider the following set of Bochner spaces

$$L^2(I;X) = \left\{ w : (0,T) \to X \,\middle|\, \int_0^T \|w(t)\|_X^2 dt < \infty \right\},$$

$$H^1(I;X_0,X_1) = \{ w \in L^2(I;X_0) \mid \partial_t w \in L^2(I,X_1) \},$$

that are equipped with their natural norms and where the time derivative ∂_t is understood in the sense of distributions. In particular, every function in $H^1(I;X_0,X_1)$ is continuous on I with values in X. For $X_0 = X = X_1$ we simply write $H^1(I;X)$. We can now proceed and state the space-time variational formulation of the considered quasic-static linear Biot model (2.21):
Find $\mathbf{u} \in H^1\left(I;\mathbf{H}^1(\Omega)\right) \cap L^2\left(I;\mathbf{H}_0^1(\Omega)\right)$, $\mathbf{q} \in L^2\left(I;\mathbf{H}(\mathrm{div};\Omega)\right)$ and $p \in H^1\left(I;L^2(\Omega)\right)$ such that:

$$\begin{aligned}
\int_I 2\mu\langle \boldsymbol{\varepsilon}(\mathbf{u}) : \boldsymbol{\varepsilon}(\mathbf{v})\rangle d\tau + \int_I \langle \lambda \nabla\cdot\mathbf{u} - \alpha p, \nabla\cdot\mathbf{v}\rangle d\tau &= \int_I \langle \mathbf{f}_\sigma, \mathbf{v}\rangle d\tau, \\
\int_I \langle \mathbf{k}^{-1}\mathbf{q}, \mathbf{z}\rangle d\tau - \int_I \langle p, \nabla\cdot\mathbf{z}\rangle d\tau &= \int_I \langle \rho_f \mathbf{g}, \mathbf{z}\rangle d\tau, \qquad (3.1) \\
\int_I \left\langle \frac{\partial}{\partial t}\left(c_M p + \alpha \nabla\cdot\mathbf{u}\right), w \right\rangle d\tau + \int_I \langle \nabla\cdot\mathbf{q}, w\rangle d\tau &= \int_I \langle f_m, w\rangle d\tau,
\end{aligned}$$

for all $\mathbf{v} \in L^2\left(I;\mathbf{H}_0^1(\Omega)\right)$, $\mathbf{z} \in L^2\left(I;\mathbf{H}(\mathrm{div};\Omega)\right)$ and $w \in L^2\left(I;L^2(\Omega)\right)$, given $\mathbf{f}_\sigma \in L^2\left(I;\mathbf{L}^2(\Omega)\right)$ and $f_m \in L^2\left(I;L^2(\Omega)\right)$. Here, we have the Lamé parameters μ and λ, and the coupling term α. The permeability is represented by $\mathbf{k}$, the fluid density by ρ_f, and the gravitational acceleration by $\mathbf{g}$. The compressibility term is represented by c_M. Recall that we use bold letters for variables, functions or spaces that represent vectors or tensors, and the identity tensor will be denoted by $\mathbf{I}$.

3.1.1 Semi-Discretization in time: continuous Galerkin cG(r)

The time interval I is decomposed in N subintervals $I_n = (t_{n-1}, t_n]$, where n=1, ..., N, $0 = t_0 < t_1 < \ldots < t_{n-1} < t_n = T$ and $\tau_n = t_n - t_{n-1}$. The time step size is denoted by $\tau = \max_{1\le n\le N} \tau_n$. In order to define a higher order cG scheme in time, we need to introduce the space of piecewise polynomials of order r with coefficients in a Banach space X and the associated Bochner space $\mathcal{X}_\tau^r(X)$ and $\mathcal{Y}_\tau^r(X)$:

$$\begin{aligned}
\mathbb{P}_r(I_n;X) &:= \left\{ \psi_n : I_n \to X \,\middle|\, \psi_n(t) = \sum_{j=0}^{r} \xi_n^j t^j,\ \xi_n^j \in X,\ j = 0, ..., r \right\}, \\
\mathcal{X}_\tau^r(X) &:= \left\{ \psi_\tau \in C(\bar{I};X) \ \middle|\ \psi_{\tau|_{I_n}} = \psi_n \in \mathbb{P}_r(\bar{I}_n;X); \forall n \in \{1, ..., N\} \right\}, \\
\mathcal{Y}_\tau^r(X) &:= \left\{ \psi_\tau \in L^2(I;X) \ \middle|\ \psi_{\tau|_{I_n}} = \psi_n \in \mathbb{P}_r(I_n;X); \forall n \in \{1, ..., N\} \right\}.
\end{aligned}$$

We can now state a semi-discrete variational form of the system (3.1). We mention that the test functions ψ_n are vanishing on $I \setminus I_n$. The semi-discrete scheme reads as:
Find $\mathbf{u}_\tau \in \mathcal{X}_\tau^r\left(\mathbf{H}^1(\Omega)\right)$, $\mathbf{q}_\tau \in \mathcal{X}_\tau^r\left(\mathbf{H}(\mathrm{div};\Omega)\right)$ and $p_\tau \in \mathcal{X}_\tau^r\left(L^2(\Omega)\right)$, such that

$$
\begin{aligned}
2\mu\int_{I_n}\langle\boldsymbol{\varepsilon}(\mathbf{u}_\tau):\boldsymbol{\varepsilon}(\mathbf{v}_\tau)\rangle d\tau+\int_{I_n}\langle\lambda\nabla\cdot\mathbf{u}_\tau+\alpha p_\tau,\nabla\cdot\mathbf{v}_\tau\rangle d\tau &= \int_{I_n}\langle\mathbf{f}_\sigma,\mathbf{v}_\tau\rangle d\tau,\\
\int_{I_n}\langle\mathbf{k}^{-1}\mathbf{q}_\tau,\mathbf{z}_\tau\rangle d\tau-\int_{I_n}\langle p_\tau,\nabla\cdot\mathbf{z}_\tau\rangle d\tau &= \int_{I_n}\langle\rho_f\mathbf{g},\mathbf{z}_\tau\rangle d\tau,\\
\int_{I_n}\left\langle\frac{\partial}{\partial t}\left(c_M p_\tau+\alpha\nabla\cdot\mathbf{u}_\tau\right),w_\tau\right\rangle d\tau+\int_{I_n}\langle\nabla\cdot\mathbf{q}_\tau,w_\tau\rangle d\tau &= \int_{I_n}\langle f_m,w_\tau\rangle d\tau,
\end{aligned}
$$

for all $\mathbf{v}_\tau \in \mathcal{Y}_\tau^{r-1}\left(\mathbf{H}_0^1(\Omega)\right)$, $\mathbf{z}_\tau \in \mathcal{Y}_\tau^{r-1}\left(\mathbf{H}(\mathrm{div};\Omega)\right)$ and $w_\tau \in \mathcal{Y}_\tau^{r-1}\left(L^2(\Omega)\right)$, and satisfying the continuity constraints $\mathbf{u}_{\tau|I_n}(t_{n-1}) = \mathbf{u}_{\tau|I_{n-1}}(t_{n-1})$, $\mathbf{q}_{\tau|I_n}(t_{n-1}) = \mathbf{q}_{\tau|I_{n-1}}(t_{n-1})$ and $p_{\tau|I_n}(t_{n-1}) = p_{\tau|I_{n-1}}(t_{n-1})$.

We represent $\mathbf{u}_{\tau|I_n}$, $\mathbf{q}_{\tau|I_n}$, and $p_{\tau|I_n}$ in terms of the basis functions with respect to the time variable of $\mathcal{X}_\tau^r\left(\mathbf{H}^1(\Omega)\right)$, $\mathcal{X}_\tau^r\left(\mathbf{H}(\mathrm{div};\Omega)\right)$, and $\mathcal{X}_\tau^r\left(L^2(\Omega)\right)$, respectively. For this, let t_n^j, for $j = 0,\ldots,r$ be the $(r+1)$ Gauss quadrature points on I_n. We define ψ_n^j to be the Lagrange polynomial of degree r, which satisfies $\psi_n^j(t_n^i) = \hat{\delta}_{ji}$, with $\hat{\delta}$ being the Kronecker symbol. Now we express our variables as a linear combination of the basis functions

$$
\mathbf{u}_{\tau|I_n}(t)=\sum_{j=0}^{r}\mathbf{u}_n^j\psi_n^j(t),\quad \mathbf{q}_{\tau|I_n}(t)=\sum_{j=0}^{r}\mathbf{q}_n^j\psi_n^j(t),\quad p_{\tau|I_n}(t)=\sum_{j=0}^{r}p_n^j\psi_n^j(t).
$$

Then, by taking $\mathbf{v}_\tau = \mathbf{v}\psi_n^i$, $\mathbf{z}_\tau = \mathbf{z}\psi_n^i$ and $w_\tau = w\psi_n^i$,$i = 0,\ldots,r$ in the semi-discrete problem above, we get the equivalent formulation on each time interval I_n:
Find $\mathbf{u}_n^j \in \mathbf{H}_0^1(\Omega)$, $\mathbf{q}_n^j \in \mathbf{H}(\mathrm{div};\Omega)$ and $p_n^j \in L^2(\Omega)$ for every $j = 0,...,r$ such that

$$
\begin{aligned}
2\mu\langle\boldsymbol{\varepsilon}(\mathbf{u}_n^i),\boldsymbol{\varepsilon}(\mathbf{v})\rangle+\langle\lambda\nabla\cdot\mathbf{u}_n^i-\alpha p_n^i,\nabla\cdot\mathbf{v}\rangle &= \langle\mathbf{f}_\sigma,\mathbf{v}\rangle,\\
\langle\mathbf{k}^{-1}\mathbf{q}_n^i,\mathbf{z}\rangle-\langle p_n^i,\nabla\cdot\mathbf{z}\rangle &= \langle\rho_f\mathbf{g},\mathbf{z}\rangle,\\
\sum_{j=0}^{r}\left\{\alpha_{ij}\langle c_M p_n^j+\alpha\nabla\cdot\mathbf{u}_n^j,w\rangle\right\}+\beta_{ii}\langle\nabla\cdot\mathbf{q}_n^i,w\rangle &= \beta_{ii}\langle f_m,w\rangle.
\end{aligned}
$$

holds true $\forall i = 0,..,r$ and for all $\mathbf{v} \in \mathbf{H}_0^1(\Omega)$, $\mathbf{z} \in \mathbf{H}(\mathrm{div};\Omega)$ and $w \in L^2(\Omega)$. The coefficients above are defined by $\alpha_{ij} := \int_{I_n}\partial_t(\psi_n^j)\psi_n^i dt$ and $\beta_{ii} := \int_{I_n}\phi_n^i\psi_n^i dt$, see [13, 14] for more details.

3.1.2 Semi-Discretization in time: discontinuous Galerkin dG(r)

We can now state a semi-discrete variational form of the system (3.1) using discontinuous Galerkin finite elements in time. We mention that the test functions ψ_n are vanishing on $I\setminus I_n$. The semi-discrete scheme reads as:

Find $\mathbf{u}_\tau \in \mathcal{Y}_\tau^r\left(\mathbf{H}^1(\Omega)\right)$, $\mathbf{q}_\tau \in \mathcal{Y}_\tau^r(\mathbf{H}(\mathrm{div};\Omega))$ and $p_\tau \in \mathcal{Y}_\tau^r\left(L^2(\Omega)\right)$, such that

$$
\begin{aligned}
2\mu\int_{I_n}\langle\boldsymbol{\varepsilon}(\mathbf{u}_\tau):\boldsymbol{\varepsilon}(\mathbf{v}_\tau)\rangle d\tau+\int_{I_n}\langle\lambda\nabla\cdot\mathbf{u}_\tau+\alpha p_\tau,\nabla\cdot\mathbf{v}_\tau\rangle d\tau&=\int_{I_n}\langle\mathbf{f}_\sigma,\mathbf{v}_\tau\rangle d\tau,\\
\int_{I_n}\langle\mathbf{k}^{-1}\mathbf{q}_\tau,\mathbf{z}_\tau\rangle d\tau-\int_{I_n}\langle p_\tau,\nabla\cdot\mathbf{z}_\tau\rangle d\tau&=\int_{I_n}\langle\rho_f\mathbf{g},\mathbf{z}_\tau\rangle d\tau,\\
\int_{I_n}\left\langle\frac{\partial}{\partial t}\left(c_M p_\tau+\alpha\nabla\cdot\mathbf{u}_\tau\right),w_\tau\right\rangle d\tau+\int_{I_n}\langle\nabla\cdot\mathbf{q}_\tau,w_\tau\rangle d\tau&\\
+\langle\left[c_M p_\tau+\alpha\nabla\cdot\mathbf{u}_\tau\right]_{n-1},w_\tau(t_n^+)\rangle&=\int_{I_n}\langle f_m,w_\tau\rangle d\tau,
\end{aligned}
$$

for all $\mathbf{v}_\tau \in \mathcal{Y}_\tau^r\left(\mathbf{H}_0^1(\Omega)\right)$, $\mathbf{z}_\tau \in \mathcal{Y}_\tau^r(\mathbf{H}(\mathrm{div};\Omega))$ and $w_\tau \in \mathcal{Y}_\tau^r\left(L^2(\Omega)\right)$. We also use the notations $[w_\tau]_{n-1} = w_\tau^+(t_{n-1}) - w_\tau^-(t_{n-1})$, $w_\tau^+(t_{n-1}) = w_{\tau|_{I_n}}(t_{n-1})$ and $w_\tau^-(t_{n-1}) = w_{\tau|_{I_{n-1}}}(t_{n-1})$.

We represent $\mathbf{u}_{\tau|I_n}$, $\mathbf{q}_{\tau|I_n}$, and $p_{\tau|I_n}$ in terms of the basis functions with respect to the time variable of $\mathcal{Y}_\tau^r\left(\mathbf{H}^1(\Omega)\right)$, $\mathcal{Y}_\tau^r(\mathbf{H}(\mathrm{div};\Omega))$, and $\mathcal{Y}_\tau^r\left(L^2(\Omega)\right)$, respectively. For this, let t_n^j, for $j=0,\ldots,r$ be the $(r+1)$ Gauss quadrature points on I_n. We define ψ_n^j to be the Lagrange polynomial of degree r, which satisfies $\psi_n^j(t_n^i)=\hat{\delta}_{ji}$, with $\hat{\delta}$ being the Kronecker symbol. Now we express our variables as a linear combination of the basis functions

$$
\mathbf{u}_{\tau|I_n}(t)=\sum_{j=0}^{r}\mathbf{u}_n^j\psi_n^j(t),\quad \mathbf{q}_{\tau|I_n}(t)=\sum_{j=0}^{r}\mathbf{q}_n^j\psi_n^j(t),\quad p_{\tau|I_n}(t)=\sum_{j=0}^{r}p_n^j\psi_n^j(t).
$$

Then, by taking $\mathbf{v}_\tau=\mathbf{v}\psi_n^i$, $\mathbf{z}_\tau=\mathbf{z}\psi_n^i$ and $w_\tau=w\psi_n^i$,$i=0,\ldots,r$ in the semi-discrete problem above, we get the equivalent formulation on each time interval I_n:
Find $\mathbf{u}_n^j \in H_0^1(\Omega)$, $\mathbf{q}_n^j \in \mathbf{H}(\mathrm{div};\Omega)$ and $p_n^j \in L^2(\Omega)$ for every $j=0,...,r$ such that

$$
\begin{aligned}
2\mu\langle\boldsymbol{\varepsilon}(\mathbf{u}_n^i),\boldsymbol{\varepsilon}(\mathbf{v})\rangle+\langle\lambda\nabla\cdot\mathbf{u}_n^i-\alpha p_n^i,\nabla\cdot\mathbf{v}\rangle &= \langle\mathbf{f}_\sigma,\mathbf{v}\rangle,\\
\langle\mathbf{k}^{-1}\mathbf{q}_n^i,\mathbf{z}\rangle-\langle p_n^i,\nabla\cdot\mathbf{z}\rangle &= \langle\rho_f\mathbf{g},\mathbf{z}\rangle,\\
\sum_{j=0}^{r}\left\{\alpha_{ij}\langle c_M p_n^j+\alpha\nabla\cdot\mathbf{u}_n^j,w\rangle\right\}+\beta_{ii}\langle\nabla\cdot\mathbf{q}_n^i,w\rangle &= \beta_{ii}\langle f_m,w\rangle\\
&- \psi_n^i(t_{n-1}^+)\left\langle c_M p_{n-1}^- +\alpha\nabla\cdot\mathbf{u}_{n-1}^-+),w\right\rangle,
\end{aligned}
$$

holds true $\forall i=0,..,r$ and for all $\mathbf{v}\in\mathbf{H}_0^1(\Omega)$, $\mathbf{z}\in\mathbf{H}(\mathrm{div};\Omega)$ and $w\in L^2(\Omega)$. The coefficients above are defined by $\alpha_{ij} := \int_{I_n}\partial_t(\psi_n^j)\psi_n^i dt+\psi_n^{j+}(t_{n-1})\psi_n^{i+}(t_{n-1})$ and $\beta_{ii}:=\int_{I_n}\phi_n^i\psi_n^i dt$, see [13, 14] for more details.

3.1.3 Discretization in space: cG(p+1)-MFEM(p)

Let $\mathcal{K}_h$ be a regular decomposition of Ω into quadrilateral elements K for $d=2$, and hexahedral elements for $d=3$. We use quadrilateral and hexahedral elements because the implementation in deal II is tailored to it [10]. We denote by h_K the diameter of the element K, and by h the global discretization mesh diameter by

$h = \max_{K\in\mathcal{K}_h} h_K$. We introduce the next finite element spaces following lines of Brezzi & Fortin [31]

$$\mathbb{P}_{p1,p2}(K) := \left\{ \phi : K \to \mathbb{R} \,\middle|\, \phi(\mathbf{x}) = \sum_{i=0}^{p_1}\sum_{j=0}^{p_2} \phi_{i,j} x_1^i x_2^j,\ \phi_{i,j} \in \mathbb{R} \right\} \text{ and}$$

$$\mathbb{P}_{p1,p2,p3}(K) := \left\{ \phi : K \to \mathbb{R} \,\middle|\, \phi(\mathbf{x}) = \sum_{i=0}^{p_1}\sum_{j=0}^{p_2}\sum_{k=0}^{p_3} \phi_{i,j,k} x_1^i x_2^j x_3^k,\ \phi_{i,j,k} \in \mathbb{R} \right\},$$

which are spaces of polynomials of degree p_1, p_2, and p_3 for the component x_1, x_2, and x_3 of the position vector $\mathbf{x}$. With that, we define the following vector-valued space

$$\mathbb{Q}_p^d(K) := \begin{cases} \left\{ \phi : K \to \mathbb{R}^2 \,|\, \phi \in \mathbb{P}_{p,p}(K) \times \mathbb{P}_{p,p}(K) \right\}, & \text{if } d = 2 \\ \left\{ \phi : K \to \mathbb{R}^3 \,|\, \phi \in \mathbb{P}_{p,p,p}(K) \times \mathbb{P}_{p,p,p}(K) \times \mathbb{P}_{p,p,p}(K) \right\}, & \text{if } d = 3. \end{cases}$$

which is a space of vector-valued polynomials of degree p at each component.

Continuous Galerkin cG(p) Here, we present the space we use for the discretization of the mechanics problem. For any arbitrary polynomial degree $p \geq 0$, the continuous Galerkin (cG(p)) space is defined as

$$\mathbf{V}_h^p := \left\{ \mathbf{v}_h \in C(\Omega) \,\middle|\, \mathbf{v}_{h|K} \in \mathbb{Q}_p^d(K), \forall K \in \mathcal{K}_h \right\}.$$

Mixed finite element method MFEM(p) In this section, we present spaces for the approximation of $\mathbf{H}(\mathrm{div};\Omega)$ that we use for the spatial discretization of the flow problem. These spaces are called Raviart-Thomas (**RT**) for $d = 2$, or Raviart-Thomas-Nedelec (**RTN**) for $d = 3$, and they are defined as follows:

$$\mathbf{RT}_p(K) := \left\{ \phi : K \to \mathbb{R}^2 \,|\, \phi \in \mathbb{P}_{p+1,p}(K) \times \mathbb{P}_{p,p+1}(K) \right\} \text{ and}$$
$$\mathbf{RTN}_p(K) := \left\{ \phi : K \to \mathbb{R}^3 \,|\, \phi \in \mathbb{P}_{p+1,p,p}(K) \times \mathbb{P}_{p,p+1,p}(K) \times \mathbb{P}_{p,p,p+1}(K) \right\}.$$

Then, for any arbitrary polynomial degree $p \geq 0$, the mixed finite element (MFEM(p)) spaces are defined as

$$\mathbf{Z}_h^p := \begin{cases} \left\{ \mathbf{z}_h \in \mathbf{H}(\mathrm{div};\Omega) \,\middle|\, \mathbf{z}_{h|K} \in \mathbf{RT}_p(K), \forall K \in \mathcal{K}_h \right\}, & \text{if } d = 2 \\ \left\{ \mathbf{z}_h \in \mathbf{H}(\mathrm{div};\Omega) \,\middle|\, \mathbf{z}_{h|K} \in \mathbf{RTN}_p(K), \forall K \in \mathcal{K}_h \right\}, & \text{if } d = 3, \end{cases}$$

and

$$W_h^p := \begin{cases} \left\{ w_h \in L^2(\Omega) \,\middle|\, w_{h|K} \in \mathbb{P}_{p,p}(K), \forall K \in \mathcal{K}_h \right\}, & \text{if } d = 2 \\ \left\{ w_h \in L^2(\Omega) \,\middle|\, w_{h|K} \in \mathbb{P}_{p,p,p}(K), \forall K \in \mathcal{K}_h \right\}, & \text{if } d = 3. \end{cases}$$

The spaces cG(p+1) and MFEM(p) are not uniformly inf-sup stable for poromechanics problems. However, a small enough h can be used to avoid oscillations [105].

We now proceed by formulating a fully discrete scheme dG(r)-cG(p+1)-MFEM(p) for solving (3.1). The fully discrete scheme for solving (3.1) on each time interval I_n reads as follows:

For every $i \in \{0, ..., r\}$, find $\mathbf{u}_{n,h}^i \in \mathbf{V}_h^{p+1}$, $\mathbf{q}_{n,h}^i \in \mathbf{Z}_h^p$ and $p_{n,h}^i \in W_h^p$, such that:

$$
\begin{aligned}
2\mu\langle\boldsymbol{\varepsilon}(\mathbf{u}_{n,h}^i), \boldsymbol{\varepsilon}(\mathbf{v}_{n,h})\rangle + \langle\lambda\nabla\cdot\mathbf{u}_h^i - \alpha p_{n,h}^i, \nabla\cdot\mathbf{v}_{n,h}\rangle &= \langle\mathbf{f}_\sigma(t_{n,i}), \mathbf{v}_h\rangle \\
\langle\mathbf{k}^{-1}\mathbf{q}_{n,h}^i, \mathbf{z}_h\rangle - \langle p_{n,h}^i, \nabla\cdot\mathbf{z}_h\rangle &= \langle\rho_f\mathbf{g}, \mathbf{z}_h\rangle, \\
\sum_{j=0}^{r}\Big\{\alpha_{ij}\langle c_M p_{n,h}^j + \alpha\nabla\cdot\mathbf{u}_h^j, w_h\rangle\Big\} + \beta_{ii}\langle\nabla\cdot\mathbf{q}_{n,h}^i, w_h\rangle &= \beta_{ii}\langle f_m(t_{n,i}), w_h\rangle \\
&+ \psi_n^i(t_{n-1}^+)\left\langle(c_M p_{n-1}^- + \alpha\nabla\cdot\mathbf{u}_{n-1}^-), w_h\right\rangle.
\end{aligned}
$$

for all $\mathbf{v}_h \in \mathbf{V}_h^{p+1}$, $\mathbf{z}_h \in \mathbf{Z}_h^p$ and $w_h \in W_h^p$.

It is beyond the scope of this work to give a comprehensive review on all spatial discretization. However, we mention discretizations that have been developed and analyzed for Biot's equations: finite volumes [66, 87], mixed finite elements methods [6, 76, 85, 86], nonconforming finite elements [62], the MINI element [104], continuous or discontinuous Galerkin [38, 39, 41, 101, 111, 122, 131], high-order methods [21], Galerkin least squares [73], isogeometric analysis [123, 124], multiscale methods [34, 35, 47], and combinations of the above-mentioned ones [17, 76, 84, 91–94, 128]. Adaptive computations were considered, for example, in the work of Ern and Meunier [52]. A Monte Carlo approach was proposed in the work of Rahrah and Vermolen [100]. For a discussion on the stability of different spatial discretizations, we refer to the recent papers [59, 105].

3.1.4 Lower order space-time discretization dG(0)-cG(1)-MFEM(0)

For the lowest polynomial degree in time and space, $r = p = 0$, we have the following nodal point $\hat{t}_0 = \frac{1}{2}$ and quadrature weights $\hat{w}_0 = 1$. Here, the test and trial time's functions are $\hat{\psi}_0 = 1$, then the assemblies in time are evaluated as $\alpha_{0,0} = 1$, $\beta_{0,0} = \tau_n$. Find $\mathbf{u}_{n,h}^0, \in \mathbf{V}_h^1$, $\mathbf{q}_{n,h}^0 \in \mathbf{Z}_h^0$ and $p_{n,h}^0 \in W_h^0$, such that

$$
\begin{aligned}
2\mu\langle\boldsymbol{\varepsilon}(\mathbf{u}_{n,h}^0), \boldsymbol{\varepsilon}(\mathbf{v}_{n,h})\rangle + \langle\lambda\nabla\cdot\mathbf{u}_{n,h}^0 - \alpha p_{n,h}^0, \nabla\cdot\mathbf{v}_{n,h}\rangle &= \langle\mathbf{f}_\sigma(t_{n,0}), \mathbf{v}_h\rangle, && (3.2)\\
\langle\mathbf{K}^{-1}\mathbf{q}_{n,h}^0, \mathbf{z}_h\rangle - \langle p_{n,h}^0, \nabla\cdot\mathbf{z}_h\rangle &= \langle\rho_f\mathbf{g}, \mathbf{z}_h\rangle, && (3.3)\\
\langle c_M p_{n,h}^0 + \alpha\nabla\cdot\mathbf{u}_h^0, w_h\rangle + \tau_n\langle\nabla\cdot\mathbf{q}_{n,h}^0, w_h\rangle &= \left\langle c_M p_{n-1}^- + \alpha\nabla\cdot\mathbf{u}_{n-1}^-, w_h\right\rangle \\
&+ \tau_n\langle f_m(t_{n,0}), w_h\rangle, && (3.4)
\end{aligned}
$$

for all $\mathbf{v}_{n,h} \in \mathbf{V}_h^1$, $\mathbf{z}_{n,h} \in \mathbf{Z}_h^0$ and $w_{n,h} \in W_h^0$.

Backward Euler. The scheme above is algebraically equivalent to a backward Euler scheme, and both are linearly convergent with respect to the time variable.

The only difference lies on the nodal point of the time interval, where $\hat{t}_0 = 1$ for backward Euler. In other words, backward Euler calculates the solution at the end point of the time interval, while $dG(0)$ calculates it for the middle point of the time interval.

3.2 Solvers for coupled problems

Coupled problems are present in many physical examples. For instance, the models presented in chapter 2.6 show the coupling between fluid flow and mechanical deformation in a porous domain. There are two approaches that can be used to solve coupled problems, the monolithic (fully coupled) scheme and the splitting (weakly coupled) scheme. In general, the monolithic schemes ensure that the numerical solution is consistent with the underlying continuous differential equations. Despite obvious advantages, the monolithic solver for fully coupled problems is more difficult to implement, and have difficulties solving the resulting linear system, particularly in the context of existing legacy code for separate physics. Due to the complexities associated with the fully coupled scheme, weakly coupled or iteratively coupled approaches are still used as industry standard [37, 42, 65, 68, 69, 80, 82, 90–92, 106–108, 125, 130]. An iteratively coupled approach takes somewhat of a middle path; at each time step, it decouples the flow and mechanics, but iterates so that convergence is achieved. Different alternation of iterative cycles in flow and mechanics, i.e., single- [4] and multi-rate schemes [3, 5, 48, 74], multiscale methods [47] and algebraic solvers can be considered. General Schur complement based preconditioners [8, 36, 37, 40, 58, 58, 94, 126, 127] and preconditioners which are robust with respect to the model parameters [1, 9, 60, 61, 77, 102, 103] are examples of algebraic solvers. For other splitting schemes, see for example the works of Turska et al. [118, 119].

We will be using the following algebraic system of equations (Eqs. 3.5), in order to illustrate the monolithic and splitting approach. Nevertheless, these approaches can also be translated to the variational formulation of a coupled problem, see Paper A-F. Let $\mathbf{A} \in \mathbb{R}^{n \times n}$ be the algebraic elastic operator from the mechanics problem, $\mathbf{C} \in \mathbb{R}^{m \times m}$ be the algebraic operator from the flow problem and $\mathbf{B} \in \mathbb{R}^{n \times m}$ be the coupling term. The vector solution $\mathbf{x} = \{\mathbf{u}\}$ represents the discrete approximation of the mechanics deformation and $\mathbf{y} = \{\mathbf{q}, p\}^\top$ represents the discrete approximation of the flow problem solution. Find $\mathbf{x} \in \mathbb{R}^n$ and $\mathbf{y} \in \mathbb{R}^m$ such that

$$\begin{aligned} \mathbf{A}\,\mathbf{x} - \mathbf{B}\,\mathbf{y} &= \mathbf{b}, \\ \mathbf{B}^\top \mathbf{x} + \mathbf{C}\,\mathbf{y} &= \mathbf{c}, \end{aligned} \tag{3.5}$$

for the given discrete approximation of the right hand side $\mathbf{b} \in \mathbb{R}^n$ and $\mathbf{c} \in \mathbb{R}^m$.

3.2.1 Monolithic scheme

A monolithic scheme solves Problem 3.5 in a fully coupled way. This provides an unconditionally stable approach. However, it requires assembling of a bigger matrix

$\mathbf{M} \in \mathbb{R}^{(n+m)\times(n+m)}$, composed by smaller block matrices

$$\mathbf{M} := \begin{pmatrix} \mathbf{A} & -\mathbf{B} \\ \mathbf{B}^\top & \mathbf{C} \end{pmatrix}.$$

In practice, this scheme is typically difficult to solve iteratively, leading to an ill-conditioned system which needs the use of preconditioners [53, 54, 107]. Therefore, construction of efficient preconditioning techniques for the algebraic systems is an open question and a matter of ongoing scientific research, see for example [36, 56, 126].

3.2.2 Splitting scheme

Jacobi and Gauss-Seidel methods are examples of iterative splitting schemes. The stability of these iterative methods depends on the matrix involved. There are also more sophisticated methods like Successive over-relaxation method (SOR), that adds a parameter in order to stabilize the iterative method [117]. Splitting schemes extend to systems of equations that have a block structure (3.5). For instance, one of these splitting schemes is the exact Uzawa type splitting scheme [57, 120].
Solve for $\mathbf{x}$ and $\mathbf{y}$

$$\begin{pmatrix} \mathbf{A} & -\mathbf{B} \\ \mathbf{0} & (\mathbf{C}+\mathbf{S}) \end{pmatrix} \begin{pmatrix} \mathbf{x} \\ \mathbf{y} \end{pmatrix} = \begin{pmatrix} \mathbf{b} \\ \mathbf{c} - \mathbf{B}^\top \mathbf{A}^{-1} b \end{pmatrix},$$

where $\mathbf{S} = \mathbf{B}^\top \mathbf{A}^{-1} \mathbf{B}$. This method is exact and converge in one iteration. Nevertheless, $\mathbf{A}^{-1}$ is practically unavailable in poromechanics problems. We therefore introduce an Inexact Uzawa splitting scheme [114, 132]. This scheme is obtained by approximating operator $\mathbf{S}$. In this case, we consider a diagonal approximation of $\mathbf{S} \approx s\,\mathbf{I}$, with the stabilization parameter $s \geq 0$, and $\mathbf{B}^\top \mathbf{A}^{-1} \mathbf{b} \approx \mathbf{B}^\top \mathbf{x}^{i-1} - \mathbf{S}\mathbf{y}^{i-1}$. For $i > 0$, given $\mathbf{x}^0$ and $\mathbf{y}^0$, solve for $\mathbf{x}^i$ and $\mathbf{y}^i$ until convergence

$$\begin{pmatrix} \mathbf{A} & -\mathbf{B} \\ \mathbf{0} & (\mathbf{C}+\mathbf{S}) \end{pmatrix} \begin{pmatrix} \mathbf{x}^i \\ \mathbf{y}^i \end{pmatrix} = \begin{pmatrix} \mathbf{b} \\ \mathbf{c} + \mathbf{S}\mathbf{y}^{i-1} - \mathbf{B}^\top \mathbf{x}^{i-1} \end{pmatrix}. \tag{3.6}$$

It is essential to understand the efficiency, stability and convergence of these iterative splitting schemes applied to poromechanics problems, in order to ensure the robustness and accuracy of the resulting computations. Papers A, C, D and E develop, study, and analyse monolithic and splitting schemes for poromechanics problems.

Fixed-stress splitting method The fixed-stress splitting method is the most widely used solver for poromechanics. It consists of solving the flow problem by first fixing the volumetric mean total stress, and then the mechanics problem is solved from the values obtained at the previous flow step. The method can be written algebraically as Eq. (3.6) where the stabilization parameter is given by $s = \frac{\alpha^2}{\lambda}$ and the matrix is given by

$$\mathbf{S} = \begin{pmatrix} 0 & 0 \\ 0 & s\mathbf{C}_p \end{pmatrix},$$

where the matrix $\mathbf{C}_p$ represents the algebraic operator of the flow problem corresponding to the pressure component.

A lot of research has been done on this method in recent years. The unconditional stability of the fixed-stress splitting method is shown in [69], using a von Neumann analysis. In addition, the stability and convergence of the fixed-stress splitting method was rigorously established in [80]. In Paper E, we prove the convergence of the fixed-stress split method in energy norm for linear and heterogeneous poromechanics problems.

3.3 Linearizations schemes

In Section 2, we discussed the equations that govern fluid flow in deformable porous media. Some of these equations are non-linear, leading to non-linear variational problems. Here, we will use a prototype non-linear problem (Eq. 3.7) to illustrate two linearization techniques: Newton's method and the L-scheme.
For V and W, two normed vector spaces $U \subset V$, find $\mathbf{x} \in U$ such that

$$\mathbf{F}(\mathbf{x}) = 0, \tag{3.7}$$

given a non-linear function $\mathbf{F} : U \to W$.

The function $\mathbf{F}$ is called Fréchet differentiable at $\mathbf{x}$ if there exists a bounded operator $A : V \to W$ such that

$$\lim_{\|\mathbf{h}\|_V \to 0} \frac{\|\mathbf{F}(\mathbf{x}+\mathbf{h}) - \mathbf{F}(\mathbf{x}) - A\mathbf{h}\|_W}{\|\mathbf{h}\|_V} = 0.$$

If such operator A exists and is unique, we write $D\mathbf{F}(\mathbf{x}) = A$. Similarly to the Fréchet derivative on a Banach space, the Gateaux derivative is often used to formalize the directional derivative.

$$D\mathbf{F}(\mathbf{x};\mathbf{y}) = \lim_{h \to 0} \frac{\|\mathbf{F}(\mathbf{x}+h\mathbf{y}) - \mathbf{F}(\mathbf{x})\|_W}{h}.$$

The Gateaux derivative generalized the idea of directional derivatives and it is useful for problems that has complicated non-linearities, for instance Eqs. (2.18).

3.3.1 Newton's method

The first choice of a linearization method is the well-recognized Newton method. In this case, a solution $\mathbf{x} \in U$ of Eq. (3.7) is approximated iteratively as follows:
For $i > 0$, given $\mathbf{x}^0 \in U$, find $\mathbf{x}^{i+1} \in U$ such that

$$\mathbf{F}(\mathbf{x}^i) + D\mathbf{F}(\mathbf{x}^i; \delta\mathbf{x}^{i+1}) = 0, \tag{3.8}$$

where $\delta\mathbf{x}^{i+1} = \mathbf{x}^{i+1} - \mathbf{x}^i$ and i is the iteration index.

This method has quadratic convergence, but the convergence is local. This means that the starting value for the iterations should not be too far from the (unknown)

solution. To increase the robustness of the Newton method, one can first perform some L-scheme iterations, which are later described, and then switch to Newton's method [78]. Another way to increase the robustness of Newton's method is by applying line search strategy [29, 30].

3.3.2 L-scheme

The idea of the L-scheme [78, 95] is to solve the non-linear problem (3.7) iteratively by linearising in the following way:
For $i > 0$, given $\mathbf{x}^0 \in U$, find $\mathbf{x}^{i+1} \in U$ such that

$$\mathbf{F}(\mathbf{x}^i) + L\delta\mathbf{x}^{i+1} = 0, \tag{3.9}$$

where $L \in \mathbb{R}$ is a linearization parameter of choice.

When $i \to \infty$, we must have $\mathbf{x}^i \to \mathbf{x}$, obviously ensuring the consistency of the scheme. The L-scheme can be interpreted as either a stabilized fixed-point method or as quasi-Newton method. Additionally, it is very robust but only linearly convergent. It can be applied to non-smooth, but monotonically increasing scalar functions $\mathbf{F}(\cdot)$ [95]. For the case of Hölder continuous but not Lipschitz functions $\mathbf{F}(\cdot)$, we refer to [28, 98]. The L-scheme can be speeded up by using the Anderson acceleration [7, 29]. The main advantages of the L-scheme are

- It does not involve the computation of derivatives.
- The arising linear systems are well-conditioned.
- It can be applied to non-smooth non-linearities.
- It is easy to understand and implement.

The L-scheme is currently being used for: transport of a surfactant in variably saturated porous media [64, 83], Biot's model coupled with heat equation [32] and two phase flow in porous media [109]. Also, this method can perfectly be used in combination with other methods, like domain decomposition [109] and preconditioning [2].

Chapter 4

Introduction to the papers

Here we will summarize the scientific results. We first show the convergence of the L-scheme for a non-linear Biot model in Paper A. Second, we extend the results from Paper A to a higher order discretization in time. Third, in Paper C, we will analyze Newton's method and extend the model in Paper A to Biot's model under large deformation. And fourth, we will develop a new splitting scheme that allows parallel computations in the time domain.

Additionally, we will show two collaborative papers. The first one, Paper E, is related to optimizing the fixed stress splitting method through a stabilization parameter. The second one, Paper F, is a short conference paper that compiles and discusses the theoretical convergence of L-scheme and Newton's method in the monolithic and splitting version.

4.1 Main results

4.1.1 Paper A: Robust iterative schemes for non-linear poromechanics

Authors: M. Borregales, F.A. Radu, K.Kumar and J.M. Nordbotten

Journal: Computational Geosciences 22, 4 (2018)

In this paper, we proposed and analyzed two linearization schemes for a non-linear extension of Biot's model. We consider the case when the relative density of the flow and the bulk modulus in the porous material are non-linear. These non-linearities are the first but necessary steps to, later on, consider extensions of Biot's model to multiphase flow, elastodynamics, and poromechanics under large deformation.

The paper combines linearization techniques [78, 98, 99] and splitting schemes (fixed-stress and undrained splitting schemes) [70, 82] for solving Biot's model. We proposed a monolithic and a splitting L-scheme for solving a non-linear Biot model. The existence and uniqueness of a solution for both schemes, as well as their global,

linear, and robust convergence, is shown rigorously. Concretely, by robust, it is meant that the convergence of the schemes proposed is guaranteed regardless of the starting guess for the iteration (global convergence) and independently of the discretization parameters.

We performed an implicit discretization in time using backward Euler, linear conformal Galerkin elements for the space discretization of the mechanics problem and mixed finite elements (the lowest order Raviart-Thomas elements) for the flow problem. Two illustrative numerical examples, an academic one and a non-linear extension of Mandel's problem, were implemented for testing the performance of the schemes. Both examples show results in agreement with the convergence analysis developed in the paper.

4.1.2 Paper B: Higher order space-time elements for a non-linear Biot model

Authors: M. Borregales and F.A. Radu.

Journal: Numerical Mathematics and Advanced Applications ENUMATH 2017, Lecture Notes in Computational Science and Engineering.

In this paper, we applied the monolithic and splitting L-scheme developed in Paper A to a higher order finite element space-time discretization. We note that the non-linear Biot model in Paper A can be understood as the singular limit of the fully dynamic Biot-Allard system [81]. The quasi-static characteristic of the Biot model comes in due to neglecting the solid's velocity in the mechanical problem Eq. 2.4. In this regard, the non-linear Biot model in Paper A does not allow application to problems with higher dynamics in the solids deformation.

Here, we applied a higher order space-time discretization to a non-linear Biot model [11, 12, 14] linearized by L-scheme. We believe that this methodology can be extended for more complex non-linear models, elastodynamics and to the fully-dynamic Biot-Allard system [81].

The major challenge we faced in this work was related to the implementation of the numerical experiment. We use the open-source finite element library deal.II [10] in all our implementations, but it does not allow $d+1$ mesh for a space-time domain. Therefore, we used the DTM++ framework [71, 72] in order to incorporate a family of continuous and discontinuous high order finite element methods for the time discretization.

The most important observation of this work is that the convergence of the monolithic and splitting L-scheme are not affected by the mesh size and time step size. These results are in accordance with the theoretical results from Paper A. However, the convergence is slightly dependent on the order of the spatial discretization.

4.1.3 Paper C: Iterative solvers for Biot model under small and large deformation

Authors: M. Borregales, K.Kumar, J.M. Nordbotten and F.A. Radu.

Journal: arXiv:1905.12996

In this paper, we proposed and analyzed several iterative schemes for solving Biot's model under small and large deformation. This paper extends the non-linear Biot model in Paper A to include geometrical non-linearities. We proposed two linearization schemes based on Newtons methods: a monolithic Newton method and the alternate Newton's method. Additionally, we proposed two linearization schemes based on the L-schemes proposed in Paper A.

The linear Biot model is a good model for small deformations, but it becomes inappropriate for moderate to large deformations, which are common in the context of phenomena such as swelling and damage, and for soft materials such as gels and tissues. The non-linearities for the Biot model under large deformations are more complex than the ones encountered in Paper A, and they include geometrical non-linearities for both the flow and the mechanics problem.

The main contribution of this paper is the convergence analysis of the monolithic Newton method and the alternate Newton's method under the assumption of small deformation. The analysis in this paper showed second order convergence for the monolithic Newton method and linear convergence for the alternate Newton method. The alternate Newton method requires a stabilization parameter, based on the undrained splitting scheme [68], otherwise the convergence cannot be guaranteed. Two numerical examples for large deformation (2D and 3D) show agreement between convergence analysis and the computations.

4.1.4 Paper D: A parallel-in-time fixed-stress splitting method for Biot's consolidation model

Authors: M. Borregales, K. Kumar, F.A. Radu, C. Rodrigo and F.J. Gaspar

Journal: Computers & Mathematics with Applications (2018)

In this paper, we proposed and analyzed a new splitting scheme that allows parallel computation. The partially parallel fixed-stress exploit the quasi-static nature of the mechanics problem. This new approach forgets about the sequential nature of the temporal variable and considers the time direction as a further direction for parallelization.

Among splitting schemes for Biot model, the fixed-stress splitting method is the most widely used [26, 70, 80]. This sequential-implicit method basically consists of solving the flow problem first by fixing the volumetric mean total stress, and then the mechanics part is solved from the solution obtained at the previous flow step. The multirate iterative coupling schemes [3, 5], where multiple finer time steps for flow

are taken within one coarse mechanics time step, exploit the different time scales for the mechanics and flow problems. In [37], the authors present a very interesting approach which consists of re-interpreting the fixed-stress splitting scheme as a preconditioned-Richardson iteration with a particular block-triangular preconditioning operator. Recently, in [56], an inexact version of the fixed-stress splitting scheme has been successfully proposed as smoother in a geometric multigrid framework, which provides an efficient monolithic solver for Biots problem.

All the previously mentioned algorithms are based on a time-marching approach, in which each time step is solved after the other in a sequential manner. Therefore, they do not allow the parallelization of the temporal variable. Parallel-in-time integration methods, however, are receiving a lot of interest nowadays because of the advent of massively parallel systems with thousands of threads, permitting to reduce drastically the computing time [55].

As the main contribution, we develop a new version of the fixed-stress splitting method for poromechanics problems where it is partially parallel-in-time. We further rigorously show its convergence. Another contribution of this paper is a new proof for the convergence of the fixed-stress splitting algorithm in the semi-discrete case. The theoretical results are sustained by numerical computations. Moreover, a fully parallel-in-time version of the presented method is introduced.

The main benefit of the new method is that the mechanics can be solved in a parallel-in-time manner. We have rigorously analyzed the convergence of the proposed method. If the chosen stabilization term is large enough, the method is shown to be convergent. The theoretical results indicates a similar behavior as when using the classical fixed-stress splitting method, in terms of convergence rate and stabilization parameter size. We further performed numerical tests by using two well-known benchmark problems. The numerical results confirm the theoretical findings. We observe that the new scheme is very efficient, using around 20% of the wall time of the classic fixed-stress scheme. Nevertheless, the parallel implementation has still to be optimized.

4.2 Related work

4.2.1 Paper E: Robust fixed stress splitting for Biots equations in heterogeneous media

Authors: J.W. Both, M. Borregales, J.M. Nordbotten K. Kumar, and J.M. Nordbotten

Journal: Applied Mathematics Letters (2017)

In this paper, we proposed an optimized fixed stress splitting method. The fixed stress method has been the standard splitting method for Biot's model. Nevertheless, it was designed based on a physical notion. The method is based on imposing

constant volumetric mean total stress in the first half step of fluid flow. By interpreting the fixed stress method as a stabilized fixed point iteration, we are able to study it in a more rigorous mathematical setting.

The main contribution is the global and linear convergence in energy norms of the fixed stress method. Additionally, we propose a new optimized stabilization parameter. This parameter depends on all mechanical parameters and shows stable iteration counts. Numerical test cases show no significant increase of iterations when switching from a homogeneous to a heterogeneous medium or from two to three dimensions, demonstrating the robustness of the splitting scheme with respect to heterogeneities. Still, further numerical studies of the fixed stress method [27, 112] show that the optimal stabilization parameter does not solely depend on the Lamé parameters, but also other physical material parameters, the physical characteristics of the problem and numerical discretization parameters.

4.2.2 Paper F: L-scheme and Newton based solvers for a nonlinear Biot model

Authors: F.A. Radu, M. Borregales, F.J. Gaspar, K. Kumar and C. Rodrigo.

Journal: Proceedings: 6th European Conference on Computational Mechanics (Solids, Structures and Coupled Problems), 7th European Conference on Computational Fluid Dynamics (2018)

In this paper, we propose convergent iterative solvers based on the L-scheme and Newton's method for a nonlinear Biot model. More precisely, the first Lamé coefficient (λ) and the fluid compressibility are assumed to be nonlinear.

An important assumption is that the nonlinearities are required to be monotonically increasing and Lipschitz continuous. For a justification of the validity of the considered model, we refer to the book [115]. We remark that the results of the present paper can easily be extended to a model containing geometrical nonlinearity in the mechanics equation (Paper C), as long as it is monotonically increasing, Lipschitz continuous, and the coupling term remains linear.

The main contribution of this paper is the compilation of different nonlinear solvers based on the L-scheme, the Newton method, and the undrained splitting method. The only quadratic convergent scheme is the monolithic Newton. The splitting Newton method also requires a stabilization parameter, otherwise the linear convergence cannot be guaranteed. The analysis of the schemes and illustrative numerical experiments were presented in Paper C.

4.3 Conclusions and outlook

This thesis concerns iterative solvers for poromechanics problems. We proposed several solvers based on the L-scheme, Newton method, monolithic and splitting meth-

ods. The convergence and the performance of each solver were rigorously analyzed for linear and non-linear poromechanics problems.

The monolithic L-scheme is easy to understand, easy to implement, and it is computationally efficient. Nevertheless, the stability of the scheme had to be studied to assure convergence. We showed that it is globally convergent, and it is robust for different parameters, space discretizations, and time discretizations if the non-linearities are monotonically increasing. In contrast, the monolithic Newton method shows quadratic convergence and the convergence is warranted for small deformation poromechanics and relatively small time-steps.

Splitting schemes are attractive for solving coupled problems because the previous knowledge of solving each separate problem can be used straight forward. They are also computationally efficient because one needs to solve smaller problems. However, the splitting schemes show stability problems, especially when the coupling between flow and mechanics is strong. We combined splitting schemes with linearization schemes for solving poromechanics problems.

The monolithic and splitting L-scheme have similar linear convergence rate. However, the splitting version is much faster, and it is suitable for preconditioning monolithic L-scheme or Newton's method. The global, linear, and robust convergence of the L-scheme is warranted if the non-linearities are monotonically increasing. However, the non-linearities presented for large deformation poromechanics are not necessarily monotone. Still, the L-scheme shows convergence and excellent performance for the example we considered.

We believe that the solvers developed here will bring excellent performance in the case of multi-phase flow and reactive transport combined with deformation. In these cases, the non-linearities arise in the flow model in the diffusion term, in the time derivative term, and/or in the Biot's coupling term. By incorporating these non-linearities, the numerical models for CO_2 storage might bring better predictions. In the case of hyperelastic porous material, the new solvers might increase the understanding of the mechanical behaviour of biological tissues. However, the techniques for convergence analysis must be further developed to consider non-monotone non-linearities.

For further research, the convergence analysis of these solvers can also be extended to poromechanics problems with other dynamic models. This is particularly useful for wave propagation and dynamic permeability in deformable porous media. An example of that is liquefaction occurring during earthquakes. Several approaches can be considered in this case. For instance, different time discretization order between the flow and mechanics problem can be applied. Another interesting approach is obtaining a parallel solver by decoupling the flow and mechanics problem in the time domain. In this way, a parallel solver can exploit efficiently the computational resources we have access to nowadays.

Bibliography

[1] Adler, J., Gaspar, F., Hu, X., Rodrigo, C., and Zikatanov, L. (2018). Robust Block Preconditioners for Biot's Model. In *Domain Decomposition Methods in Science and Engineering XXIV*, pages 3–16. Springer International Publishing. doi: 10.1007/978-3-319-93873-8.

[2] Ahmed, E., Fumagalli, A., Budisa, A., Keilegavlen, E., Nordbotten, J., and Radu, F. (2019). Robust linear domain decomposition schemes for reduced non-linear fracture flow models. *arXiv:1906.05831 [math.NA]* .

[3] Almani, T., Kumar, K., Dogru, A., Singh, G., and Wheeler, M. (2016). Convergence Analysis of Multirate Fixed-Stress Split Iterative Schemes for Coupling Flow with Geomechanics. *Comput. Methods. Appl. Mech. Eng. 311*, 180–207. doi: 10.1016/j.cma.2016.07.036.

[4] Almani, T., Kumar, K., and Wheeler, M. F. (2017). Convergence and error analysis of fully discrete iterative coupling schemes for coupling flow with geomechanics. *Comput. Geosci. 21*(5-6), 1157–1172. doi: 10.1007/s10596-017-9691-7.

[5] Almani, T., Manea, A., Kumar, K., and Dogru, A. H. (2019). Convergence of the undrained split iterative scheme for coupling flow with geomechanics in heterogeneous poroelastic media. *Comput. Geosci.* doi: 10.1007/s10596-019-09860-5.

[6] Ambartsumyan, I., Khattatov, E., Nordbotten, J., and Yotov, I. (2018). A multipoint stress mixed finite element method for elasticity on simplicial grids. *arXiv:1805.09920v3 [math.NA]* .

[7] Anderson, D. (1965). Iterative Procedures for Nonlinear Integral Equations. *J. ACM 12*(4), 547–560. doi: 10.1145/321296.321305.

[8] Axelsson, O., Blaheta, R., and Byczanski, P. (2012). Stable discretization of poroelasticity problems and efficient preconditioners for arising saddle point type matrices. *Comput. Vis. Sci. 15*(4), 191–207. doi: 10.1007/s00791-013-0209-0.

[9] Bærland, T., Lee, J. J., Mardal, K.-A., and Winther, R. (2017). Weakly imposed symmetry and robust preconditioners for Biot's consolidation model. *Comput. Methods Appl. Math. 17*(3), 377–396. doi: 10.1515/cmam-2017-0016.

[10] Bangerth, W., Kanschat, G., Heister, T., Heltai, L., and Kanschat, G. (2016). The deal.II library version 8.4. *J. Numer. Math. 24*, 135–141. doi: 10.1515/jnma-2016-1045.

[11] Bause, M. (2019). Iterative coupling of mixed and discontinuous Galerkin methods for poroelasticity. In *Numerical Mathematics and Advanced Applications ENUMATH 2017*, pages 551–560. Springer International Publishing. doi: 10.1007/978-3-319-96415-7.

[12] Bause, M. and Köcher, U. (2015). Variational time discretization for mixed finite element approximations of nonstationary diffusion problems. *J. Comput. Appl. Math 289*, 208–224. doi: 10.1016/j.cam.2015.02.015.

[13] Bause, M., Radu, F., and Köcher, U. (2017). Error analysis for discretizations of parabolic problems using continuous finite elements in time and mixed finite elements in space. *Numerische Mathematik 137*(4), 773–818. doi: 10.1007/s00211-017-0894-6.

[14] Bause, M., Radu, F., and Köcher, U. (2017). Space–time finite element approximation of the Biot poroelasticity system with iterative coupling. *Comput. Methods. Appl. Mech. Eng 320*(Supplement C), 745–768. doi: 10.1016/j.cma.2017.03.017.

[15] Bear, J. (1988). Dynamics of Fluids in Porous Media. Dover Civil and Mechanical Engineering Series. Dover. ISBN 9780486656755.

[16] Berger, L. (2015). A Low Order Finite Element Method for Poroelasticity with Applications to Lung Modelling. Ph.D. thesis.

[17] Berger, L., Bordas, R., Kay, D., and Tavener, S. (2017). A stabilized finite element method for finite-strain three-field poroelasticity. *Comput. Mech. 60*(1), 51–68. doi: 10.1007/s00466-017-1381-8.

[18] Biot, M. A. (1941). General theory of three-dimensional consolidation. *J. Appl. Phys. 12*(2), 155–164. doi: 10.1063/1.1712886.

[19] Biot, M. A. (1955). Theory of Elasticity and Consolidation for a Porous Anisotropic Solid. *J. Appl. Phys. 26*(2), 182–185. doi: 10.1063/1.1721956.

[20] Bociu, L., Guidoboni, G., Sacco, R., and Webster, J. T. (2016). Analysis of Nonlinear Poro-Elastic and Poro-Visco-Elastic Models. *Archive for Rational Mechanics and Analysis 222*(3), 1445–1519. doi: 10.1007/s00205-016-1024-9.

[21] Boffi, D., Botti, M., and Di Pietro, D. A. (2016). A nonconforming high-order method for the Biot problem on general meshes. *SIAM J. Sci. Comput. 38*(3), A1508–A1537. doi: 10.1137/15M1025505.

[22] Borregales, M., Kumar, K., Nordbotten, J., and Radu, F. (2019). Iterative solvers for Biot model under small and large deformation. *arXiv:1905.12996v1 [math.NA]*, [C].

[23] Borregales, M., Kumar, K., Radu, F., Rodrigo, C., and Gaspar, F. (2019). A parallel-in-time fixed-stress splitting method for Biot's consolidation model. *Comput. Math. Appl. 77*(6), 1466–1478. doi: 10.1016/j.camwa.2018.09.005, [D].

[24] Borregales, M., Nordbotten, J., Kumar, K., and Radu, F. (2017). Robust iterative schemes for non-linear poromechanics. *Comput. Geosci. 22*(4), 1021–1038. doi: 10.1007/s10596-018-9736-6, [A].

[25] Borregales, M. and Radu, F. (2019). Higher order space-time elements for a non-linear Biot model. In *Numerical Mathematics and Advanced Applications ENUMATH 2017*, pages 541–549. Springer International Publishing. doi: 10.1007/978-3-319-96415-7, [B].

[26] Both, J., Borregales, M., Nordbotten, J., Kumar, K., and Radu, F. (2017). Robust fixed stress splitting for Biot's equations in heterogeneous media. *Appl. Math. Letters 68*, 101–108. doi: 10.1016/j.aml.2016.12.019, [F].

[27] Both, J. and Köcher, U. (2019). Numerical investigation on the fixed-stress splitting scheme for Biot's equations: Optimality of the tuning parameter. In *Numerical Mathematics and Advanced Applications ENUMATH 2017*. Springer International Publishing. doi: 10.1007/978-3-319-96415-7.

[28] Both, J., Kumar, K., Nordbotten, J., Pop, I., and Radu, F. (2019). Iterative Linearisation Schemes for Doubly Degenerate Parabolic Equations. In *Numerical Mathematics and Advanced Applications ENUMATH 2017*, pages 49–63. Springer International Publishing, Cham. ISBN 978-3-319-96415-7. doi: 10.1007/978-3-319-96415-7.

[29] Both, J., Kumar, K., Nordbotten, J., and Radu, F. (2019). Anderson accelerated fixed-stress splitting schemes for co nsolidation of unsaturated porous media. *Comput. Math. Appl. 77*(6), 1479–1502. doi: 10.1016/j.camwa.2018.07.033.

[30] Both, J., Kumar, K., Nordbotten, J., and Radu, F. (2019). The gradient flow structures of thermo-poro-visco-elastic processes in porous media. *arXiv:1907.03134v1 [math.NA]* .

[31] Brezzi, F. and Fortin, M. (2012). Mixed and hybrid finite element methods, volume 15 of *Springer Ser. Comput. Math.* Springer-Verlag New York. ISBN 978-1-4612-7824-5.

[32] Brun, M., Ahmed, E., Berre, I., Nordbotten, J., and Radu, F. (2019). Monolithic and splitting based solution schemes for fully coupled quasi-static thermo-poroelasticity with nonlinear convective transport. *arXiv:1902.05783v1 [math.NA]* .

[33] Brun, M. K., Ahmed, E., Nordbotten, J. M., and Radu, F. A. (2019). Well-posedness of the fully coupled quasi-static thermo-poroelastic equations with nonlinear convective transport. *J. Math. Anal. Appl 471*(1), 239–266. doi: 10.1016/j.jmaa.2018.10.074.

[34] Castelletto, N., Hajibeygi, H., and Tchelepi, H. A. (2017). Multiscale finite-element method for linear elastic geomechanics. *J. Comput. Phys. 331*, 337–356. doi: 10.1016/j.jcp.2016.11.044.

[35] Castelletto, N., Klevtsov, S., Hajibeygi, H., and Tchelepi, H. (2019). Multiscale two-stage solver for Biot's poroelasticity equations in subsurface media. *Comput. Geosci. 23*(2), 207–224. doi: 10.1007/s10596-018-9791-z.

[36] Castelletto, N., White, J., and Ferronato, M. (2016). Scalable algorithms for three-field mixed finite element coupled poromechanics. *J. Comput. Phys. 327*, 894–918. doi: 10.1016/j.jcp.2016.09.063.

[37] Castelletto, N., White, J., and Tchelepi, H. (2015). Accuracy and convergence properties of the fixed-stress iterative solution of two-way coupled poromechanics. *Int. J. Numer. Anal. Meth. Geomech. 39*(14), 1593–1618. doi: 10.1002/nag.2400.

[38] Chaabane, N. and Rivière, B. (2018). A Sequential Discontinuous Galerkin Method for the Coupling of Flow and Geomechanics. *J. Sci. Comput. 74*(1), 375–395. doi: 10.1007/s10915-017-0443-6.

[39] Chaabane, N. and Rivière, B. (2018). A splitting-based finite element method for the Biot poroelasticity system. *Comput. Math. Appl. 75*(7), 2328–2337. doi: 10.1016/j.camwa.2017.12.009.

[40] Chan, S.-H., Phoon, K.-K., and Lee, F. H. (2001). A modified Jacobi preconditioner for solving ill-conditioned Biots consolidation equations using symmetric quasi-minimal residual method. *Internat. J. Numer. Anal. Methods Geomech. 25*, 1001–1025. doi: 10.1002/nag.164.

[41] Chen, Y., Luo, Y., and Feng, M. (2013). Analysis of a discontinuous Galerkin method for the Biot's consolidation problem. *Appl. Math. Comput. 219*(17), 9043–9056. doi: 10.1016/j.amc.2013.03.104.

[42] Chin, L., Thomas, L., Sylte, J., and Pierson, R. (2002). Iterative Coupled Analysis of Geomechanics and Fluid Flow for Rock Compaction in Reservoir Simulation. *Oil & Gas Sci. Technol. 57*(5), 485–497. doi: 10.2516/ogst:2002032.

[43] Ciralet, P. (1988). Mathematical Elasticity. Nord-Holland. ISBN 9780444825704.

[44] Cookson, A., Lee, J., Michler, C., Chabiniok, R., Hyde, E., Nordsletten, D., Sinclair, M., Siebes, M., and Smith, N. (2012). A novel porous mechanical framework for modelling the interaction between coronary perfusion and myocardial mechanics. *J. Biomech. 45*(5), 850–855. doi: 10.1016/j.jbiomech.2011.11.026.

[45] Coussy, O. (1995). Mechanics of Porous Continua. Wiley, New York. ISBN 9780471952671.

[46] Coussy, O. (2004). Poromechanics. J. Willey & Sons, Ltd. ISBN 9780470849200.

[47] Dana, S., Ganis, B., and Wheeler, M. (2018). A multiscale fixed stress split iterative scheme for coupled flow and poromechanics in deep subsurface reservoirs. *J. Comput. Phys. 352*, 1–22. doi: 10.1016/j.jcp.2017.09.049.

[48] Delpopolo, C. L., Bonaventura, L., Scotti, A., and Formaggia, L. (2019). A conservative implicit multirate method for hyperbolic problems. *Comput. Geosci. 23*(4), 647–664. doi: 10.1007/s10596-018-9764-2.

[49] Detournay, E. and Cheng, A. H.-D. (1993). Fundamentals of Poroelasticity. In *Analysis and Design Methods*, volume 2. Pergamon Press. doi: 10.1016/B978-0-08-040615-2.50011-3.

[50] Doster, F. and Nordbotten, J. (2015). Full Pressure Coupling for Geomechanical Multi-phase Multi-component Flow Simulations.

[51] Dutta-Roy, T., Wittek, A., and Miller, K. (2008). Biomechanical modelling of normal pressure hydrocephalus. *Journal of biomechanics 41*(10), 2263—2271. doi: 10.1016/j.jbiomech.2008.04.014.

[52] Ern, A. and Meunier, S. (2009). A posteriori error analysis of Euler-Galerkin approximations to coupled elliptic-parabolic problems. *ESAIM: M2AN 43*(2), 353–375. doi: 10.1051/m2an:2008048.

[53] Gai, X. (2014). A coupled geomechanics and reservoir flow model on parallel computers. Ph.D. thesis.

[54] Gai, X., Dean, R., Wheeler, M., and Liu, R. (2003). Coupled Geomechanical and Reservoir Modeling on Parallel Computers. *Society of Petroleum Engineers* .

[55] Gander, M. J. (2015). 50 Years of Time Parallel Time Integration. In Carraro, T., Geiger, M., Körkel, S., and Rannacher, R. (editors), *Multiple Shooting and Time Domain Decomposition Methods*, pages 69–113. Springer International Publishing, Cham. ISBN 978-3-319-23321-5.

[56] Gaspar, F. and Rodrigo, C. (2017). On the fixed-stress split scheme as smoother in multigrid methods for coupling flow and geomechanics. *Comput. Methods. Appl. Mech. Eng 326*(Supplement C), 526–540. doi: 10.1016/j.cma.2017.08.025.

[57] Glowinski, R. and Le Tallec, P. (1989). Augmented Lagrangian and Operator-Splitting Methods in Nonlinear Mechanics. In *Studies in Applied and Numerical Mathematics*, page 302. Society for Industrial and Applied Mathematics. ISBN 978-0-89871-230-8. doi: 10.1137/1.9781611970838. Doi:10.1137/1.9781611970838.

[58] Haga, J., Osnes, H., and Langtangen, H. (2012). A parallel block preconditioner for large-scale poroelasticity with highly heterogeneous material parameters. *Comput. Geosci. 16*(3), 723–734. doi: 10.1007/s10596-012-9284-4.

[59] Haga, J. B., Osnes, H., and Langtangen, H. P. (2012). On the causes of pressure oscillations in low-permeable and low-compressible porous media. *Int. J. Numer. Anal. Meth. Geomech. 36*(12), 1507–1522. doi: 10.1002/nag.1062. Doi: 10.1002/nag.1062.

[60] Hong, Q., Kraus, J., Lymbery, M., and Philo, F. (2019). Conservative discretizations and parameter-robust preconditioners for Biot and multiple-network flux-based poroelasticity models. *Numer Linear Algebra Appl 26*(4), e2242. doi: 10.1002/nla.2242. Doi: 10.1002/nla.2242.

[61] Hong, Q., Kraus, J., Lymbery, M., and Wheeler, M. (2019). Parameter-robust convergence analysis of fixed-stress split iterativemethod for multiple-permeability poroelasticity systems. *arXiv:1812.11809v2* .

[62] Hu, X., Rodrigo, C., Gaspar, F., and Zikatanov, L. (2017). A nonconforming finite element method for the Biot's consolidation model in poroelasticity. *J. Comput. Appl. Math 310*, 143–154. doi: 10.1016/j.cam.2016.06.003. Numerical Algorithms for Scientific and Engineering Applications.

[63] Hyde, E. (2014). Multi-scale parameterisation of static and dynamic continuum porous perfusion models using discrete anatomical data. Ph.D. thesis, Oxford University, UK.

[64] Illiano, D., Pop, I., and Radu, F. (2019). Iterative schemes for surfactant transport in porous media. *arXiv:1906.00224 [math.NA]* .

[65] Jha, B. and Juanes, R. (2007). A locally conservative finite element framework for the simulation of coupled flow and reservoir geomechanics. *Acta Geotechnica 2*(3), 139–153. doi: 10.1007/s11440-007-0033-0.

[66] Keilegavlen, E. and Nordbotten, J. (2017). Finite volume methods for elasticity with weak symmetry. *Int. J. Numer. Meth. Engng 112*(8), 939–962. doi: 10.1002/nme.5538. Doi: 10.1002/nme.5538.

[67] Kim, J. (2018). A new numerically stable sequential algorithm for coupled finite-strain elastoplastic geomechanics and flow. *Comput. Methods. Appl. Mech. Eng. 335*, 538–562. doi: 10.1016/j.cma.2018.02.024.

[68] Kim, J., Tchelepi, H., and Juanes, R. (2011). Stability and convergence of sequential methods for coupled flow and geomechanics: Drained and undrained splits. *Comput. Methods. Appl. Mech. Eng. 200*(23–24), 2094–2116. doi: 10.1016/j.cma.2011.02.011.

[69] Kim, J., Tchelepi, H., and Juanes, R. (2011). Stability and convergence of sequential methods for coupled flow and geomechanics: Fixed-stress and fixed-strain splits. *Comput. Methods. Appl. Mech. Eng. 200*(13–16), 1591–1606. doi: 10.1016/j.cma.2010.12.022.

[70] Kim, J., Tchelepi, H. A., and Juanes, R. (2011). Stability, Accuracy, and Efficiency of Sequential Methods for Coupled Flow and Geomechanics. *SPE Journal 16*(02), 249–262. doi: 10.2118/119084-PA.

[71] Köcher, U. (2015). Variational Space-Time Methods for the Elastic Wave Equation and the Diffusion Equation. Ph.D. thesis, Helmut-Schmidt-Universität.

[72] Köcher, U., Bruchhäuser, M. P., and Bause, M. (2019). Efficient and scalable data structures and algorithms for goal-oriented adaptivity of space–time FEM codes. *SoftwareX 10*, 100239. doi: 10.1016/j.softx.2019.100239.

[73] Korsawe, J. and Starke, G. (2005). A Least-Squares Mixed Finite Element Method for Biot's Consolidation Problem in Porous Media. *SIAM J. Numer. Anal. 43*(1), 318–339. doi: 10.1137/S0036142903432929.

[74] Kumar, K., Almani, T., Singh, G., and Wheeler, M. F. (2016). Multirate undrained splitting for coupled flow and geomechanics in porous media. In *Numerical mathematics and advanced applications—ENUMATH 2015*, volume 112, pages 431–440. Springer. doi: 10.1007/978-3-319-39929-4.

[75] Landau, L. and Lifshitz, E. (1987). Chapter II - Viscous Fluids, pages 44–94. Pergamon. ISBN 978-0-08-033933-7.

[76] Lee, J. (2016). Robust Error Analysis of Coupled Mixed Methods for Biot's Consolidation Model. *Journal of Scientific Computing 69*(2), 610–632. doi: 10.1007/s10915-016-0210-0.

[77] Lee, J. J., Mardal, K.-A., and Winther, R. (2017). Parameter-robust discretization and preconditioning of Biot's consolidation model. *SIAM J. Sci. Comput. 39*(1), A1–A24. doi: 10.1137/15M1029473.

[78] List, F. and Radu, F. (2016). A study on iterative methods for solving Richards' equation. *Comput. Geosci. 20*(2), 341–353. doi: 10.1007/s10596-016-9566-3.

[79] Marsden, J. E. and Hughes, T. J. R. (1994). Mathematical Foundations of Elasticity. Dover Publications Inc., New York. ISBN 0486678652.

[80] Mikelić, A., Wang, B., and Wheeler, M. (2014). Numerical convergence study of iterative coupling for coupled flow and geomechanics. *Comput. Geosci. 18*(3-4), 325–341. doi: 10.1007/s10596-013-9393-8.

[81] Mikelić, A. and Wheeler, M. (2012). Theory of the dynamic Biot-Allard equations and their link to the quasi-static Biot system. *J. Math. Phys. 53*(12), 123702. doi: 10.1063/1.4764887.

[82] Mikelić, A. and Wheeler, M. (2013). Convergence of iterative coupling for coupled flow and geomechanics. *Comput. Geosci. 18*(3-4), 325–341. doi: 10.1007/s10596-012-9318-y.

[83] Mitra, K. and Pop, I. (2019). A modified L-scheme to solve nonlinear diffusion problems. *Comput. Methods. Appl. Mech. Eng. 77*(6), 1722–1738. doi: 10.1016/j.camwa.2018.09.042.

[84] Murad, M. A. and Loula, A. F. D. (1992). Improved accuracy in finite element analysis of Biot's consolidation problem. *Comput. Methods Appl. Mech. Engrg. 95*(3), 359–382. doi: 10.1016/0045-7825(92)90193-N.

[85] Murad, M. A. and Loula, A. F. D. (1994). On stability and convergence of finite element approximations of Biot's consolidation problem. *Internat. J. Numer. Methods Engrg. 37*(4), 645–667. doi: 10.1002/nme.1620370407.

[86] Murad, M. A., Thomée, V., and Loula, A. F. D. (1996). Asymptotic behavior of semidiscrete finite-element approximations of Biot's consolidation problem. *SIAM J. Numer. Anal. 33*(3), 1065–1083. doi: 10.1137/0733052.

[87] Nordbotten, J. (2016). Stable Cell-Centered Finite Volume Discretization for Biot Equations. *SIAM J. Numer. Anal. 54*(2), 942–968. doi: 10.1137/15M1014280.

[88] Nordbotten, J. and Celia, M. (2012). Geological Storage of CO2. John Wiley & Sons. ISBN 978-0-470-88946-6.

[89] Peter, B., Johannes, K., Robert, S., and Mary, W. (2013). Simulation of Flow in Porous Media, Applications in Energy and Environment. DE GRUYTER. ISBN 978-3-11-028221-4.

[90] Pettersen, O. (2012). Coupled Flow and Rock Mechanics Simulation Optimizing the coupling term for faster and accurate computation. *Int. J. Numer. Anal. Model. 9*(3), 628–643.

[91] Phillips, P. and Wheeler, M. (2007). A coupling of mixed and continuous Galerkin finite element methods for poroelasticity I: the continuous in time case. *Comput. Geosci. 11*(2), 131–144. doi: 10.1007/s10596-007-9045-y.

[92] Phillips, P. J. and Wheeler, M. F. (2007). A coupling of mixed and continuous Galerkin finite element methods for poroelasticity. II. The discrete-in-time case. *Comput. Geosci. 11*(2), 145–158. doi: 10.1007/s10596-007-9045-y.

[93] Phillips, P. J. and Wheeler, M. F. (2008). A coupling of mixed and discontinuous Galerkin finite-element methods for poroelasticity. *Comput. Geosci. 12*(4), 417–435. doi: 10.1007/s10596-008-9082-1.

[94] Phoon, K. K., Toh, K. C., Chan, S. H., and Lee, F. H. (2002). An efficient diagonal preconditioner for finite element solution of Biot consolidation equations. *J. Numer. Methods Engrg. 55*, 377–400. doi: 10.1002/nme.500.

[95] Pop, I., Radu, F., and Knabner, P. (2004). Mixed finite elements for the Richards' equation: linearization procedure. *J. Comput. Appl. Math. 168*(1–2), 365–373. doi: 10.1016/j.cam.2003.04.008.

[96] Prevost, J. (2013). One-Way versus Two-Way Coupling in Reservoir-Geomechanical Models, pages 517–526. American Society of Civil Engineers. doi: 10.1061/9780784412992.061.

[97] Radu, F., Borregales, M., Kumar, K., Gaspar, F., and Rodrigo, C. (2018). L-scheme and Newton based solvers for a nonlinear Biot model. *ECCOMAS Proceedings Glasgow*, [E].

[98] Radu, F., Kumar, K., Nordbotten, J., and Pop, I. (2018). A robust, mass conservative scheme for two-phase flow in porous media including Hoelder continuous nonlinearities. *IMA J. Num. Anal. 38*, 884–920. doi: 10.1093/imanum/drx032.

[99] Radu, F., Nordbotten, J., Pop, I., and Kumar, K. (2015). A robust linearization scheme for finite volume based discretizations for simulation of two-phase flow in porous media. *J. Comput. Appl. Math. 289*, 134–141. doi: 10.1016/j.cam.2015.02.051.

[100] Rahrah, M. and Vermolen, F. (2018). Monte Carlo Assessment of the Impact of Oscillatory and Pulsating Boundary Conditions on the Flow Through Porous Media. *Transport in Porous Media 123*(1), 125–146. doi: 10.1007/s11242-018-1028-z.

[101] Reed, M. B. (1984). An investigation of numerical errors in the analysis of consolidation by finite elements. *Internat. J. Numer. Anal. Methods Geomech. 8*, 243—257. doi: 10.1002/nag.1610080304.

[102] Rhebergen, S., Wells, G. N., Katz, R. F., and Wathen, A. J. (2014). Analysis of block preconditioners for models of coupled magma/mantle dynamics. *SIAM J. Sci. Comput. 36*(4), A1960–A1977. doi: 10.1137/130946678.

[103] Rhebergen, S., Wells, G. N., Wathen, A. J., and Katz, R. F. (2015). Three-field block preconditioners for models of coupled magma/mantle dynamics. *SIAM J. Sci. Comput. 37*(5), A2270–A2294. doi: 10.1137/14099718X.

[104] Rodrigo, C., Gaspar, F., Hu, X., and Zikatanov, L. (2016). Stability and monotonicity for some discretizations of the Biot's consolidation model. *Comput. Methods. Appl. Mech. Eng. 298*, 183–204. doi: 10.1016/j.cma.2015.09.019.

[105] Rodrigo, C., Hu, X., Ohm, P., Adler, J., Gaspar, F., and Zikatanov, L. (2018). New stabilized discretizations for poroelasticity and the Stokes' equations. *Comput. Methods. Appl. Mech. Eng. 341*, 467–484. doi: 10.1016/j.cma.2018.07.003.

[106] Samier, P. and De Gennaro, S. (2007). Practical Iterative Coupling of Geomechanics With Reservoir Simulation. doi: 10.2118/106188-MS.

[107] Settari, A. and Mourits, F. (1998). A Coupled Reservoir and Geomechanical Simulation System. *Society of Petroleum Engineers* doi: 10.2118/50939-PA.

[108] Settari, A. and Walters, D. (2001). Advances in Coupled Geomechanical and Reservoir Modeling With Applications to Reservoir Compaction. *Society of Petroleum Engineers 6*(3). doi: 10.2118/74142-PA.

[109] Seus, D., Radu, F., and Rohde, C. (2019). A Linear Domain Decomposition Method for Two-Phase Flow in Porous Media. In *Numerical Mathematics and Advanced Applications ENUMATH 2017*, pages 603–614. Springer International Publishing. doi: 10.1007/978-3-319-96415-7.

[110] Showalter, R. (2000). Diffusion in Poro-Elastic Media. *J. Math Anal. Appl. 251*(1), 310–340. doi: 10.1006/jmaa.2000.7048.

[111] Simoni, L., Secchi, S., and Schrefler, B. A. (2008). Numerical difficulties and computational procedures for thermo-hydro-mechanical coupled problems of saturated porous media. *Computational Mechanics 43*(1), 179–189. doi: 10.1007/s00466-008-0302-2.

[112] Storvik, E., Both, J., Kumar, K., Nordbotten, J., and Radu, F. (2019). On the optimization of the fixed-stress splitting for Biot's equations. *Int. J. Numer. Meth. Eng.* doi: 10.1002/nme.6130.

[113] Sumner, M. (1999). Handbook of Soil Science. Taylor & Francis. ISBN 9780849331367.

[114] Tamellini, L., Formaggia, L., Miglio, E., and Scotti, A. (2012). An Uzawa iterative scheme for the simulation of floating bodies. *Computers & Fluids 68*, 148–158. doi: 10.1016/j.compfluid.2012.07.024.

[115] Temam, R. and Miranville, A. (2005). Mathematical Modeling in Continuum Mechanics. Cambridge. ISBN 9780521617239.

[116] Terzaghi, K. (1943). Wiley: New York. ISBN 9780470172766. doi: 10.1002/9780470172766.ch1.

[117] Trefethen, L. and Bau, D. (2016). Numerical Linear Algebra. Society for Industrial & Applied Mathematics,U.S. ISBN 0898713617.

[118] Turska, E. and Schrefler, B. (1993). On convergence conditions of partitioned solution procedures for consolidation problems. *Comput. Methods. Appl. Mech. Eng. 106*(1), 51–63. doi: 10.1016/0045-7825(93)90184-Y.

[119] Turska, E., Wisniewski, K., and Schrefler, B. (1994). Error propagation of staggered solution procedures for transient problems. *Comput. Methods. Appl. Mech. Eng. 114*(1), 177–188. doi: 10.1016/0045-7825(94)90168-6.

[120] Uzawa, H. and Arrow, K. (1989). Iterative methods for concave programming, pages 135–148. Cambridge University Press. ISBN 9780521361743. doi: 10.1017/CBO9780511664496.011.

[121] Vadacca, L., Colciago, C. M., Micheletti, S., and Scotti, A. (2018). Effects of the Anisotropy of the Fault Zone Permeability on the Timing of Triggered Earthquakes: Insights from 3D-Coupled Fluid Flow and Geomechanical Deformation Modeling. *Pure and Applied Geophysics 175*(12), 4131–4144. doi: 10.1007/s00024-018-1936-4.

[122] Vermeer, P. A. and Verruijt, A. (1981). An accuracy condition for consolidation by finite elements. *Internat. J. Numer. Analyt. Methods Geomech. 5*(1), 1–14. doi: 10.1002/nag.1610050103.

[123] Vignollet, J., May, S., and de Borst, R. (2015). On the numerical integration of isogeometric interface elements. *Internat. J. Numer. Methods Engrg. 102*(11), 1733–1749. doi: 10.1002/nme.4867.

[124] Vignollet, J., May, S., and de Borst, R. (2016). Isogeometric analysis of fluid-saturated porous media including flow in the cracks. *Internat. J. Numer. Methods Engrg. 108*(9), 990–1006. doi: 10.1002/nme.5242.

[125] Wan, J. (2003). Stabilized Finite Element Methods for Coupled Geomechanics and Multiphase Flow. Ph.D. thesis, Stanford University, Stanford, California.

[126] White, J., Castelletto, N., and Tchelepi, H. (2016). Block-partitioned solvers for coupled poromechanics: A unified framework. *Comput. Methods. Appl. Mech. Eng. 303*, 55–74.

[127] White, J. A. and Borja, R. I. (2011). Block-preconditioned Newton-Krylov solvers for fully coupled flow and geomechanics. *Comput. Geosci. 15*(4), 647–659. doi: 10.1007/s10596-011-9233-7.

[128] Yi, S.-Y. and Bean, M. (2016). Iteratively coupled solution strategies for a four-field mixed finite element method for poroelasticity. *International Journal for Numerical and Analytical Methods in Geomechanics 41*(2), 159–179. doi: 10.1002/nag.2538.

[129] Zakerzadeh, R. and Zunino, P. (2019). A computational framework for fluid–porous structure interaction with large structural deformation. *Meccanica 54*(1-2), 101–121. doi: 10.1007/s11012-018-00932-x.

[130] Zienkiewicz, O., Paul, D., and Chan, A. (1988). Unconditionally stable staggered solution procedure for soil-pore fluid interaction problems. *Int. J. Numer. Meth. Engng. 26*(5), 1039–1055. doi: 10.1002/nme.1620260504.

[131] Zienkiewicz, O. C. and Shiomi, T. (1984). Dynamic behaviour of saturated porous media; the generalized Biot formulation and its numerical solution. *Internat. J. Numer. Anal. Methods Geomech. 8*, 71—96. doi: 10.1002/nag.1610080106.

[132] Zulehner, W. (2002). Analysis of Iterative Methods for Saddle Point Problems: A Unified Approach *71*(238), 479–505.

Part II

Included papers

Paper C

Iterative solvers for Biot model under small and large deformation

M. Borregales, K.Kumar, J.M. Nordbotten and F.A. Radu. *Arxiv:1905.12996 2019*

Iterative solvers for Biot model under small and large deformation

Manuel Borregales* Kundan Kumar†
Jan Martin Nordbotten* Florin Adrian Radu*

30/05/2019

Abstract

We consider L-scheme and Newton based solvers for Biot model under small or large deformation. The mechanical deformation follows the Saint Venant-Kirchoff constitutive law. Further, the fluid compressibility is assumed to be nonlinear. A Lagrangian frame of reference is used to keep track of the deformation. We perform an implicit discretization in time (backward Euler) and propose two linearization schemes for solving the nonlinear problems appearing within each time step: Newton's method and L-scheme. The linearizations are used monolithically or in combination with a splitting algorithm. The resulting schemes can be applied for any spatial discretization. The convergences of all schemes are shown analytically for cases under small deformation. Illustrative numerical examples are presented to confirm the applicability of the schemes, in particular, for large deformation. ***Index terms***— Large deformation, Biot's Model, L-scheme, Newton's Method, Poroelasticity

*Department of Mathematics, University of Bergen, PO Box 7800, Bergen, Norway; Emails: {Manuel.Borregales, Jan.Nordbotten, Florin.Radu}@uib.no

†Department of Mathematics and Computer Science, Karlstad University, 651 88 Karlstad, Sweden; Email: Kundan.Kumar@kau.se

1 Introduction

The coupling of flow and mechanics in a porous medium, typically referred to as poromechanics, plays a crucial role in many socially relevant applications. These include geothermal energy extraction, energy storage in the subsurface, CO_2 sequestration, and understanding of biological tissues. The increased role played by computing in the development and optimisation of (industrial) technologies for these applications implies the need for improved mathematical models in poromechanics and robust numerical solvers for them.

The most common mathematical model for coupled flow and mechanics in porous media is the linear, quasi-stationary Biot model [8, 9, 10, 52]. The model consists of two coupled partial differential equations, representing balance of forces for the mechanics and conservation of mass and momentum for (single-phase) flow in porous media.

In terms of modelling, Biot's model has been extended to unsaturated flow [14, 37], multiphase flow [27, 28, 34, 36, 48], thermo-poro-elasticity [19], and reactive transport in porous media [33, 49], where nonlinearities arise in the flow model, specifically in the diffusion term, the time derivative term and/or in Biot's coupling term. The mechanics model can also be extended to the elasto-plastic [3, 56], the fracture propagation [35] and the hyperelasticity [20, 21], where the nonlinearities appear in the constitutive law of the material, in the compatibility condition and/or the conservation of momentum equation. Furthermore, elastodynamics or non-stationary Biot, i.e. Biot-Allard model [38], includes a convolution in the coupling term of both mechanics and flow equations. In this paper, we are going to explore a general case that allows large deformations. The mechanical deformation follows the Saint Venant-Kirchoff constitutive law and the fluid compressibility in the fluid equation is assumed to be nonlinear. This model formulation is needed to later consider extensions of Biot's model to plasticity, more general hyperelastic materials, and elastodynamics.

Finding closed-form solutions for coupled problems is very difficult, and commonly based on various simplifications. We, therefore, resort to numerical approximations. In general, there are two approaches to solve such problems, the fully coupled and the weakly coupled scheme. In general the fully coupled schemes for fluid potential and mechanical deformation are stable, have excellent convergence properties, and ensure that the numerical solution is consistent with the underlying continuous differential equations

[29, 55]. Despite obvious advantages, the monolithic solver for the fully coupled problem are more difficult to implement, and have difficulties solving the resulting linear system, particularly in the context of existing legacy codes for separate physics. In the weakly coupled approach, while marching in time, we time-lag the flow problem (or the mechanics), thereby fully decoupling the two problems. Due to the complexities associated with the fully coupled scheme, the industry standard remains to use weakly coupled or iteratively coupled approaches [18, 42, 51, 59]. An iteratively coupled approach takes somewhat of a middle path; at each time step, it decouples the flow and mechanics, but iterates so that the convergence is achieved. Weakly coupled schemes, wherein there are not iterations within time step, have in particular been questioned in previous works [17, 22, 42, 45]; they have been shown to lack robustness and even convergence, if not properly designed. In order to ensure the robustness and accuracy of the resulting computations, it is therefore essential to understand the efficiency, stability, and convergence of iterative coupling schemes, in particular in the presence of nonlinearities.

In this work, we present monolithic and splitting approaches for solving this nonlinear system, that is, nonlinear compressibility and the Saint Venant-Kirchoff constitutive law for stress-strain. Moreover, we rigorously study the convergence of our schemes, including the Newton based ones, under the assumption of small deformations. As for splitting approach, we use the undrained split method, see [31, 39]. We use linear conformal Galerkin elements for the discretization of the mechanics equation and mixed finite elements for the flow equation [7, 23, 30, 43, 58]. Precisely, the lowest order Raviart-Thomas elements are used [16]. We expect, however, that the solution strategy discussed herein will be applicable to other combinations of spatial discretizations such as those discussed in [40, 50] and the references therein. Backward Euler is used for the temporal discretization.

To summarise, the new contributions of this paper are

- We propose Newton and L-scheme based monolithic and splitting schemes for solving the Biot model under small or large deformation.
- The convergence analysis of all schemes is shown rigorously under the assumption of small deformations.
- We provide a benchmark for the convergence of splitting algorithms for a general nonlinear Biot model that includes large deformations.

We mention some relevant works in this direction. For the convergence analysis of the undrained split method applied to the linear Biot model, we refer to [5, 6, 12, 24, 25, 39]. For a discussion on the stabilization/tuning parameter used in the undrained split approach, we refer to [12, 15]. A theoretical investigation on the optimal choice for this parameter is performed in [53]. The linearization is based on either Newton's method, or the L-scheme [37, 44, 48] or a combination of them [14, 37]. For monolithic and splitting schemes based solely on L-scheme, we refer to [11]. Multirate time discretizations or higher order space-time Galerkin method has also been proposed for the linear Biot model in [1] and [6], respectively.

The paper is structured as follows. In the next section, we present the mathematical model. In Section 3, we propose four iterative schemes. Section 4 shows the analysis of iterative schemes under the assumption of small deformations. Numerical results are presented in Section 5 followed by the conclusion in Section 6.

2 Governing equations

We consider a fluid flow problem in a poroelastic bounded reference domain $\Omega \subset \mathbb{R}^d$, $d \in \{2, 3\}$ under large deformation. A Lagrangian frame of reference is used to keep track of the invertible transformation $x := \{x(X,t) = X + \mathbf{u}(X,t) : X \in \Omega \to x \in \Omega_t\}$, where Ω_t is the deformed domain at time t and $\mathbf{u}$ represents the deformation field. The gradient of the transformation and its determinant are given by $\mathbf{F} = \nabla\, x(X,t)$ and $J = \det(\mathbf{F})$. All differentials are with respect to the undeformed coordinates X, unless otherwise stated.

We will now write the conservation of momentum and mass equation in Ω. The conservation of momentum represents the balance between the first Piola-Kirchhoff poroelastic stress $\mathbf{\Pi}$ in Ω and the forces acting on Ω_t, and is given by

$$-\nabla \cdot \mathbf{\Pi} = \rho_b \mathbf{g}, \tag{1}$$

where $\rho_b = J\varrho_b$ is the bulk density in Ω, ϱ_b is the bulk density in Ω_t and $\mathbf{g}$ is gravity.

We exploit the relation $\mathbf{\Pi} = \mathbf{F}\mathbf{\Sigma}$ since the constitutive laws are developed for the second Piola-Kirchhoff poroelastic stress $\mathbf{\Sigma}$. This stress tensor is composed of the effective mechanical stress $\mathbf{\Sigma}^{eff}$ and the pore pressure p by

the following relation

$$\boldsymbol{\Sigma} = \boldsymbol{\Sigma}^{eff} - J\mathbf{F}^{-1}\mathbf{F}^{\top}p,$$

where $J\mathbf{F}^{-1}\mathbf{F}^{\top}$ ensures that pressure p exerts an isotropic stress in Ω_t. We assume an isotropic poroelastic material with constant shear modulus μ and a nonlinear function of the volumetric strain $\mathfrak{c}(\cdot)$ [11, 54]. The effective stress is given by Saint Venant-Kirchhoff constitutive law: $\boldsymbol{\Sigma}^{\mathbf{eff}} = \mathbf{2}\mu\mathbf{E} + \mathfrak{c}\left(\mathrm{tr}(\mathbf{E})\right)$, where the Green strain tensor $\mathbf{E}$ is defined by
$\mathbf{E} = \frac{1}{2}\left(\nabla\mathbf{u} + \nabla^{\top}\mathbf{u} + (\nabla\mathbf{u})^{\top}\nabla\mathbf{u}\right)$.

The conservation of fluid mass is given by

$$\dot{\Gamma} + \nabla\cdot\mathbf{q} = S_f. \tag{2}$$

We consider a fluid mass $\Gamma = J\rho_f\phi$ of a slightly compressible fluid, where ϕ is the porosity and ρ_f the fluid density and S_f the source term in Ω respectively. The time derivative of the fluid content $\dot{\Gamma} = \dot{\Gamma}(\mathbf{u}, p)$ is considered to be a function of the pressure and the pore volume change due to the deformation field. We consider Darcy's law

$$\mathbf{q} = -\mathbf{K}(\mathbf{u})\left(\nabla p - \rho_f\mathbf{g}_0\right), \tag{3}$$

where the flux variable $\mathbf{q}$ is the first Piola transform of the corresponding flux variable in Ω_t, $\mathbf{K} = J\mathbf{F}^{-1}\mathbf{k}\mathbf{F}^{-\top}$ is the corresponding transformation of the mobility tensor $\mathbf{k}$ in Ω_t and $\Upsilon = \mathbf{F}^{\top}\mathbf{g}$. Finally, the general nonlinear Biot model considered in this paper reads as:

Find $(\mathbf{u}, \mathbf{q}, p)$ such that

$$\begin{aligned} -\nabla\cdot\boldsymbol{\Pi}(\nabla\mathbf{u}, p) &= \varrho_b\mathbf{g}, && \text{in } \Omega\times]0,T[,\\ \mathbf{q} &= -\mathbf{K}(\mathbf{u})\left(\nabla p - \rho_f\Upsilon\right), && \text{in } \Omega\times]0,T[,\\ \dot{\Gamma}(\mathbf{u}, p) + \nabla\cdot\mathbf{q} &= S_f, && \text{in } \Omega\times]0,T[. \end{aligned} \tag{4}$$

To complete the model we consider Dirichlet boundary conditions (BC) and initial conditions given by $(\mathbf{u}_0, p_0)$ such that $\Gamma(\mathbf{u}_0, p_0) = \Gamma_0$ and $\boldsymbol{\Pi}(\mathbf{u}_0, p_0) = \boldsymbol{\Pi}_0$ at time $t = 0$. The functions Γ_0 and $\boldsymbol{\Pi}_0$ are supposed to be given (and to be sufficiently regular).

In practice, the initial data $\mathbf{u}_0$ and p_0 are not independent and can be obtained by solving the flow equation for p_0 and then solving the mechanics equation for getting $\mathbf{u}_0$.

3 Iterative schemes

In this section, we present several monolithic and splitting iterative schemes for solving Eqs. (4). First, we propose the Newton method which is well known for having quadratic convergence. Secondly, we combine the Newton method with a stabilized splitting scheme based on the undrained split method. Finally, for the third and fourth schemes, we propose monolithic and splitting L-schemes. The iterative schemes will be written using an incremental formulation. In this regard, we introduce naturally defined residuals for the nonlinear Eqs. (4).

$$\begin{aligned}
\mathcal{F}_{\text{mech}}(\mathbf{u}, p) &= -\nabla \cdot \boldsymbol{\Pi}\left(\nabla \mathbf{u}, p\right) - \rho_b \mathbf{g}, \\
\mathcal{F}_{\text{darcy}}(\mathbf{u}, p) &= \mathbf{q} + \mathbf{K}(\mathbf{u})\left(\nabla p - \rho_f \Upsilon\right), \\
\mathcal{F}_{\text{mass}}(\mathbf{u}, p) &= \dot{\Gamma}(\mathbf{u}, p) + \nabla \cdot \mathbf{q} - S_f.
\end{aligned} \tag{5}$$

We will denote by $\delta(\cdot)^i = (\cdot)^i - (\cdot)^{i-1}$ the incremental operator, i the incremental counter, $\partial_{(\cdot)}$ the partial derivative operator respect to $(\cdot)$.

3.1 A monolithic Newton solver

The Newton method is usually the first choice of the linearization methods due to its quadratic convergence. However, the convergence is local and it requires relatively small time steps to ensure the quadratic convergence [47]. The method starts by using initial solution $(\mathbf{u}^0, \mathbf{q}^0, p^0)$, solves for $(\delta\mathbf{u}^i, \delta\mathbf{q}^i, \delta p^i)$ satisfying

$$\begin{aligned}
-\nabla \cdot \left(\partial_{\mathbf{u}} \boldsymbol{\Pi}\left(\nabla \mathbf{u}^{i-1}, p^{i-1}\right) \nabla \delta \mathbf{u}^i - \partial_p \boldsymbol{\Pi}\left(\nabla \mathbf{u}^{i-1}, p^{i-1}\right) \delta p^i\right) &= -\mathcal{F}_{mech}(\mathbf{u}^{i-1}, p^{i-1}), \\
\delta \mathbf{q}^i + \mathbf{K}(\mathbf{u}^{i-1}) \nabla \delta p^{i-1} + \partial_{\mathbf{u}} \mathbf{K}(\mathbf{u}^{i-1}) \nabla p^{i-1} \delta \mathbf{u}^i &= -\mathcal{F}_{darcy}(\mathbf{u}^{i-1}, p^{i-1}), \\
\partial_p \dot{\Gamma}(\mathbf{u}^{i-1}, p^{i-1}) \delta p^i + \partial_{\mathbf{u}} \dot{\Gamma}(\mathbf{u}^{i-1}, p^{i-1}) \delta \mathbf{u}^i + \nabla \cdot \delta \mathbf{q}^i &= -\mathcal{F}_{mass}(\mathbf{u}^{i-1}, p^{i-1}),
\end{aligned} \tag{6}$$

and finally updates the variables

$$\left(\mathbf{u}^i, \mathbf{q}^i, p^i\right) = \left(\mathbf{u}^{i-1}, \mathbf{q}^{i-1}, p^{i-1}\right) + \left(\delta\mathbf{u}^i, \delta\mathbf{q}^i, \delta p^i\right).$$

3.2 A splitting Newton solver

The splitting Newton method combines a splitting method with the Newton linearization. We introduce a stabilization parameter $L_s \geq 0$ to stabilize the

mechanics equation. The precise condition on L_s to ensure convergence is shown in Theorem 2. The method consists on two steps: starting with the initial condition $(\mathbf{u}^0, \mathbf{q}^0, p^0)$:

Step 1: solve for $(\delta\mathbf{q}^i, \delta p^i)$

$$\begin{aligned} \delta\mathbf{q}^i + \mathbf{K}(\mathbf{u}^{i-1})\nabla\delta p^{i-1} &= -\mathcal{F}_{darcy}(\mathbf{u}^{i-1}, p^{i-1}), \\ \partial_p\dot{\Gamma}(\mathbf{u}^{i-1}, p^{i-1})\delta p^i + \nabla\cdot\delta\mathbf{q}^i &= -\mathcal{F}_{mass}(\mathbf{u}^{i-1}, p^{i-1}), \end{aligned} \tag{7}$$

and update the variables

$$\left(\mathbf{q}^i, p^i\right) = \left(\mathbf{q}^{i-1}, p^{i-1}\right) + \left(\delta\mathbf{q}^i, \delta p^i\right).$$

Step 2: solve for $\delta\mathbf{u}^i$ satisfying

$$-\nabla\cdot\left(\partial_{\mathbf{u}}\mathbf{\Pi}\left(\nabla\mathbf{u}^{i-1}, p^i\right)\nabla\delta\mathbf{u}^i - L_s(\nabla\cdot\delta\mathbf{u}^i)\,\mathbf{I}\right) = -\mathcal{F}_{mech}(\mathbf{u}^{i-1}, p^i), \tag{8}$$

and update the variable

$$\mathbf{u}^i = \mathbf{u}^{i-1} + \delta\mathbf{u}^i.$$

The stability of the scheme is controlled by L_s as it is shown in [47].

3.3 A monolithic L-scheme

The L-scheme can be interpreted as either a stabilized Picard method or a quasi-Newton method. This scheme is robust but only linearly convergent. Moreover, it can be applied to non-smooth but monotonically increasing nonlinearities. For example, for the case of Hölder continuous (not Lipschitz) nonlinearities we refer to [13]. As it is a fixed point scheme, it can be speeded up by using the Anderson acceleration [2, 15]. To summarize, the main advantages of the L-scheme are:

- It does not involve computation of derivatives.
- The arising linear systems are well-conditioned.
- It can be applied to non-smooth nonlinearities.
- It is easy to understand and implement.

A monolithic L-scheme requires three constant tensors $\mathbf{L_u},\ \mathbf{L}_p,\ \mathbf{L_q} \in \mathbb{R}^{d\times d}$ and two positive constants L_p and $L_{\mathbf{u}}$ as linearization parameters. A practical choice of the linearization parameters will be discussed in the numerical section. We refer to [11, 22] for a discussion regarding the best choice for the linearization parameters L_p and $L_{\mathbf{u}}$.

The method starts with the given initial solution $(\mathbf{u}^0, \mathbf{q}^0, p^0)$ and solve for $(\delta\mathbf{u}^i, \delta\mathbf{q}^i, \delta p^i)$

$$\begin{aligned} -\nabla\cdot\mathbf{L_u}\nabla\delta\mathbf{u}^i - \nabla\cdot\mathbf{L}_p\delta p^i &= -\mathcal{F}_{mech}(\mathbf{u}^{i-1}, p^{i-1}),\\ \delta\mathbf{q}^i + \mathbf{K}(\mathbf{u}^{i-1})\nabla\delta p^i + \mathbf{L_q}\delta\mathbf{u}^i &= -\mathcal{F}_{darcy}(\mathbf{u}^{i-1}, p^{i-1}),\\ L_p\delta p^i + L_{\mathbf{u}}\delta\mathbf{u}^i + \nabla\cdot\delta\mathbf{q}^i &= -\mathcal{F}_{mass}(\mathbf{u}^{i-1}, p^{i-1}), \end{aligned} \tag{9}$$

and then update the variables

$$\left(\mathbf{u}^i, \mathbf{q}^i, p^i\right) = \left(\mathbf{u}^{i-1}, \mathbf{q}^{i-1}, p^{i-1}\right) + \left(\delta\mathbf{u}^i, \delta\mathbf{q}^i, \delta p^i\right).$$

3.4 A splitting L-scheme

The splitting scheme requires less linearization terms: two constants $\mathbf{L_u} \in \mathbb{R}^{d\times d}$, $L_p \geq 0$ and a positive stabilisation term L_s. This makes it suitable for quick implementation since there is no need to calculate any Jacobian. The method is split in two steps, given initial solution $(\mathbf{u}^0, \mathbf{q}^0, p^0)$:

Step 1: solve for $(\delta\mathbf{q}^i, \delta p^i)$

$$\begin{aligned} \delta\mathbf{q}^i + \mathbf{K}(\mathbf{u}^{i-1})\nabla\delta p^i &= -\mathcal{F}_{darcy}(\mathbf{u}^{i-1}, p^{i-1}),\\ L_p\delta p^i + \nabla\cdot\delta\mathbf{q}^i &= -\mathcal{F}_{mass}(\mathbf{u}^{i-1}, p^{i-1}), \end{aligned} \tag{10}$$

update the variables

$$\left(\mathbf{q}^i, p^i\right) = \left(\mathbf{q}^{i-1}, p^{i-1}\right) + \left(\delta\mathbf{q}^i, \delta p^i\right).$$

Step 2: solve for $\delta\mathbf{u}^i$

$$-\nabla\cdot\left(\mathbf{L_u}\nabla\delta\mathbf{u}^i + L_s(\nabla\delta\cdot\mathbf{u}^i)\ \mathbf{I}\right) = -\mathcal{F}_{mech}(\mathbf{u}^{i-1}, p^i), \tag{11}$$

and then update the variables

$$\mathbf{u}^i = \mathbf{u}^{i-1} + \delta\mathbf{u}^i.$$

4 The Biot model under small deformations

The convergence analysis of the iterative schemes proposed cannot be addressed with standard techniques [11, 15, 14, 37, 39]. This is due to the nonlinearities being non-monotone. Nevertheless, a rigorous analysis can be performed for the case of small deformations. Accordingly, we assume the porous medium to be under small deformation and present the convergence of the iterative schemes proposed in the previous section.

Under small deformation, the different between Ω_t and Ω can be neglected. The gradient of the transformation is approximated by $\mathbf{F} \approx \mathbf{I}$ and the determinant of the transformation by $J \approx 1$. Additionally, the Green strain tensor $\mathbf{E}$ can be approximated by the infinitesimal strain tensor $\mathbf{E} \approx \varepsilon = \frac{1}{2}\left(\nabla \mathbf{u} + (\nabla \mathbf{u})^\top\right)$. Then, the poroelastic stress tensor can be expressed by

$$\mathbf{\Pi}(\mathbf{u}, p) = \sigma(\mathbf{u}, p) = 2\mu\varepsilon(\nabla \mathbf{u}) + \mathfrak{c}(\mathrm{tr}(\varepsilon(\nabla \mathbf{u}))) - \alpha p \mathbf{I}, \tag{12}$$

where α is the Biot constant. The mobility tensor is considered isotropic $\mathbf{K}(\mathbf{u}, p) = k\mathbf{I}$, but the results of the convergence analysis can be extended without difficulties to a more general anisotropic case. Additionally, the time derivative of the volumetric deformation is approximated by $\dot{J} \approx \nabla \cdot \dot{\mathbf{u}}$. In this regard the fluid mass can be expressed as

$$\Gamma(\mathbf{u}, p) = \Gamma_0 + c_f\left(\mathfrak{b}(p) - \mathfrak{b}(p_0)\right) + \alpha \nabla \cdot (\mathbf{u} - \mathbf{u}_0), \tag{13}$$

where the relative density $\mathfrak{b}(\cdot)$ is a nonlinear function of the pressure p. The variational formulation for the Biot model, under small deformation, reads as follows:

For each $t \in (0, T]$, find $\mathbf{u}(t) \in \left(H_0^1(\Omega)\right)^d$, $\mathbf{q} \in H^1(\mathrm{div}, \Omega)$ and $p(t) \in L^2(\Omega)$ such that there holds

$$\begin{aligned}
(\varepsilon(\mathbf{u}), \varepsilon(\mathbf{v})) + (\mathfrak{c}(\nabla \cdot \mathbf{u}) - \alpha p, \nabla \cdot \mathbf{v}) &= (\rho_b \mathbf{g}, \mathbf{v}), \quad \forall \mathbf{v} \in \left(H(\Omega)\right)^d, \\
(\mathbf{K}^{-1}\mathbf{q}, \mathbf{z}) - (p, \nabla \cdot \mathbf{z}) &= (\rho_f \mathbf{g}, \mathbf{z}), \quad \forall \mathbf{z} \in H^1(\mathrm{div}, \Omega), \\
\left(\dot{\mathfrak{b}}(p)) + \alpha \nabla \cdot \dot{\mathbf{u}}, w\right) + \tau\left(\nabla \cdot \mathbf{q}, w\right) &= \tau\left(S_f, w\right), \quad \forall w \in L^2(\Omega),
\end{aligned} \tag{14}$$

with the initial condition

$$(\mathfrak{b}(p_0)) + \alpha \nabla \cdot \mathbf{u}_0, w) = 0, \ \forall w \in L^2(\Omega). \tag{15}$$

In the above, we have used the standard notations. We denote by $L^2(\Omega)$ the space of square integrable functions and by $H^1(\Omega)$ the Sobolev space $H^1(\Omega) = \{v \in L^2(\Omega)\,;\, \nabla v \in L^2(\Omega)^d\}$. Furthermore, $H^1_0(\Omega)$ will be the space of functions in $H^1(\Omega)$ vanishing on $\partial\Omega$ and $H(\mathrm{div};\Omega)$ the space of vector valued function having all the components and the divergence in $L^2(\Omega)$. As usual we denote by $(\cdot,\cdot)$ the inner product in $L^2(\Omega)$, and by $||\cdot||$ its associated norm.

Next, we make structural assumptions on the nonlinearities:

(A1) $\mathfrak{c}$, $\mathfrak{b} : \mathbb{R} \to \mathbb{R}$ differentiable with $\mathfrak{c}'$ and $\mathfrak{b}'$ Lipschitz continuous.

(A2) There exists a constant $\alpha_{\mathfrak{c}}$ such that $\mathfrak{c}'(\xi) > \alpha_{\mathfrak{c}}$, $\forall\, \xi \in \mathbb{R}$.

(A3) There exists a constant $\alpha_{\mathfrak{b}}$ such that $\mathfrak{b}'(\xi) > \alpha_{\mathfrak{b}}$, $\forall\, \xi \in \mathbb{R}$.

(A4) There exists constant $k_m > 0$ and k_M such that $k_m \leq k(\vec{\xi}) \leq k_M$, $\forall \vec{\xi} \in \Omega$.

For the discretization of problem (14) we use conformal Galerkin finite elements for the displacement variable and mixed finite elements for the flow [23, 43]. More precisely, we use linear elements for the displacement and lowest order Raviart-Thomas elements [16] for the flow. Backward Euler is used for the temporal discretization.

Let $\Omega = \cup_{K\in\mathcal{T}_h} K$ be a regular decomposition of Ω into d-simplices. We denote by h the mesh size. The discrete spaces are given by

$$\begin{aligned}
\mathbf{V}_h &:= \{\mathbf{v}_h \in H^1(\Omega)^d\,;\, \mathbf{v}_{h|K} \in \mathbb{P}_1^d\,,\, \forall K \in \mathcal{T}_h\},\\
W_h &:= \{w_h \in L^2(\Omega)\,;\, w_{h|K} \in \mathbb{P}_0\,,\, \forall K \in \mathcal{T}_h\},\\
\mathbf{Z}_h &:= \{\vec{z}_h \in H(\mathrm{div};\Omega)\,;\, \vec{z}_{h|K}(\vec{x}) = \vec{a} + b\vec{x},\, \vec{a} \in \mathbb{R}^d,\, b \in \mathbb{R},\, \forall K \in \mathcal{T}_h\},
\end{aligned}$$

where $\mathbb{P}_0, \mathbb{P}_1$ denote the spaces of constant functions and of linear polynomials, respectively. For $N \in \mathbb{N}$, we discretize the time interval uniformly and define the time step $\tau = \frac{T}{N}$ and $t_n = n\tau$. We use the index n for the primary variable $\mathbf{u}^n$, $\mathbf{q}^n$ and p^n at corresponding time step t_n. In this way, the fully discrete weak problem reads:

For $n \geq 1$ and given $\left(\mathbf{u}_h^{n-1}, \mathbf{q}_h^{n-1}, p_h^{n-1}\right)$ find $(\mathbf{u}_h^n, \mathbf{q}_h^n, p_h^n) \in (\mathbf{V}_h, \mathbf{Z}_h, W_h)$, such that

$$
\begin{aligned}
(\varepsilon(\mathbf{u}_h^n), \varepsilon(\mathbf{v}_h)) + (\mathfrak{c}(\nabla \cdot \mathbf{u}_h^n), \nabla \cdot \mathbf{v}_h) - \alpha\,(p_h^n, \nabla \cdot \mathbf{v}_h) &= (\rho_b \mathbf{g}, \mathbf{v}_h), \\
(\mathbf{K}^{-1}\mathbf{q}_h^n, \mathbf{z}_h) - (p_h^n, \nabla \cdot \mathbf{z_h}) &= (\rho_f \mathbf{g}, \mathbf{z}_h)\,, \\
\big(\mathfrak{b}(p_h^n) - \mathfrak{b}(p_h^{n-1}), w_h\big) + \alpha\,\big(\nabla \cdot (\mathbf{u}_h^n - \mathbf{u}_h^{n-1}), w_h\big) & \\
+\tau\,(\nabla \cdot \mathbf{q}_h^n, \nabla w_h) &= \tau(S_f, w_h),
\end{aligned}
\tag{16}
$$

for all $(\mathbf{v}_h, \mathbf{z}_h, w_h) \in (\mathbf{V}_h, \mathbf{Z}_h, W_h)$.

Following the notation previously introduced, we denote by n the time level, whereas i will refer to the iteration number of the Newton method. We further denote the approximate solution of the linearized problem (16) by $(\mathbf{u}_h^{n,i}, \mathbf{q}_h^{n,i}, p_h^{n,i})$. At this stage we can introduce the notations

$$
\begin{aligned}
\mathbf{e}_{\mathbf{u}}^{n,i} &= \mathbf{u}_h^{n,i} - \mathbf{u}_h^n, \\
\mathbf{e}_{\mathbf{q}}^{n,i} &= \mathbf{q}_h^{n,i} - \mathbf{q}_h^n, \\
e_p^{n,i} &= p_h^{n,i} - p_h^n.
\end{aligned}
$$

These will be used subsequently in the convergence analysis of the monolithic Newton method and the alternate version. For the monolithic and splitting L-scheme the convergence analysis can be found in [11].

4.1 Convergence analysis of the monolithic Newton method

In this section, we analyse the monolithic Newton method introduced in Section 3 used for solving the simplified nonlinear Biot model given in (16). As we have previously stated, we perform the analysis for the case of small deformation. Here we present a variational formulation of the scheme and demonstrate its quadratic convergence in a rigorous manner. The Newton scheme reads as follows:

For $i = 1, 2, \ldots$ solve

$$
\begin{aligned}
\left(\varepsilon(\mathbf{u}_h^{n,i}),\varepsilon(\mathbf{v}_h)\right)+\left(\mathfrak{c}(\nabla\cdot\mathbf{u}_h^{n,i-1})+\mathfrak{c}'(\nabla\cdot\mathbf{u}_h^{n,i-1})\nabla\cdot\delta\mathbf{u}_h^{n,i},\nabla\cdot\mathbf{v}_h\right)\\
-\left(\alpha p_h^{n,i},\nabla\cdot\mathbf{v}_h\right)=(\rho_b\mathbf{g},\mathbf{v}_h),\\
\left(\mathbf{K}^{-1}\mathbf{q}_h^{n,i},\mathbf{z}_h\right)-\left(p_h^{n,i},\nabla\cdot\mathbf{z_h}\right)=(\rho_f\mathbf{g},\mathbf{z}_h)\,,\\
\left(\mathfrak{b}(p_h^{n,i-1})+\mathfrak{b}'(p_h^{n,i-1})\delta p_h^{n,i}-\mathfrak{b}(p_h^{n-1}),w_h\right)+\left(\alpha\nabla\cdot(\mathbf{u}_h^{n,i}-\mathbf{u}_h^{n-1}),w_h\right)\\
+\tau\left(\nabla\cdot\mathbf{q}_h^{n,i},\nabla w_h\right)=\tau(S_f,w_h),
\end{aligned}
\tag{17}
$$

$\forall\,(\mathbf{v}_h,\mathbf{z}_h,w_h)\in(\mathbf{V}_h,\mathbf{Z}_h,W_h)$, where the initial approximation $(\mathbf{u}_h^{n,0}\mathbf{q}_h^{n,0},p_h^{n,0})$ is taken as the solution at the previous time step, that is $(\mathbf{u}_h^{n-1},\mathbf{q}_h^{n-1},p_h^{n-1})$.

In order to prove the convergence of the considered Newton method, the following lemmas will be used.

Lemma 1. *Let $\{x_n\}_{n\geq 0}$ be a sequence of real positive number satisfying*

$$
x_n\leq ax_{n-1}^2+bx_{n-1}\ \forall n\geq 1, \tag{18}
$$

where $a,b\geq 0$. Assuming that

$$
ax_0^2+b\leq 1
$$

holds, then the sequence $\{x_n\}_{n\geq 0}$ converges to zero.

Proof. The result can be shown by induction, see page 52 in [46] for more details. □

Lemma 2. *If $f:\mathbb{R}\to\mathbb{R}$ is differentiable and f' is Lipschitz continuous, then there holds*

$$
|f(x)-f(y)+f'(y)(y-x)|\leq\frac{L_{f'}}{2}|y-x|^2,\quad\forall\,x,y\in\mathbb{R}.
$$

Proof. See page 350 in [32], for example. □

Next, the following result provides the quadratic convergence of the Newton method (17) for τ sufficiently small.

Theorem 1. *Assuming (A1)-(A4), the Newton method in* (17) *converges quadratically if $\tau=O(h^d)$.*

Proof. By subtracting equations (16) from (17), taking as test functions $\mathbf{e}_{\mathbf{u}}^{n,i}$, $\mathbf{e}_{\mathbf{q}}^{n,i}$ and $e_p^{n,i}$ and rearranging some terms to the right hand side we obtain,

$$\begin{aligned}
&\left(\varepsilon(\mathbf{e}_{\mathbf{u}}^{n,i}), \varepsilon(\mathbf{e}_{\mathbf{u}}^{n,i})\right) + \left(\mathfrak{c}'(\nabla\cdot\mathbf{u}_h^{n,i-1})\nabla\cdot\mathbf{e}_{\mathbf{u}}^{n,i}, \nabla\cdot\mathbf{e}_{\mathbf{u}}^{n,i}\right) - \alpha\left(e_p^{n,i}, \nabla\cdot\mathbf{e}_{\mathbf{u}}^{n,i}\right) \\
&\quad = \left(\mathfrak{c}(\nabla\cdot\mathbf{u}_h^{n}) - \mathfrak{c}(\nabla\cdot\mathbf{u}_h^{n,i-1}) + \mathfrak{c}'(\nabla\cdot\mathbf{u}_h^{n,i-1})\nabla\cdot\mathbf{e}_{\mathbf{u}}^{n,i-1}, \nabla\cdot\mathbf{e}_{\mathbf{u}}^{n,i}\right), \quad (19)\\
&\qquad \left(\mathbf{K}^{-1}\mathbf{e}_{\mathbf{q}}^{n,i}, \mathbf{e}_{\mathbf{q}}^{n,i}\right) - \left(e_p^{n,i}, \nabla\cdot\mathbf{e}_{\mathbf{q}}^{n,i}\right) = 0, \quad (20)\\
&\left(\mathfrak{b}'(p_h^{n,i-1})\left(p_h^{n,i} - p_h^{n}\right), e_p^{n,i}\right) + \alpha\left(\nabla\cdot\mathbf{e}_{\mathbf{u}}^{n,i}, e_p^{n,i}\right) + \tau\left(\nabla\cdot\mathbf{e}_{\mathbf{q}}^{n,i}, e_p^{n,i}\right) \\
&\quad = \left(\mathfrak{b}(p_h^{n,i-1}) - \mathfrak{b}(p_h^{n-1}) + \mathfrak{b}'(p_h^{n,i-1})\left(p_h^{n,i-1} - p_h^{n}\right), e_p^{n,i}\right), \quad (21)
\end{aligned}$$

where we have rewritten,

$$\begin{aligned}
\mathfrak{c}'(\nabla\cdot\mathbf{u}_h^{n,i-1})\nabla\cdot\delta\mathbf{u}_h^{n,i} &= \mathfrak{c}'(\nabla\cdot\mathbf{u}_h^{n,i-1})\nabla\cdot(\mathbf{u}_h^{n,i} - \mathbf{u}_h^{n,i-1}) \\
&= \mathfrak{c}'(\nabla\cdot\mathbf{u}_h^{n,i-1})(\nabla\cdot\mathbf{u}_h^{n,i} - \nabla\cdot\mathbf{u}_h^{n}) \\
&\quad -\mathfrak{c}'(\nabla\cdot\mathbf{u}_h^{n,i-1})(\nabla\cdot\mathbf{u}_h^{n,i-1} - \nabla\cdot\mathbf{u}_h^{n}) \\
&= \mathfrak{c}'(\nabla\cdot\mathbf{u}_h^{n,i-1})\left(\nabla\cdot\mathbf{e}_{\mathbf{u}}^{n,i} - \nabla\cdot\mathbf{e}_{\mathbf{u}}^{n,i-1}\right),
\end{aligned}$$

We obtain an analogous expression for the term with $\mathfrak{b}'(\cdot)$. From (A1), $\mathfrak{c}(\cdot)$ is differentiable with $\mathfrak{c}'(\cdot)$ Lipschitz continuous, then from Lemma 2 we have,

$$|\mathfrak{c}(x) - \mathfrak{c}(y) + \mathfrak{c}'(y)(y-x)| \leq \frac{L_{\mathfrak{c}'}}{2}|x-y|^2, \quad \forall\, x, y \in \mathbb{R}, \tag{22}$$

where $L_{\mathfrak{c}'}$ represents the Lipshitz constant of $\mathfrak{c}'(\cdot)$. Then, by using Young's inequality $(a,b) \leq \dfrac{||a||^2}{2\gamma} + \dfrac{\gamma||b||^2}{2}$, for $\gamma \geq 0$, and by choosing $x = \nabla\cdot\mathbf{u}_h^n$ and $y = \nabla\cdot\mathbf{u}_h^{n,i-1}$ in (22), from (19) we obtain the following bound, for any $\gamma \geq 0$

$$\begin{aligned}
&||\varepsilon(\mathbf{e}_{\mathbf{u}}^{n,i})||^2 + \left(\mathfrak{c}'(\nabla\cdot\mathbf{u}_h^{n,i-1})\nabla\cdot\mathbf{e}_{\mathbf{u}}^{n,i}, \nabla\cdot\mathbf{e}_{\mathbf{u}}^{n,i}\right) - \alpha\left(e_p^{n,i}, \nabla\cdot\mathbf{e}_{\mathbf{u}}^{n,i}\right) \\
&\qquad \leq \frac{L_{\mathfrak{c}'}^2}{8\gamma}||\nabla\cdot\mathbf{e}_{\mathbf{u}}^{n,i-1}||_{L^4(\Omega)}^4 + \frac{\gamma}{2}||\nabla\cdot\mathbf{e}_{\mathbf{u}}^{n,i}||^2.
\end{aligned} \tag{23}$$

Next, by using the inverse inequality for discrete spaces $||\cdot||_{L^4(\Omega)} \leq Ch^{-d/4}||\cdot||$

[41], (pg. 111) the latter reads,

$$\begin{aligned} ||\varepsilon(\mathbf{e}_{\mathbf{u}}^{n,i})||^2 + \left(\mathfrak{c}'(\nabla\cdot\mathbf{u}_h^{n,i-1})\nabla\cdot\mathbf{e}_{\mathbf{u}}^{n,i}, \nabla\cdot\mathbf{e}_{\mathbf{u}}^{n,i}\right) - \alpha\left(e_p^{n,i}, \nabla\cdot\mathbf{e}_{\mathbf{u}}^{n,i}\right) \\ \leq C_1 h^{-d}\frac{L_{\mathfrak{c}'}^2}{8\gamma}||\nabla\cdot\mathbf{e}_{\mathbf{u}}^{n,i-1}||^4 + \frac{\gamma}{2}||\nabla\cdot\mathbf{e}_{\mathbf{u}}^{n,i}||^2. \end{aligned} \tag{24}$$

Finally, by using (A2) and choosing $\gamma = \alpha_{\mathfrak{c}}$, we obtain the following inequality,

$$||\varepsilon(\mathbf{e}_{\mathbf{u}}^{n,i})||^2 + \frac{\alpha_{\mathfrak{c}}}{2}||\nabla\cdot\mathbf{e}_{\mathbf{u}}^{n,i}||^2 - \alpha\left(e_p^{n,i}, \nabla\cdot\mathbf{e}_{\mathbf{u}}^{n,i}\right) \leq C_1 h^{-d}\frac{L_{\mathfrak{c}'}^2}{8\alpha_{\mathfrak{c}}}||\nabla\cdot\mathbf{e}_{\mathbf{u}}^{n,i-1}||^4. \tag{25}$$

In a similar way, we obtain the following expression from (21),

$$\tau\left(\nabla\cdot\mathbf{e}_{\mathbf{q}}^{n,i}, e_p^{n,i}\right) + \frac{\alpha_{\mathfrak{b}}}{2}||e_p^{n,i}||^2 + \alpha\left(\nabla\cdot\mathbf{e}_{\mathbf{u}}^{n,i}, e_p^{n,i}\right) \leq C_2 h^{-d}\frac{L_{\mathfrak{b}'}^2}{8\alpha_{\mathfrak{b}}}||e_p^{n,i-1}||^4. \tag{26}$$

Adding (25), (26), and (20) multiplied by τ yields,

$$\begin{aligned} \tfrac{\alpha_{\mathfrak{c}}}{2}||\nabla\cdot\mathbf{e}_{\mathbf{u}}^{n,i}||^2 + \tfrac{\alpha_{\mathfrak{b}}}{2}||e_p^{n,i}||^2 + \left(\mathbf{K}^{-1}\mathbf{e}_{\mathbf{q}}^{n,i}, \mathbf{e}_{\mathbf{q}}^{n,i}\right) &\leq C_1 h^{-d}\frac{L_{\mathfrak{c}'}^2}{8\alpha_{\mathfrak{c}}}||\nabla\cdot\mathbf{e}_{\mathbf{u}}^{n,i-1}||^4 \\ &+ C_2 h^{-d}\tfrac{L_{\mathfrak{b}'}^2}{8\alpha_{\mathfrak{b}}}||e_p^{n,i-1}||^4. \end{aligned} \tag{27}$$

By defining $\alpha_{\mathfrak{c},\mathfrak{b}} = \min\left(\alpha_{\mathfrak{c}}, \alpha_{\mathfrak{b}}, \frac{\tau}{k_M}\right)$ and $C_{\mathfrak{c},\mathfrak{b}} = \max\left(\frac{C_1 L_{\mathfrak{c}'}^2}{\alpha_{\mathfrak{c}}}, \frac{C_2 L_{\mathfrak{b}'}^2}{\alpha_{\mathfrak{b}}}\right)$ we can rewrite (27) as

$$\|\nabla\cdot\mathbf{e}_{\mathbf{u}}^{n,i}\|^2 + \|e_p^{n,i}\|^2 + \|\mathbf{e}_{\mathbf{q}}^{n,i}\|^2 \leq \frac{C_{\mathfrak{c},\mathfrak{b}}h^{-d}}{\alpha_{\mathfrak{c},\mathfrak{b}}}\left(\|\nabla\cdot\mathbf{e}_{\mathbf{u}}^{n,i-1}\|^4 + \|e_p^{n,i-1}\|^4\right). \tag{28}$$

Using $\|\nabla\cdot\mathbf{e}_{\mathbf{u}}^{n,0}\| \leq C\tau$, $\|e_p^{n,0}\| \leq C\tau$ (which can be proven) and Lemma 1, the quadratic convergence of Newton's method is ensured if

$$\frac{C_{\mathfrak{c},\mathfrak{b}}h^{-d}}{\alpha_{\mathfrak{c},\mathfrak{b}}}\tau^2 \leq 1$$

which holds true for $\tau = O(h^{\frac{d}{2}})$. □

4.2 Convergence analysis of the alternate splitting Newton scheme

In this section we present the splitting Newton scheme for solving the nonlinear Biot model given in (16). We present the solver in a variational form and demonstrate its linear convergence.
Let $i \geq 1$, $L_s \geq 0$ and $(\mathbf{u}_h^{n,i-1}, \mathbf{q}_h^{n,i-1}, p_h^{n,i-1}) \in (\mathbf{V}_h, \mathbf{Z}_h, W_h)$ be given.

Step 1: find $(\mathbf{q}_h^{n,i}, p_h^{n,i}) \in (\mathbf{Z}_h, W_h)$ such that

$$\begin{aligned} \left(\mathbf{K}^{-1}\mathbf{q}_h^{n,i}, \mathbf{z}_h\right) - \left(p_h^{n,i}, \nabla\cdot\mathbf{z}_h\right) &= \left(\rho_f \mathbf{g}, \mathbf{z}_h\right), \\ \left(\mathfrak{b}(p_h^{n,i-1}) + \mathfrak{b}'(p_h^{n,i-1})\delta p_h^{n,i} - \mathfrak{b}(p_h^{n-1}), w_h\right) + \tau\left(\nabla\cdot\mathbf{q}_h^{n,i}, \nabla w_h\right) & \\ +\alpha\left(\nabla\cdot(\mathbf{u}_h^{n,i-1} - \mathbf{u}_h^{n-1}), w_h\right) &= \tau(S_f, w_h), \end{aligned} \tag{29}$$

$\forall\, (\mathbf{z}_h, w_h) \in (\mathbf{Z}_h, W_h)$

Step 2: find $\mathbf{u}_h^{n,i} \in \mathbf{V}_h$ such that

$$\begin{aligned} \left(\varepsilon(\mathbf{u}_h^{n,i}), \varepsilon(\mathbf{v}_h)\right) + \left(\mathfrak{c}(\nabla\cdot\mathbf{u}_h^{n,i-1}) + \mathfrak{c}'(\nabla\cdot\mathbf{u}_h^{n,i-1})\nabla\cdot\delta\mathbf{u}_h^{n,i}, \nabla\cdot\mathbf{v}_h\right) & \\ + \left(L_s\nabla\cdot\delta\mathbf{u}_h^{n,i}, \nabla\cdot\mathbf{v}_h\right) - \alpha\left(p_h^{n,i}, \nabla\cdot\mathbf{v}_h\right) = \left(\rho_b\mathbf{g}, \mathbf{v}_h\right), & \end{aligned} \tag{30}$$

$\forall \mathbf{v}_h \in \mathbf{V}_h$.

Theorem 2. *Assuming (A1)-(A4) and $L_s \geq \frac{\alpha^2}{\alpha_{\mathfrak{b}}}$, the alternate Newton splitting method in (29)-(30) converges linearly if τ is small enough.*

Proof. The proof is similar to that of Theorem 1. Nevertheless, for the sake of completion we give it in Appendix A. □

5 Numerical examples

In this section, we present numerical experiments that illustrate the performance of the proposed iterative schemes. We study two test problems: a 2D academic problem with a manufactured analytical solution, and a 3D large deformation case on a unit cube. All numerical experiments were implemented using the open-source finite element library Deal II [4]. For all numerical experiments, a Backward Euler scheme has been used for the time discretization. We consider continuous linear Galerkin FE for $\mathbf{u}$, lowest order of Raviart-Thomas FE and discontinuous Galerkin FE for $\mathbf{q}$ and p. However,

we would like to mention that any stable discretization can be considered instead. For all cases, as stopping criterion for the schemes, we use

$$\|p^i - p^{i-1}\| + \|\mathbf{q}^i - \mathbf{q}^{i-1}\| + \|\mathbf{u}^i - \mathbf{u}^{i-1}\| \leq 10^{-8}.$$

Test problem 1: an academic example for Biot's model under small deformation

We solve the nonlinear Biot problem under small deformation in the unit-square $\Omega = (0,1)^2$ and until final time $T = 1$. This test case was proposed in [11] to study the performance of the monolithic and splitting L-scheme. We extend the Newton method and the alternate Newton method described in Section 4.

Here, we introduce a manufactured right hand side such that the problem admits the following analytical solution

$$\begin{aligned} p(x,y,t) = tx(1-x)y(1-y), \quad \mathbf{q}(x,y,t) = -k\nabla p, \\ u_1(x,y,t) = u_2(x,y,t) = tx(1-x)y(1-y), \end{aligned}$$

which has homogeneous boundary values for p and $\mathbf{u}$.

For infinitesimal deformations and rotations, there is no distinction between the reference and the deformed domains. In this regard, we solve problem (16) using the iterative schemes proposed in Section 4. The mesh size and the time step are set as $h = \tau = 0.1$. For this case, all initial conditions are zero. The linearization parameters L_p and $L_{\mathbf{u}}$ are equal to the Lipschitz constant $L_{\mathfrak{b}}$ and $L_{\mathfrak{c}}$ corresponding to the nonlinearities $\mathfrak{b}(\cdot)$ and $\mathfrak{c}(\cdot)$ [11].

In order to study the performance of the considered schemes, we propose four coefficient functions for $\mathfrak{b}(\cdot)$ and two for $\mathfrak{c}(\cdot)$, and define four test cases as given in Table 1. Figure 1 shows the performance of the numerical methods at the last time step $T = 1$. The monolithic Newton method shows quadratic convergence in all cases. Nevertheless, the alternate Newton and the L-scheme methods show linear convergence as predicted in Section 4.

Figure 2 shows the performance of the considered schemes for different time steps. The Newton method has better convergence for smaller time steps while the L-scheme has it for larger time steps; all this is in agreement with the Theorems 1 and 2. The performance of the considered schemes are independent of the mesh discretization.

Test problem 2: a unit cube under large deformation

Table 1: The coefficient functions $\mathfrak{b}(\cdot), \mathfrak{c}(\cdot)$ for test problem 1.

Case	$\mathfrak{b}(p)$	$\mathfrak{c}(\nabla \cdot \mathbf{u})$
1	e^p	$(\nabla \cdot \mathbf{u})^3 + \nabla \cdot \mathbf{u}$
2	e^p	$(\nabla \cdot \mathbf{u})^3$
3	e^p	$\sqrt[3]{\nabla \cdot \mathbf{u}^5} + \nabla \cdot \mathbf{u}$
4	p^2	$\nabla \cdot \mathbf{u}^2$

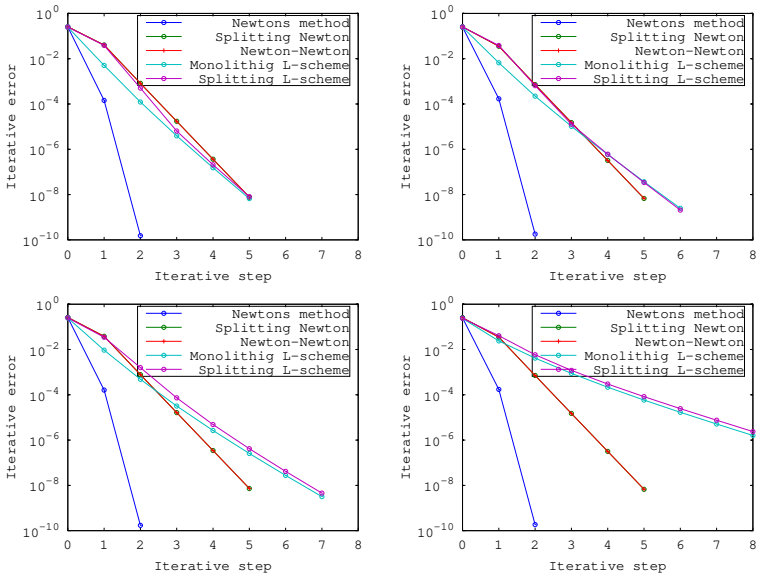

Figure 1: Iterative error at each iteration for different methods: to the right $\mathfrak{b}(p) = e^p$, $\mathfrak{c}(\nabla \cdot \mathbf{u}) = \sqrt[3]{\mathbf{u}^5} + \nabla \cdot \mathbf{u}$, to the left $\mathfrak{b}(p) = p^2$, $\mathfrak{c}(\nabla \cdot \mathbf{u}) = \nabla \cdot \mathbf{u}^2$.

We now solve a large deformation problem on the unit-cube $\Omega = (0,1)^3$. A Lagrangian frame of reference is necessary to keep track of the deformed domain Ω_t at time t. We study the performance of the iterative schemes presented in Section 3 for solving Eqs. (4). The material is supposed to be isotropic and with constant Lamé parameters μ and $\mathfrak{c}(\cdot)$. We consider a Lagrangian fluid mass $m_f = \rho_f J \phi$ of a slightly compressible fluid, where ϕ is the porosity. Under this assumption, the time derivative of the fluid content reads as

$$\dot{\Gamma}(\mathbf{u}, p) = c_p J(\mathbf{u}) \phi \dot{p} + c_\alpha \dot{J}(\mathbf{u}),$$

where the compressibility c_p and Biot's coefficient $c_\alpha = J \frac{\partial \phi}{\partial J} + \phi \approx 1$ for

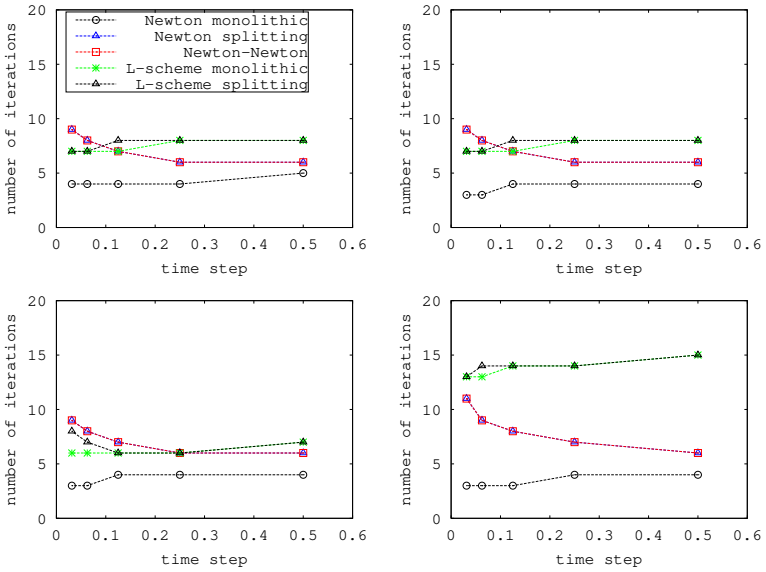

Figure 2: Number of iteration for different time steps: to the right $\mathfrak{b}(p) = e^p$, $\mathfrak{c}(\nabla \cdot \mathbf{u}) = \sqrt[3]{\mathbf{u}^5} + \nabla \cdot \mathbf{u}$, to the left $\mathfrak{b}(p) = p^2$, $\mathfrak{c}(\nabla \cdot \mathbf{u}) = \nabla \cdot \mathbf{u}^2$.

simplicity. We will compare the iterative schemes for a torsion case on a unit cube. On the top face, we apply the rotation tensor $\mathbf{R}(\theta)$ of a time dependent angle $\theta(t) = \pi/4\ t$, which gives a rotation of $\pi/4$ at $T = 1$. We set homogeneous initial condition for $(\mathbf{q}_0, p_0)$ and $\nabla \mathbf{u}_0 = (\mathbf{R}(\theta) - \mathbf{I})$. In the alternate Newton method, the stabilization parameter is set to $L_s = 1$. In the L-scheme method, the linearisation tensor parameters are set as follows: $\mathbf{L_u} = \partial_{\mathbf{u}} \mathbf{\Pi} (\nabla \mathbf{u}_0, p_0)$, $\mathbf{L}_p = \partial_p \mathbf{\Pi} (\nabla \mathbf{u}_0, p_0)$, $\mathbf{L_q} = \partial_p \mathbf{K} (\nabla \mathbf{u}_0)$, $L_p = \partial_p \mathbf{\Gamma} (\nabla \mathbf{u}_0, p_0)$ and $L_{\mathbf{u}} = \partial_{\mathbf{u}} \mathbf{\Gamma} (\nabla \mathbf{u}_0, p_0)$. The mesh size and the time step are set as $h = \tau = 2^{-3}$. We denote by top face of the unit-cube the region $z = 1$, the bottom face $z = 0$ and the lateral faces are $x = 0$, $x = 1$, $y = 0$ and $y = 1$. The boundary conditions are listed in Table 2 and the displacement and pressure field are shown in Figure 4.

We compare the performance of the schemes proposed in Section 3 and we observe that the numerical convergence is in accordance with the theory developed in Section 4, even though the analysis is done for small deformation. Newton's method has quadratic convergence for the smaller time steps and linear convergence for the larger time steps. In contrast, the monolithic L-scheme has the same rate of convergence regardless of size of the time

Table 2: Boundary conditions for Traction and Rotation case respectively.

Face	Flow	Mechanics
Top	$p = 0$	$\mathbf{u} = (\mathbf{R}(\theta(t)) - \mathbf{I})\, X_0$
Bottom	$p = 0$	$\mathbf{u} \cdot \vec{n} = 0$
Lateral	$p = 0$	$\vec{\Pi} \cdot \vec{n} = 0$

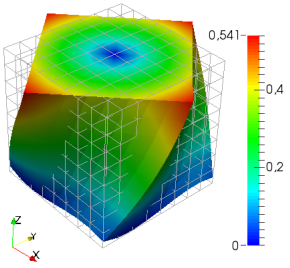

Figure 3: Magnitude of the deformation field and the fluid flow field for torsion.

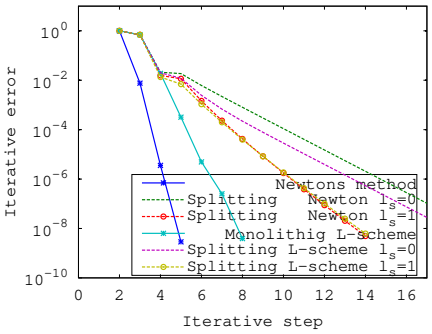

Figure 4: Iterative error at each iteration step for each iterative schemes.

step (see Figure 4). All splitting schemes have better convergence when the stability term is used (we use $L_s = 1.0$).

6 Conclusions

We considered Biot's model under small and large deformation. Different nonlinear solvers based on the L-scheme, Newton's method, and the

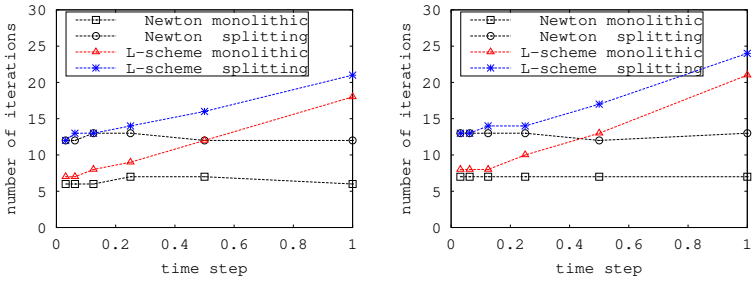

Figure 5: Number of iterations at time $t = 1.0$ using different time steps: to the left $h = 1/2^3$, and $h = 1/2^4$ to the right.

undrained splitting method were presented. The only quadratic convergent scheme is the monolithic Newton method. The splitting Newton method also requires a stabilization parameter, otherwise the (linear) convergence cannot be guaranteed. The analysis of the schemes and illustrative numerical experiments were presented.

We tested the performance of the schemes on two test problems: a unit square under small deformation and a unit cube under large deformation. To summarise, we make the following remarks:

- Monolithic and splitting L-schemes are robust with respect to the choice of the linearization parameter, the mesh size, and time step size.

- The stabilization parameter L_s has a strong influence on the speed of the convergence of the splitting Newton scheme.

- The splitting L-scheme can be used both as a robust solver or even as a preconditioner (as it is established in [26, 57]) to improve the performance of the monolithic Newton method and the L-scheme.

A Convergence proof of the alternate Newton method

The following result provides the linear convergence of the alternate Newton method in (29)- (30) for τ sufficiently small.

Theorem 3. *Assuming (A1)-(A4) and* $L_s \geq \frac{\alpha^2}{\alpha_{\mathfrak{b}}}$*, the alternate Newton splitting method in* (29)-(30) *converges linearly if* τ *is small enough.*

Proof. By subtracting problems (29)-(30) and (16), taking as test functions $\mathbf{e}_{\mathbf{q}}^{n,i}$, $e_p^{n,i}$ and $\mathbf{e}_{\mathbf{u}}^{n,i}$, and rearranging some elements to the right hand side we obtain,

$$\left(\mathbf{K}^{-1}\mathbf{e}_{\mathbf{q}}^{n,i}, \mathbf{e}_{\mathbf{q}}^{n,i}\right) - \left(e_p^{n,i}, \nabla\cdot\mathbf{e}_{\mathbf{q}}^{n,i}\right) = 0, \tag{31}$$

$$\begin{aligned}\left(\mathfrak{b}'(p_h^{n,i-1})(p_h^n - p_h^{n,i}), e_p^{n,i}\right) + \alpha\left(\nabla\cdot\mathbf{e}_{\mathbf{u}}^{n,i-1}, e_p^{n,i}\right) + \tau\left(\nabla\cdot\mathbf{e}_{\mathbf{q}}^{n,i}, e_p^{n,i}\right)\\ = \left(\mathfrak{b}(p_h^n) - \mathfrak{b}(p_h^{n,i-1}) - \mathfrak{b}'(p_h^{n,i-1})(p_h^n - p_h^{n,i-1}), e_p^{n,i}\right).\end{aligned} \tag{32}$$

The mechanics equation then gives,

$$\begin{aligned}(\varepsilon(\mathbf{e}_{\mathbf{u}}^{n,i}), \varepsilon(\mathbf{e}_{\mathbf{u}}^{n,i})) + \left(\mathfrak{c}'(\nabla\cdot\mathbf{u}_h^{n,i-1})\nabla\cdot\mathbf{e}_{\mathbf{u}}^{n,i}, \nabla\cdot\mathbf{e}_{\mathbf{u}}^{n,i}\right)\\ + L_s\left(\nabla\cdot\delta\mathbf{u}_h^{n,i}, \nabla\cdot\mathbf{e}_{\mathbf{u}}^{n,i}\right) - \alpha\left(e_p^{n,i}, \nabla\cdot\mathbf{e}_{\mathbf{u}}^{n,i}\right)\\ = \left(\mathfrak{c}(\nabla\cdot\mathbf{u}_h^n) - \mathfrak{c}(\nabla\cdot\mathbf{u}_h^{n,i-1}) + \mathfrak{c}'(\nabla\cdot\mathbf{u}_h^{n,i-1})\nabla\cdot\mathbf{e}_{\mathbf{u}}^{n,i-1}, \nabla\cdot\mathbf{e}_{\mathbf{u}}^{n,i}\right).\end{aligned} \tag{33}$$

By using similar steps as in Theorem 1, we obtain the following

$$\begin{aligned}||\varepsilon(\mathbf{e}_{\mathbf{u}}^{n,i})||^2 + \left(\mathfrak{c}'(\nabla\cdot\mathbf{u}_h^{n,i-1})\nabla\cdot\mathbf{e}_{\mathbf{u}}^{n,i}, \nabla\cdot\mathbf{e}_{\mathbf{u}}^{n,i}\right)\\ + L_s\left(\nabla\cdot(\mathbf{e}_{\mathbf{u}}^{n,i} - \mathbf{e}_{\mathbf{u}}^{n,i-1}), \nabla\cdot\mathbf{e}_{\mathbf{u}}^{n,i}\right) - \alpha\left(e_p^{n,i}, \nabla\cdot\mathbf{e}_{\mathbf{u}}^{n,i}\right)\\ \leq \frac{L_{\mathfrak{c}'}^2}{8\gamma_1}||\nabla\cdot\mathbf{e}_{\mathbf{u}}^{n,i-1}||_{L^4(\Omega)}^4 + \frac{\gamma_1}{2}||\nabla\cdot\mathbf{e}_{\mathbf{u}}^{n,i}||^2.\end{aligned} \tag{34}$$

Next, by using the inverse inequality $||\cdot||_{L^4(\Omega)} \leq Ch^{-d/4}||\cdot||$ [41], and by using the following formula $(x-y,x) = \frac{||x||^2}{2} + \frac{||x-y||^2}{2} - \frac{||y||^2}{2}$, by choosing $x = \nabla\cdot\mathbf{e_u}^{n,i}$ and $y = \nabla\cdot\mathbf{e}_{\mathbf{u}}^{n,i-1}$, we obtain from (34)

$$||\varepsilon(\mathbf{e}_{\mathbf{u}}^{n,i})||^2 + \left(\mathfrak{c}'(\nabla\cdot\mathbf{u}_h^{n,i-1})\nabla\cdot\mathbf{e}_{\mathbf{u}}^{n,i}, \nabla\cdot\mathbf{e}_{\mathbf{u}}^{n,i}\right) + \tfrac{L_s}{2}\|\nabla\cdot(\mathbf{e}_{\mathbf{u}}^{n,i} - \mathbf{e}_{\mathbf{u}}^{n,i-1})\|^2$$
$$\tfrac{L_s}{2}\|\nabla\cdot\mathbf{e}_{\mathbf{u}}^{n,i}\|^2 - \alpha\left(e_p^{n,i}, \nabla\cdot\mathbf{e}_{\mathbf{u}}^{n,i}\right) + \leq C_1 h^{-d}\frac{L_{\mathfrak{c}'}^2}{8\gamma_1}||\nabla\cdot\mathbf{e}_{\mathbf{u}}^{n,i-1}||^4$$
$$+\tfrac{\gamma_1}{2}||\nabla\cdot\mathbf{e}_{\mathbf{u}}^{n,i}||^2 + \tfrac{L_s}{2}\|\nabla\cdot\mathbf{e}_{\mathbf{u}}^{n,i-1}\|^2. \tag{35}$$

Finally, by reorganizing (35), using (A2) and choosing $\gamma_1 = \alpha_{\mathfrak{c}}$, we obtain the following inequality,

$$\begin{aligned} &||\varepsilon(\mathbf{e}_{\mathbf{u}}^{n,i})||^2 + \left(\tfrac{\alpha_{\mathfrak{c}}+L_s}{2}\right)\|\nabla\cdot\mathbf{e}_{\mathbf{u}}^{n,i}\|^2 + \tfrac{L_s}{2}\|\nabla\cdot\delta\mathbf{e}_{\mathbf{u}}^{n,i}\|^2 \\ &\leq C_1 h^{-d}\frac{L_{\mathfrak{c}'}^2}{8\alpha_{\mathfrak{c}}}||\nabla\cdot\mathbf{e}_{\mathbf{u}}^{n,i-1}||^4 + \frac{L_s}{2}\|\nabla\cdot\mathbf{e}_{\mathbf{u}}^{n,i-1}\| + \alpha\left(e_p^{n,i}, \nabla\cdot\mathbf{e}_{\mathbf{u}}^{n,i}\right). \end{aligned} \tag{36}$$

In a similar way, we obtain the following expression from (21),

$$\frac{\tau}{k_M}||\mathbf{e}_{\mathbf{q}}^{n,i}||^2 + \frac{\alpha_{\mathfrak{b}}}{2}||e_p^{n,i}||^2 \leq C_2 h^{-d}\frac{L_{\mathfrak{b}'}^2}{8\alpha_{\mathfrak{b}}}||e_p^{n,i-1}||^4 - \alpha\left(\nabla\cdot\mathbf{e}_{\mathbf{u}}^{n,i-1}, e_p^{n,i}\right). \tag{37}$$

Adding equations (36) and (37) yields,

$$\begin{aligned} &\tfrac{\tau}{k_M}||\mathbf{e}_{\mathbf{q}}^{n,i}||^2 + \tfrac{\alpha_{\mathfrak{b}}}{2}||e_p^{n,i}||^2 + ||\varepsilon(\mathbf{e}_{\mathbf{u}}^{n,i})||^2 + \tfrac{L_s}{2}\|\nabla\cdot\delta\mathbf{e}_{\mathbf{u}}^{n,i}\|^2 + \left(\tfrac{\alpha_{\mathfrak{c}}+L_s}{2}\right)\|\nabla\cdot\mathbf{e}_{\mathbf{u}}^{n,i}\|^2 \\ &\leq C_2 h^{-d}\frac{L_{\mathfrak{b}'}^2}{8\alpha_{\mathfrak{b}}}||e_p^{n,i-1}||^4 + C_1 h^{-d}\frac{L_{\mathfrak{c}'}^2}{8\alpha_{\mathfrak{c}}}||\nabla\cdot\mathbf{e}_{\mathbf{u}}^{n,i-1}||^4 \\ &+\tfrac{L_s}{2}\|\nabla\cdot\mathbf{e}_{\mathbf{u}}^{n,i-1}\|^2 + \alpha\left(\nabla\cdot\delta\mathbf{e}_{\mathbf{u}}^{n,i}, e_p^{n,i}\right). \end{aligned} \tag{38}$$

By using Young's inequality $(a,b) \leq \frac{||a||^2}{2\gamma} + \frac{\gamma||b||^2}{2}$, for $\gamma > 0$ and choosing $b = e_p^{n,i}$ and $a = \nabla\cdot\delta\mathbf{e}_{\mathbf{u}}^{n,i}$ we bound the coupling term (for $\gamma_2 > 0$),

$$\alpha\left(\nabla\cdot\delta\mathbf{e}_{\mathbf{u}}^{n,i}, e_p^{n,i}\right) \leq \frac{\alpha^2}{2\gamma_2}\|\nabla\cdot\delta\mathbf{e}_{\mathbf{u}}^{n,i-1}\|^2 + \frac{\gamma_2}{2}\|e_p^{n,i}\|^2. \tag{39}$$

Then by using (39) and choosing $\gamma_2 = \frac{\alpha_{\mathfrak{b}}}{2}$ we obtain from (38)

$$\begin{aligned} &\tfrac{\tau}{k_M}||\mathbf{e}_{\mathbf{q}}^{n,i}||^2 + \tfrac{\alpha_{\mathfrak{b}}}{4}||e_p^{n,i}||^2 + ||\varepsilon(\mathbf{e}_{\mathbf{u}}^{n,i})||^2 + \left(\tfrac{L_s}{2} - \tfrac{\alpha^2}{2\alpha_{\mathfrak{b}}}\right)\|\nabla\cdot\delta\mathbf{e}_{\mathbf{u}}^{n,i}\|^2 \\ &+ \left(\tfrac{\alpha_{\mathfrak{c}}+L_s}{2}\right)\|\nabla\cdot\mathbf{e}_{\mathbf{u}}^{n,i}\|^2 \leq \tfrac{h^{-d}}{8}\left(C_2\tfrac{L_{\mathfrak{b}'}^2}{\alpha_{\mathfrak{b}}}||e_p^{n,i-1}||^4 + C_1\tfrac{L_{\mathfrak{c}'}^2}{\alpha_{\mathfrak{c}}}||\nabla\cdot\mathbf{e}_{\mathbf{u}}^{n,i-1}||^4\right) \\ &+\tfrac{L_s}{2}\|\nabla\cdot\mathbf{e}_{\mathbf{u}}^{n,i-1}\|^2. \end{aligned} \tag{40}$$

Since $L_s \geq \frac{\alpha^2}{\alpha_\mathfrak{b}}$, we obtain

$$\begin{aligned} &\tfrac{\tau}{k_M}||\mathbf{e}_\mathbf{q}^{n,i}||^2 + \tfrac{\alpha_\mathfrak{b}}{4}||e_p^{n,i}||^2 + \left(\tfrac{\alpha_\mathfrak{c}+L_s}{2}\right)\|\nabla\cdot\mathbf{e}_\mathbf{u}^{n,i}\|^2 \\ &\leq \tfrac{h^{-d}}{8}\left(C_2\tfrac{L_{\mathfrak{b}'}^2}{\alpha_\mathfrak{b}}||e_p^{n,i-1}||^4 + C_1\tfrac{L_{\mathfrak{c}'}^2}{\alpha_\mathfrak{c}}||\nabla\cdot\mathbf{e}_\mathbf{u}^{n,i-1}||^4\right) \\ &\qquad + \tfrac{L_s}{2}\|\nabla\cdot\mathbf{e}_\mathbf{u}^{n,i-1}\|^2. \end{aligned} \tag{41}$$

By using $\|\nabla\cdot\mathbf{e}_\mathbf{u}^{n,0}\| \leq C\tau$, $\|e_p^{n,0}\| \leq C\tau$ wich can be proven and the estimate in Lemma 1, the convergence is ensured if $\tau = O(h^{\frac{d}{2}})$.

□

Acknowledgement

The research was supported by the University of Bergen in cooperation with the FME-SUCCESS center (grant 193825/S60) funded by the Research Council of Norway. The work has also been partly supported by: the NFR-DAADppp grant 255715, the NFR-Toppforsk project 250223, the NRC-CHI grant 255510 and the NRC-IMMENS grant 255426.

References

[1] T. Almani, K. Kumar, A.H. Dogru, G. Singh, and M.F. Wheeler. Convergence Analysis of Multirate Fixed-Stress Split Iterative Schemes for Coupling Flow with Geomechanics. *Comput. Methods. Appl. Mech. Eng.*, 311:180–207, 2016.

[2] D.G. Anderson. Iterative Procedures for Nonlinear Integral Equations. *J. ACM*, 12(4):547–560, 1965.

[3] F. Armero. Formulation and finite element implementation of a multiplicative model of coupled poro-plasticity at finite strains under fully saturated conditions. *Comput. Methods. Appl. Mech. Eng.*, 171(3):205–241, 1999.

[4] W. Bangerth, G. Kanschat, T. Heister, L. Heltai, and G. Kanschat. The deal.II library version 8.4. *J. Numer. Math.*, 24:135–141, 2016.

[5] M. Bause. Iterative coupling of mixed and discontinuous Galerkin methods for poroelasticity. *Numerical Mathematics and Advanced Applications ENUMATH 2017*, pages 551–560, 2019.

[6] M. Bause, F.A. Radu, and U. Köcher. Space–time finite element approximation of the Biot poroelasticity system with iterative coupling. *Comput. Methods. Appl. Mech. Eng*, 320(Supplement C):745–768, 2017.

[7] L. Berger, R. Bordas, D. Kay, and S. Tavener. A stabilized finite element method for finite-strain three-field poroelasticity. *Comput. Mech.*, 60(1):51–68, Jul 2017.

[8] M. A. Biot. Consolidation Settlement Under a Rectangular Load Distribution. *J. Appl. Phys.*, 12(5):426–430, 1941.

[9] M. A. Biot. General theory of three-dimensional consolidation. *J. Appl. Phys.*, 12(2):155–164, 1941.

[10] M. A. Biot. Theory of Elasticity and Consolidation for a Porous Anisotropic Solid. *J. Appl. Phys.*, 26(2):182–185, 1955.

[11] M. Borregales, J.M. Nordbotten, K. Kumar, and F.A. Radu. Robust iterative schemes for non-linear poromechanics. *Comput. Geosci.*, 22(4):1021–1038, 2017.

[12] J.W. Both, M. Borregales, J.M. Nordbotten, K. Kumar, and F.A. Radu. Robust fixed stress splitting for Biot's equations in heterogeneous media. *Appl. Math. Letters*, 68:101–108, 2017.

[13] J.W. Both, K. Kumar, J.M. Nordbotten, I.S. Pop, and F.A. Radu. Linear iterative schemes for doubly degenerate parabolic equations. *Numerical Mathematics and Advanced Applications ENUMATH 2017*, pages 49–63, 2019.

[14] J.W. Both, K. Kumar, J.M. Nordbotten, and F.A. Radu. Iterative Methods for Coupled Flow and Geomechanics in Unsaturated Porous Media. *Proceedings of the Sixth Biot Conference on Poromechanics*, 68:101–108, 2017.

[15] J.W. Both, K. Kumar, J.M. Nordbotten, and F.A. Radu. Anderson accelerated fixed-stress splitting schemes for co nsolidation of unsaturated porous media. *Comput. Math. Appl.*, 77(6):1479–1502, 2019.

[16] F. Brezzi and M. Fortin. *Mixed and hybrid finite element methods*, volume 15 of *Springer Ser. Comput. Math.* Springer-Verlag New York, 2012.

[17] N. Castelletto, J.A. White, and M. Ferronato. Scalable algorithms for three-field mixed finite element coupled poromechanics. *J. Comput. Phys.*, 327:894–918, 2016.

[18] L.Y. Chin, L.K. Thomas, J.E. Sylte, and R.G. Pierson. Iterative Coupled Analysis of Geomechanics and Fluid Flow for Rock Compaction in Reservoir Simulation. *Oil & Gas Sci. Technol.*, 57(5):485–497, 2002.

[19] O. Coussy. A general theory of thermoporoelastoplasticity for saturated porous materials. *Trans. Por. Med.*, 4(3):281–293, 1989.

[20] O. Coussy. *Mechanics of Porous Continua*. Wiley, New York, 1995.

[21] O. Coussy. *Poromechanics*. J. Willey & Sons, Ltd., 2004.

[22] F. Doster and J.M. Nordbotten. Full Pressure Coupling for Geomechanical Multi-phase Multi-component Flow Simulations, 2015.

[23] X. Gai and M.F. Wheeler. Iteratively coupled mixed and Galerkin finite element methods for poro-elasticity. *Numer. Methods. Partial. Diff. Equations*, 23(4):785–797, 2007.

[24] F.J. Gaspar and C. Rodrigo. On the fixed-stress split scheme as smoother in multigrid methods for coupling flow and geomechanics. *Computer Methods in Applied Mechanics and Engineering*, 326(Supplement C):526–540, 2017.

[25] V. Girault, K. Kumar, and M.F. Wheeler. Convergence of iterative coupling of geomechanics with flow in a fractured poroelastic medium. *Comput. Geosci.*, 20(5):997–1011, 2016.

[26] J.B. Haga, H. Osnes, and H.P. Langtangen. Efficient block preconditioners for the coupled equations of pressure and deformation in highly discontinuous media. *Int. J. Numer. Anal. Meth. Geomech.*, 35(13):1466–1482, 2011.

[27] Q. Hong, J. Kraus, M. Lymbery, and F. Philo. Conservative discretizations and parameter-robust preconditioners for Biot and multiple-network flux-based poroelastic models. *arXiv: 1806.00353*, 2018.

[28] Q. Hong, J. Kraus, M. Lymbery, and M.F. Wheeler. Parameter-robust convergence analysis of fixed-stress split iterativemethod for multiple-permeability poroelasticity systems. *arXiv:1812.11809v2*, 2019.

[29] L. Jeannin, M. Mainguy, R. Masson, and S. Vidal-Gilbert. Accelerating the convergence of coupled geomechanical-reservoir simulations. *Int. J. Numer. Anal. Meth. Geomech.*, 31(10):1163–1181, aug 2007.

[30] B. Jha and R. Juanes. A locally conservative finite element framework for the simulation of coupled flow and reservoir geomechanics. *Acta Geotechnica*, 2(3):139–153, 2007.

[31] J. Kim, H.A. Tchelepi, and R. Juanes. Stability and convergence of sequential methods for coupled flow and geomechanics: Drained and undrained splits. *Comput. Methods. Appl. Mech. Eng.*, 200(23–24):2094–2116, 2011.

[32] P. Knabner and L. Angerman. *Numerical Methods for Elliptic and Parabolic Partial Differential Equations*, volume 44. Springer-Verlag New York, 2003.

[33] K. Kumar, I. Pop, and F. Radu. Convergence Analysis of Mixed Numerical Schemes for Reactive Flow in a Porous Medium. *SIAM J. Numer. Anal.*, 51(4):2283–2308, 2013. doi: 10.1137/120880938.

[34] J.J. Lee, E. Piersanti, K-A. Mardal, and M.E. Rognes. A mixed finite element method for nearly incompressible multiple-network poroelasticity. *SIAM J. Sci. Comput.*, 41(2):A722–A747, 2018.

[35] S. Lee, A. Mikelic, M.F Wheeler, and T. Wick. Phase-field modeling of proppant-filled fractures in a poroelastic medium. *Comput. Methods. Appl. Mech. Eng.*, 312:509–541, 2016.

[36] R. W. Lewis and Y. Sukirman. Finite element modelling of three-phase flow in deforming saturated oil reservoirs. *Int. J. Numer. Anal. Meth. Geomech.*, 17(8):577–598, aug 1993.

[37] F. List and F.A. Radu. A study on iterative methods for solving Richards' equation. *Comput. Geosci.*, 20(2):341–353, 2016.

[38] A. Mikelić and M.F. Wheeler. Theory of the dynamic Biot-Allard equations and their link to the quasi-static Biot system. *J. Math. Phys.*, 53(12):–, 2012.

[39] A. Mikelić and M.F. Wheeler. Convergence of iterative coupling for coupled flow and geomechanics. *Comput. Geosci.*, 18(3-4):325–341, 2013.

[40] J.M. Nordbotten. Stable Cell-Centered Finite Volume Discretization for Biot Equations. *SIAM J. Numer. Anal.*, 54(2):942–968, 2016.

[41] J. Pasciak. The Mathematical Theory of Finite Element Methods (Susanne C. Brenner and L. Ridgway Scott). *SIAM Review*, 37(3):472–473, 1995. doi: 10.1137/1037111.

[42] O. Pettersen. Coupled Flow and Rock Mechanics Simulation Optimizing the coupling term for faster and accurate computation. *Int. J. Numer. Anal. Model.*, 9(3):628–643, 2012.

[43] P.J. Phillips and M.F. Wheeler. A coupling of mixed and continuous Galerkin finite element methods for poroelasticity I: the continuous in time case. *Comput. Geosci.*, 11(2):131–144, 2007.

[44] I.S. Pop, F. Radu, and P. Knabner. Mixed finite elements for the Richards' equation: linearization procedure. *J. Comput. Appl. Math.*, 168(1–2):365–373, 2004.

[45] J.H. Prevost. *One-Way versus Two-Way Coupling in Reservoir-Geomechanical Models*, pages 517–526. American Society of Civil Engineers, 2013.

[46] F.A. Radu. *Mixed finite element discretization of Richards' equation: error analysis and application to realistic infiltration problems.* PhD thesis, University of Erlangen–Nürnberg, 2004.

[47] F.A. Radu, M. Borregales, K. Kumar, F. Gaspar, and C. Rodrigo. L-scheme and Newton based solvers for a nonlinear Biot model. *ECCOMAS Proceedings Glasgow*, 2018.

[48] F.A. Radu, J.M. Nordbotten, I.S. Pop, and K. Kumar. A robust linearization scheme for finite volume based discretizations for simulation of two-phase flow in porous media. *J. Comput. Appl. Math.*, 289:134–141, 2015.

[49] F.A. Radu and I.S. Pop. Newton method for reactive solute transport with equilibrium sorption in porous media. *J. Comput. Appl. Math.*, 234(7):2118–2127, 2010.

[50] C. Rodrigo, F.J. Gaspar, X. Hu, and L.T. Zikatanov. Stability and monotonicity for some discretizations of the Biot's consolidation model. *Comput. Methods. Appl. Mech. Eng.*, 298:183–204, 2016.

[51] A. Settari and Dale A. Walters. Advances in Coupled Geomechanical and Reservoir Modeling With Applications to Reservoir Compaction. *SPE J.*, 2001.

[52] R.E. Showalter. Diffusion in Poro-Elastic Media. *J. Math Anal. Appl.*, 251(1):310–340, 2000.

[53] E. Storvik, J.W. Both, K. Kumar, J.M. Nordbotten, and F.A. Radu. On the optimization of the fixed-stress splitting for Biot's equations. *Int. J. Numer. Meth. Eng.* to apear, 2019.

[54] R. Temam and A. Miranville. *Mathematical Modeling in Continuum Mechanics*. Cambridge, May 2005.

[55] J. Wan, L.J. Durlofsky, T.J.R. Hughes, and K. Aziz. Stabilized Finite Element Methods for Coupled Geomechanics - Reservoir Flow Simulations, 2003.

[56] D. White, B. Ganis, R. Liu, and M.F. Wheeler. Near-Wellbore Study with a Drucker-Prager Plasticity Model Coupled witha Parallel Compositional Reservoir Simulator. *Paper SPE-182627-MS SPE Reservoir Simulation Conference*, 2017.

[57] J.A. White, N. Castelletto, and H.A. Tchelepi. Block-partitioned solvers for coupled poromechanics: A unified framework. *Comput. Methods. Appl. Mech. Eng.*, 303:55–74, may 2016.

[58] S-Y. Yi and M.L. Bean. Iteratively coupled solution strategies for a four-field mixed finite element method for poroelasticity. *International Journal for Numerical and Analytical Methods in Geomechanics*, 41(2):159–179.

[59] O.C. Zienkiewicz, D.K. Paul, and A.H.C. Chan. Unconditionally stable staggered solution procedure for soil-pore fluid interaction problems. *Int. J. Numer. Meth. Engng.*, 26(5):1039–1055, may 1988.

Paper D

A parallel-in-time fixed-stress splitting method for Biot's consolidation model

M. Borregales, K. Kumar, F.A. Radu, C. Rodrigo and F.J. Gaspar

Computers and Mathematics with Applications (2018). Elsevier.

doi: 10.1016/j.camwa.2018.09.005

Computers and Mathematics with Applications 77 (2019) 1466–1478

Contents lists available at ScienceDirect

Computers and Mathematics with Applications

journal homepage: www.elsevier.com/locate/camwa

A partially parallel-in-time fixed-stress splitting method for Biot's consolidation model

Manuel Borregales [a], Kundan Kumar [a], Florin Adrian Radu [a], Carmen Rodrigo [c,*], Francisco José Gaspar [b]

[a] Department of Mathematics, University of Bergen, Allégaten 41, 50520 Bergen, Norway
[b] CWI, Centrum Wiskunde & Informatica, Science Park 123, P.O. Box 94079, 1090 Amsterdam, The Netherlands
[c] IUMA and Department of Applied Mathematics, University of Zaragoza, María de Luna, 3, 50018 Zaragoza, Spain

ARTICLE INFO

Article history:
Available online 8 October 2018

Keywords:
Iterative fixed-stress splitting scheme
Parallel-in-time
Biot's model
Poromechanics
Finite elements
Convergence analysis

ABSTRACT

In this work, we study the parallel-in-time iterative solution of coupled flow and geomechanics in porous media, modelled by a two-field formulation of Biot's equations. In particular, we propose a new version of the fixed-stress splitting method, which has been widely used as solution method of these problems. This new approach forgets about the sequential nature of the temporal variable and considers the time direction as a further direction for parallelization. The method is partially parallel-in-time. We present a rigorous convergence analysis of the method and numerical experiments to demonstrate the robust behaviour of the algorithm.

1. Introduction

The coupled poroelastic equations describe the behaviour of fluid-saturated porous materials undergoing deformation. Such coupling has been intensively investigated, starting from the pioneering one-dimensional work of Terzaghi [1], which was extended to a more general three-dimensional theory by Biot [2,3]. Biot's model was originally developed to study geophysical applications such as reservoir geomechanics, however, nowadays it is widely used in the modelling of many applications in a great variety of fields, ranging from geomechanics and petroleum engineering, to biomechanics or food processing. There is a vast literature on Biot's equations and the existence, uniqueness, and regularity of their solutions, see Showalter [4], Phillips and Wheeler [5] and the references therein.

Reliable numerical methods for solving poroelastic problems are needed for the accurate solution of multi-physics phenomena appearing in different application areas. In particular, the solution of the large linear systems of equations arising from the discretization of Biot's model is the most consuming part when real simulations are performed. For this reason, a lot of effort has been made in the last years to design efficient solution methods for these problems. Two different approaches can be adopted, the so-called monolithic or fully coupled methods and the iterative coupling methods. The monolithic approach consists of solving the linear system simultaneously for all the unknowns. The challenge here, is the design of efficient preconditioners to accelerate the convergence of Krylov subspace methods and the design of efficient smoothers in a multigrid framework. Recent advances in both directions can be found in [6–9] and the references therein. These methods usually provide unconditional stability and convergence. Iterative coupling methods, however, solve sequentially the equations for fluid flow and geomechanics, at each time step, until a converged solution within a prescribed tolerance is

* Corresponding author.
E-mail addresses: Manuel.Borregales@uib.no (M. Borregales), Kundan.Kumar@uib.no (K. Kumar), Florin.Radu@uib.no (F.A. Radu), carmenr@unizar.es (C. Rodrigo), F.J.Gaspar@cwi.nl (F.J. Gaspar).

https://doi.org/10.1016/j.camwa.2018.09.005
0898-1221/

achieved. They offer several attractive features as their flexibility, for example, since they allow to link two different codes for fluid flow and geomechanics for solving the coupled poroelastic problems. The most used iterative coupling methods are the drained and undrained splits, which solve the mechanical problem first, and the fixed-strain and fixed-stress splits, which on the contrary solve the flow problem first [10–12].

Among iterative coupling schemes, the fixed-stress splitting method is the most widely used. This sequential-implicit method basically consists of solving the flow problem first fixing the volumetric mean total stress, and then the mechanics part is solved from the values obtained at the previous flow step. In the last years, a lot of research has been done on this method. The unconditional stability of the fixed-stress splitting method is shown in [11] using a von Neumann analysis. In addition, stability and convergence of the fixed-stress splitting method have been rigorously established in [13]. Recently, in [14] the authors have proven the convergence of the fixed-stress split method in energy norm for heterogeneous problems. Estimates for the case of the multirate iterative coupling scheme are obtained in [15], where multiple finer time steps for flow are taken within one coarse mechanics time step, exploiting the different time scales for the mechanics and flow problems. In [16], the convergence of this method is demonstrated in the fully discrete case when space–time finite element methods are used. In [17], the authors present a very interesting approach which consists of re-interpreting the fixed-stress splitting scheme as a preconditioned-Richardson iteration with a particular block-triangular preconditioning operator. Recently, in [18] an inexact version of the fixed-stress splitting scheme has been successfully proposed as smoother in a geometric multigrid framework, which provides an efficient monolithic solver for Biot's problem. Finally, we mention that the fixed-stress splitting was recently applied to a non-linear poromechanics model in [19] and to consolidation of unsaturated porous media in [20].

All the previously mentioned algorithms are based on a time-marching approach, in which each time step is solved after the other in a sequential manner, and therefore they do not allow the parallelization of the temporal variable. Parallel-in-time integration methods, however, are receiving a lot of interest nowadays because of the advent of massively parallel systems with thousands of threads, permitting to reduce drastically the computing time [21]. There are various different methods introducing concurrency along the temporal dimension. The most well-known time-parallelization methods include the parallel full approximation scheme in space and time (PFASST) [22], the Parareal method [23], the Multigrid Reduction in Time algorithm (MGRIT) [24], the Space–time Multigrid method (STMG) [25], and the Space–time concurrent multigrid waveform relaxation (WRMG) with cyclic reduction [26,27]. Due to the mixed elliptic–parabolic structure of Biot's problem, the development of parallel-in-time algorithms is not intuitive.

In the present work, we introduce a very simple version of the fixed-stress splitting method for the poroelasticity problem which is partially parallel-in-time. We further show rigorously its convergence. Techniques similar with the ones from [13,14,16] are used. For completeness, in Section 3, we include a new proof for the convergence of the fixed-stress splitting algorithm in the semi-discrete case. The theoretical results are sustained by numerical computations. Moreover, a fully parallel-in-time version of the presented method is introduced.

The remainder of the paper is organized as follows. In Section 2 we briefly introduce the poroelasticity model and present the considered finite element discretizations. Section 3 is devoted to the description of the classical fixed-stress splitting algorithm. In Section 4, the partially parallel-in-time new approach based on the fixed-stress splitting algorithm is presented and its convergence analysis is derived. Section 5 illustrates the robustness of the proposed parallel-in-time fixed-stress splitting method through two numerical experiments. Finally, some conclusions are drawn in Section 6.

2. Mathematical model and discretization

The equations describing poroelastic flow and deformation are derived from the principles of fluid mass conservation and the balance of forces on the porous matrix. More concretely, according to Biot's theory [2,3], and assuming Ω a bounded open subset of $\mathbb{R}^d$, $d \in \{2, 3\}$, with regular boundary Γ, the consolidation process must satisfy on the space–time domain $\Omega \times (0, T]$ the following system of partial differential equations:

$$\begin{aligned}
\text{equilibrium equation:} \quad & -div\, \boldsymbol{\sigma}' + \alpha \nabla p &&= \rho \boldsymbol{g}, \\
\text{constitutive equation:} \quad & \boldsymbol{\sigma}' &&= 2G\boldsymbol{\varepsilon}(\boldsymbol{u}) + \lambda\, \mathrm{div}(\boldsymbol{u})\boldsymbol{I}, \\
\text{compatibility condition:} \quad & \boldsymbol{\varepsilon}(\boldsymbol{u}) &&= \tfrac{1}{2}(\nabla \boldsymbol{u} + \nabla \boldsymbol{u}^t), \\
\text{Darcy's law:} \quad & \boldsymbol{q} &&= -\tfrac{1}{\mu_f}\boldsymbol{K}\left(\nabla p - \rho_f \boldsymbol{g}\right), \\
\text{continuity equation:} \quad & \tfrac{\partial}{\partial t}\left(\tfrac{1}{\beta} p + \alpha \nabla \cdot \boldsymbol{u}\right) + \nabla \cdot \boldsymbol{q} &&= f,
\end{aligned} \tag{1}$$

where $\boldsymbol{I}$ is the identity tensor, $\boldsymbol{u}$ is the displacement vector, p is the pore pressure, $\boldsymbol{\sigma}'$ and $\boldsymbol{\varepsilon}$ are the effective stress and strain tensors for the porous medium, $\boldsymbol{g}$ is the gravity vector, $\boldsymbol{q}$ is the percolation velocity of the fluid relative to the soil, μ_f is the fluid viscosity and $\boldsymbol{K}$ is the absolute permeability tensor. The Lamé coefficients, λ and G, can be also expressed in terms of Young's modulus E and the Poisson's ratio ν as $\lambda = E\nu/((1-2\nu)(1+\nu))$ and $G = E/(2+2\nu)$. The bulk density ρ is related to the densities of the solid (ρ_s) and fluid (ρ_f) phases as $\rho = \phi\rho_f + (1-\phi)\rho_s$, where ϕ is the porosity. β is the Biot modulus and α is the Biot coefficient given by $\alpha = 1 - K_b/K_s$, where K_b is the drained bulk modulus, and K_s is the bulk modulus of the solid phase.

If considering the displacements of the solid matrix $\boldsymbol{u}$ and the pressure of the fluid p as primary variables, we obtain the so-called two-field formulation of the Biot's consolidation model. With this idea in mind, the mathematical model (1) can be rewritten as

$$-\operatorname{div}\boldsymbol{\sigma}' + \alpha\nabla p = \rho\boldsymbol{g}, \qquad \boldsymbol{\sigma}' = 2G\,\boldsymbol{\varepsilon}(\boldsymbol{u}) + \lambda\operatorname{div}(\boldsymbol{u})\boldsymbol{I}, \tag{2}$$

$$\frac{\partial}{\partial t}\left(\frac{1}{\beta}p + \alpha\nabla\cdot\boldsymbol{u}\right) - \nabla\cdot\left(\frac{1}{\mu_f}\boldsymbol{K}\left(\nabla p - \rho_f\boldsymbol{g}\right)\right) = f. \tag{3}$$

The most important feature of this mathematical model is that the equations are strongly coupled. Here, the Biot parameter α plays the role of coupling parameter between these equations. In order to ensure the existence and uniqueness of solution, we must supplement the system with appropriate boundary and initial conditions. For instance,

$$\begin{array}{llllll} p = 0, & \text{on } \Gamma_p & \text{and} & \dfrac{\boldsymbol{K}}{\mu_f}\left(\nabla p - \rho_f\boldsymbol{g}\right)\cdot\boldsymbol{n} & = & 0, \quad \text{on } \Gamma_{\mathbf{q}}, \\ \boldsymbol{u} = \boldsymbol{0}, & \text{on } \Gamma_{\mathbf{u}} & \text{and} & \boldsymbol{\sigma}'\boldsymbol{n} & = & \boldsymbol{0}, \quad \text{on } \Gamma_t, \end{array} \tag{4}$$

where $\boldsymbol{n}$ is the unit outward normal to the boundary, $\Gamma_p \cup \Gamma_{\mathbf{q}} = \Gamma_t \cup \Gamma_{\mathbf{u}} = \Gamma$, and $\Gamma_p \cap \Gamma_{\mathbf{q}} = \Gamma_t \cap \Gamma_{\mathbf{u}} = \emptyset$ with Γ_p, $\Gamma_{\mathbf{q}}$, $\Gamma_{\mathbf{u}}$ and Γ_t subsets of Γ having non null measure. For the initial time, $t = 0$, the following condition is fulfilled

$$\left(\frac{1}{\beta}p + \alpha\nabla\cdot\boldsymbol{u}\right)(\boldsymbol{x}, 0) = 0, \ \boldsymbol{x} \in \Omega. \tag{5}$$

Results about existence and uniqueness of the solution of the Biot's model (2)–(3) with initial condition (5) can be found in the works by Showalter [4] and Zenisek [28].

2.1. Semi-discretization in space

To introduce the spatial discretization of the Biot model, we choose the finite element method. We define the standard Sobolev spaces $\boldsymbol{V} = \{\boldsymbol{u} \in (H^1(\Omega))^d \mid \boldsymbol{u}|_{\Gamma_{\mathbf{u}}} = \boldsymbol{0}\}$, and $Q = \{p \in H^1(\Omega) \mid p|_{\Gamma_p} = 0\}$, with $H^1(\Omega)$ denoting the Hilbert subspace of $L_2(\Omega)$ of functions with first weak derivatives in $L_2(\Omega)$. Then, we introduce the variational formulation for the two-field formulation of the Biot's model as follows: Find $(\boldsymbol{u}(t), p(t)) \in C^1([0,T];\boldsymbol{V}) \times C^1([0,T];Q)$ such that

$$a(\boldsymbol{u}(t), \boldsymbol{v}) - \alpha(p(t), \operatorname{div}\boldsymbol{v}) = (\rho\boldsymbol{g}, \boldsymbol{v}), \ \forall\, \boldsymbol{v} \in \boldsymbol{V}, \ t \in (0,T], \tag{6}$$

$$\alpha(\operatorname{div}\partial_t\boldsymbol{u}(t), q) + \frac{1}{\beta}(\partial_t p(t), q) + b(p(t), q) = (f, q) + (\boldsymbol{K}\mu_f^{-1}\rho_f\boldsymbol{g}, \nabla q), \ \forall q \in Q, \ t \in (0,T], \tag{7}$$

where $(\cdot,\cdot)$ is the standard inner product in the space $L_2(\Omega)$, and the bilinear forms $a(\cdot,\cdot)$ and $b(\cdot,\cdot)$ are given as

$$a(\boldsymbol{u}, \boldsymbol{v}) = 2G\int_\Omega \boldsymbol{\varepsilon}(\boldsymbol{u}) : \boldsymbol{\varepsilon}(\boldsymbol{v})\, d\Omega + \lambda\int_\Omega \operatorname{div}\boldsymbol{u}\operatorname{div}\boldsymbol{v}\, d\Omega,$$

$$b(p, q) = \int_\Omega \frac{\boldsymbol{K}}{\mu_f}\nabla p\cdot\nabla q\, d\Omega.$$

Finally, the initial condition is given by

$$\left(\frac{1}{\beta}p(0) + \alpha\nabla\cdot\boldsymbol{u}(0), q\right) = 0, \quad \forall\, q \in L_2(\Omega). \tag{8}$$

It is important to consider a finite element pair of spaces $\boldsymbol{V}_h \times Q_h$ satisfying an inf–sup condition. One very simple choice would be the stabilized P1–P1 scheme firstly introduced in [29] and widely analysed in [30], in which $\boldsymbol{V}_h$ consists of the space of piecewise (with respect to a triangulation $\mathcal{T}_h$) linear continuous vector valued functions on Ω and the space Q_h consists of piecewise linear continuous scalar valued functions. Other choices would be P2–P1, that is, piecewise quadratic continuous vector valued functions for displacements and piecewise linear continuous scalar valued functions for pressure, widely studied by Murad and Loula [31–33]; or the so-called MINI element [30] in which $\boldsymbol{V}_h = \boldsymbol{V}_l \oplus \boldsymbol{V}_b$, where $\boldsymbol{V}_l$ is the space of piecewise linear continuous vector valued functions and $\boldsymbol{V}_b$ is the space of bubble functions. Discrete inf–sup stability conditions and convergence results for the stabilized P1–P1 and the MINI element were recently derived in [30].

The semi-discretized problem can be written as follows: Find $(\boldsymbol{u}_h(t), p_h(t)) \in C^1([0,T];\boldsymbol{V}_h) \times C^1([0,T];Q_h)$ such that

$$a(\boldsymbol{u}_h(t), \boldsymbol{v}_h) - \alpha(p_h(t), \operatorname{div}\boldsymbol{v}_h) = (\rho\boldsymbol{g}, \boldsymbol{v}_h), \ \forall\, \boldsymbol{v}_h \in \boldsymbol{V}_h, \ t \in (0,T], \tag{9}$$

$$\alpha(\operatorname{div}\partial_t\boldsymbol{u}_h(t), q_h) + \frac{1}{\beta}(\partial_t p_h(t), q_h) + b(p_h(t), q_h) = (f_h, q_h) + (\boldsymbol{K}\mu_f^{-1}\rho_f\boldsymbol{g}, \nabla q_h), \ \forall q_h \in Q_h, \ t \in (0,T], \tag{10}$$

giving rise to the following fully coupled algebraic/differential equations system,

$$\begin{bmatrix} 0 & 0 \\ B & M_p \end{bmatrix} \begin{bmatrix} \dot{u}_h \\ \dot{p}_h \end{bmatrix} + \begin{bmatrix} A & B^t \\ 0 & -C \end{bmatrix} \begin{bmatrix} u_h \\ p_h \end{bmatrix} = \begin{bmatrix} g_h \\ \widetilde{f}_h \end{bmatrix}, \tag{11}$$

where we have denoted $\dot{u}_h \equiv \partial_t \boldsymbol{u}_h(t)$ and $\dot{p}_h \equiv \partial_t p_h(t)$.

Remark 1. We wish to emphasize that the solver based on the fixed-stress splitting method, which we are going to propose in this work, can be applied to other different discretizations of the problem, for example, mixed finite-elements or finite volume schemes.

3. The fixed-stress splitting algorithm for the semi-discretized problem

A popular alternative for solving the poroelasticity problem in an iterative manner is the so-called fixed-stress splitting method. This scheme is based on solving the flow equation by adding the stabilization term $L\frac{\partial p}{\partial t}$ on both sides of the equation:

$$\left(\frac{1}{\beta} + L\right)\frac{\partial p}{\partial t} - \nabla \cdot \left(\frac{1}{\mu_f}\boldsymbol{K}\left(\nabla p - \rho_f \boldsymbol{g}\right)\right) = f - \alpha \frac{\partial}{\partial t}(\nabla \cdot \mathbf{u}) + L\frac{\partial p}{\partial t}, \tag{12}$$

where L is a parameter to fix, and then, the mechanics problem is solved using updated pressure. For more details about the algorithm and how to fix parameter L, see [11,13,14,16]. Thus, given an initial guess $(\boldsymbol{u}_h^0(t), p_h^0(t))$, the fixed-stress splitting algorithm gives us a sequence of approximations $(\boldsymbol{u}_h^i(t), p_h^i(t))$, $i \geq 1$ as follows:

Step 1: Given $(\boldsymbol{u}_h^{i-1}(t), p_h^{i-1}(t)) \in C^1([0,T]; \boldsymbol{V}_h) \times C^1([0,T]; Q_h)$, find $p_h^i(t) \in C^1([0,T]; Q_h)$ such that

$$\begin{aligned} &(\frac{1}{\beta} + L)(\partial_t p_h^i(t), q_h) + b(p_h^i(t), q_h) + \alpha(\operatorname{div} \partial_t \boldsymbol{u}_h^{i-1}(t), q_h) = L(\partial_t p_h^{i-1}(t), q_h) + \\ &\qquad (f_h, q_h) + (\boldsymbol{K}\mu_f^{-1}\rho_f \boldsymbol{g}, \nabla q_h), \quad \forall\, q_h \in Q_h,\ t \in (0,T], \text{ and} \\ &p_h^i(0) = p_0. \end{aligned} \tag{13}$$

Step 2: Given $p_h^i(t) \in C^1([0,T]; Q_h)$, find $\boldsymbol{u}_h^i(t) \in C^1([0,T]; \boldsymbol{V}_h)$ such that

$$a(\boldsymbol{u}_h^i(t), \boldsymbol{v}_h) = \alpha(p_h^i(t), \operatorname{div} \boldsymbol{v}_h) + (\rho \boldsymbol{g}, \boldsymbol{v}_h), \quad \forall\, \boldsymbol{v}_h \in \boldsymbol{V}_h,\ t \in (0,T]. \tag{14}$$

The algorithm starts with an initial approximation $(\boldsymbol{u}_h^0(t), p_h^0(t))$ defined along the whole time-interval. A natural choice is to take this approximation constant and equal to the values specified by the initial condition, $(\boldsymbol{u}_h^0(t), p_h^0(t)) = (\boldsymbol{u}_0, p_0)$, $t \in (0,T]$.

3.1. Convergence analysis in the semi-discrete case

Let $\delta \boldsymbol{u}_h^i(t) = \boldsymbol{u}_h^i(t) - \boldsymbol{u}_h^{i-1}(t)$ and $\delta p_h^i(t) = p_h^i(t) - p_h^{i-1}(t)$ denote the difference between two successive approximations for displacements and for pressure, respectively.

Theorem 1. *The fixed-stress splitting method given in (13)–(14) converges for any* $L \geq \frac{\alpha^2}{2(\frac{2G}{d}+\lambda)}$. *There holds*

$$\int_0^t \|\partial_t \delta p_h^i(s)\|^2\, ds \leq \frac{L}{(\frac{1}{\beta} + L)} \int_0^t \|\partial_t \delta p_h^{i-1}(s)\|^2\, ds. \tag{15}$$

Proof. We take the time derivative of the difference of two successive iterates of the mechanics equation (14) and test the resulting equation by $\mathbf{v}_h = \partial_t \delta \mathbf{u}_h^{i-1}$ to get

$$2G(\boldsymbol{\varepsilon}(\partial_t \delta \mathbf{u}_h^i), \boldsymbol{\varepsilon}(\partial_t \delta \mathbf{u}_h^{i-1})) + \lambda(\nabla \cdot \partial_t \delta \mathbf{u}_h^i, \nabla \cdot \partial_t \delta \mathbf{u}_h^{i-1}) - \alpha(\partial_t \delta p_h^i, \nabla \cdot \partial_t \delta \mathbf{u}_h^{i-1}) = 0. \tag{16}$$

By taking the difference between two successive iterates of the flow Eq. (13) and testing with $q_h = \partial_t \delta p_h^i$, we obtain

$$\frac{1}{\beta}\|\partial_t \delta p_h^i\|^2 + L(\partial_t(\delta p_h^i - \delta p_h^{i-1}), \partial_t \delta p_h^i) + b(\delta p_h^i, \partial_t \delta p_h^i) + \alpha(\nabla \cdot \partial_t \delta \mathbf{u}_h^{i-1}, \partial_t \delta p_h^i) = 0. \tag{17}$$

After summing up Eqs. (16) and (17), and using the identities

$$(\sigma, \xi) = \frac{1}{4}\|\sigma + \xi\|^2 - \frac{1}{4}\|\sigma - \xi\|^2, \quad (\sigma - \xi, \sigma) = \frac{1}{2}\left(\|\sigma\|^2 - \|\xi\|^2 + \|\sigma - \xi\|^2\right), \tag{18}$$

one has

$$\frac{G}{2}\|\boldsymbol{\varepsilon}(\partial_t \delta \mathbf{u}_h^i + \partial_t \delta \mathbf{u}_h^{i-1})\|^2 + \frac{\lambda}{4}\|\nabla \cdot (\partial_t \delta \mathbf{u}_h^i + \partial_t \delta \mathbf{u}_h^{i-1})\|^2 + \frac{1}{\beta}\|\partial_t \delta p_h^i\|^2$$

$$+\frac{1}{2}\frac{d}{dt}\|\delta p_h^i\|_B^2+\frac{L}{2}(\|\partial_t\delta p_h^i\|^2-\|\partial_t\delta p_h^{i-1}\|^2+\|\partial_t\delta p_h^i-\partial_t\delta p_h^{i-1}\|^2)$$
$$=\frac{G}{2}\|\boldsymbol{\varepsilon}(\partial_t\delta\mathbf{u}_h^i-\partial_t\delta\mathbf{u}_h^{i-1})\|^2+\frac{\lambda}{4}\|\nabla\cdot(\partial_t\delta\mathbf{u}_h^i-\partial_t\delta\mathbf{u}_h^{i-1})\|^2. \tag{19}$$

Next, we consider the time derivative of the difference of two successive iterates of the mechanics equation (14) and test by $\mathbf{v}_h=\partial_t\delta\mathbf{u}_h^i-\partial_t\delta\mathbf{u}_h^{i-1}$. By applying the Cauchy–Schwarz inequality, it follows

$$\|\nabla\cdot(\partial_t\delta\mathbf{u}_h^i-\partial_t\delta\mathbf{u}_h^{i-1})\|\leq\frac{\alpha}{\frac{2G}{d}+\lambda}\|\partial_t\delta p_h^i-\partial_t\delta p_h^{i-1}\|. \tag{20}$$

Inserting equality (16) into Eq. (19) and by applying Cauchy–Schwarz and (20) inequalities, we obtain

$$\frac{G}{2}\|\boldsymbol{\varepsilon}(\partial_t\delta\mathbf{u}_h^i+\partial_t\delta\mathbf{u}_h^{i-1})\|^2+\frac{\lambda}{4}\|\nabla\cdot(\partial_t\delta\mathbf{u}_h^i+\partial_t\delta\mathbf{u}_h^{i-1})\|^2+\frac{1}{\beta}\|\partial_t\delta p_h^i\|^2$$
$$+\frac{1}{2}\frac{d}{dt}\|\delta p_h^i\|_B^2+\frac{L}{2}(\|\partial_t\delta p_h^i\|^2+\|\partial_t\delta p_h^i-\partial_t\delta p_h^{i-1}\|^2)$$
$$\leq\frac{L}{2}\|\partial_t\delta p_h^{i-1}\|^2+\frac{\alpha^2}{4(\frac{2G}{d}+\lambda)}\|\partial_t\delta p_h^i-\partial_t\delta p_h^{i-1}\|^2.$$

Discarding the first three positive terms, taking $L\geq\frac{\alpha^2}{2(\frac{2G}{d}+\lambda)}$, and integrating from 0 to t we finally obtain (15). It implies that the scheme is a contraction. Following the same technique as in [15], from the contractive property of scheme (13)–(14) one can establish that it is convergent and show that the converged quantities satisfy the variational formulation of the semi-discretized problem (9)–(10). This completes the proof. □

Remark 2. It is easy to see that the fixed-stress splitting method in the semi-discrete case is an iterative method based on a suitable splitting for solving the differential/algebraic equation system (11). In detail, the iterative method can be written in the form

$$\begin{bmatrix}0&0\\0&(1+L)M_p\end{bmatrix}\begin{bmatrix}\dot{u}_h^i\\\dot{p}_h^i\end{bmatrix}+\begin{bmatrix}A&B^t\\0&-C\end{bmatrix}\begin{bmatrix}u_h^i\\p_h^i\end{bmatrix}=\begin{bmatrix}0&0\\-B&LM_p\end{bmatrix}\begin{bmatrix}\dot{u}_h^{i-1}\\\dot{p}_h^{i-1}\end{bmatrix}+\begin{bmatrix}g_h\\\widetilde{f}_h\end{bmatrix}. \tag{21}$$

4. The parallel-in-time fixed-stress splitting algorithm for the fully discretized problem

4.1. Parallel-in-time algorithm

For time discretization we use the backward Euler method on a uniform partition $\{t_0,t_1,\ldots,t_N\}$ of the time interval $(0,T]$ with constant time-step size τ, $N\tau=T$. Then, we have the following fully discrete scheme corresponding to (9)–(10): For $n=1,2,\ldots,N$, find $(\boldsymbol{u}_h^n,p_h^n)\in\boldsymbol{V}_h\times Q_h$ such that

$$a(\boldsymbol{u}_h^n,\boldsymbol{v}_h)-\alpha(p_h^n,\operatorname{div}\boldsymbol{v}_h)=(\rho\boldsymbol{g},\boldsymbol{v}_h),\quad\forall\,\boldsymbol{v}_h\in\boldsymbol{V}_h, \tag{22}$$
$$\alpha(\operatorname{div}\bar{\partial}_t\boldsymbol{u}_h^n,q_h)+\frac{1}{\beta}(\bar{\partial}_t p_h^n,q_h)+b(p_h^n,q_h)=(f_h^n,q_h)+(\boldsymbol{K}\mu_f^{-1}\rho_f\boldsymbol{g},\nabla q_h),\ \forall\,q_h\in Q_h, \tag{23}$$

where $\bar{\partial}_t\boldsymbol{u}_h^n:=(\boldsymbol{u}_h^n-\boldsymbol{u}_h^{n-1})/\tau$ and $\bar{\partial}_t p_h^n:=(p_h^n-p_h^{n-1})/\tau$.

We now discuss a partially parallel-in-time version of the fixed-stress splitting method. This algorithm arises in a natural way from the iterative method (21) by discretizing in time. In this way, given an initial guess $\{(\boldsymbol{u}_h^{n,0},p_h^{n,0}),n=0,1,\ldots,N\}$, the new fixed-stress splitting algorithm gives us a sequence of approximations $\{(\boldsymbol{u}_h^{n,i},p_h^{n,i}),n=0,1,\ldots,N\}$, $i\geq1$, as follows:

Step 1: Let $p_h^{0,i}=p_0$, for all $i\geq0$. For $i\geq1$, given $\{(\boldsymbol{u}_h^{n,i-1},p_h^{n,i-1}),n=0,1,\ldots,N\}$, find $p_h^{n,i}\in Q_h$, $n=1,\ldots,N$, such that $\forall\,q_h\in Q_h$ there holds

$$\left(\frac{1}{\beta}+L\right)\left(\frac{p_h^{n,i}-p_h^{n-1,i}}{\tau},q_h\right)+b(p_h^{n,i},q_h)=\alpha\left(\operatorname{div}\frac{\boldsymbol{u}_h^{n,i-1}-\boldsymbol{u}_h^{n-1,i-1}}{\tau},q_h\right)$$
$$+L\left(\frac{p_h^{n,i-1}-p_h^{n-1,i-1}}{\tau},q_h\right)+(f_h^n,q_h)+(\boldsymbol{K}\mu_f^{-1}\rho_f\boldsymbol{g},\nabla q_h). \tag{24}$$

Step 2: Given $p_h^{n,i}\in Q_h$, $n=1,\ldots,N$, find $\boldsymbol{u}_h^{n,i}\in\boldsymbol{V}_h$, $n=1,\ldots,N$, such that

$$a(\boldsymbol{u}_h^{n,i},\boldsymbol{v}_h)=\alpha(p_h^{n,i},\operatorname{div}\boldsymbol{v}_h)+(\rho\boldsymbol{g},\boldsymbol{v}_h),\quad\forall\,\boldsymbol{v}_h\in\boldsymbol{V}_h. \tag{25}$$

Remark 3. We wish to emphasize that the proposed method is partially parallel-in-time in contrast to the classical sequential fixed-stress splitting method based on time-stepping. Notice that in the Step 2 of the new algorithm, $N-1$ independent elliptic problems can be easily solved in parallel. Also the flow problem in Step 1 can be solved by using some of the well-known parallel-in-time methods for parabolic problems mentioned in the introduction: PFASST, parareal, WRMG, MGRIT, or STMG. In this work, however, this step is implemented in a classical (non-parallel) form to keep the implementation simple, since the aim of this research is to present this new version of the fixed-stress iteration.

Remark 4 (*A Fully Parallel-in-time Fixed-stress Scheme*)**.** The scheme (24)–(25) can be made fully parallel by replacing everywhere $p^{n-1,i}$ with $p^{n-1,i-1}$. The following scheme arises:

Step 1: Let $p_h^{0,i}=p_0$, for all $i\geq 0$. For $i\geq 1$, given $\{(\boldsymbol{u}_h^{n,i-1},p_h^{n,i-1}),\, n=0,1,\ldots,N\}$, find $p_h^{n,i}\in Q_h$, $n=1,\ldots,N$, such that $\forall\, q_h\in Q_h$ there holds

$$\left(\frac{1}{\beta}+L\right)\left(\frac{p_h^{n,i}-p_h^{n-1,i-1}}{\tau},q_h\right)+b(p_h^{n,i},q_h)=\alpha\left(\operatorname{div}\frac{\boldsymbol{u}_h^{n,i-1}-\boldsymbol{u}_h^{n-1,i-1}}{\tau},q_h\right)$$
$$+L\left(\frac{p_h^{n,i-1}-p_h^{n-1,i-1}}{\tau},q_h\right)+(f_h^n,q_h)+(\boldsymbol{K}\mu_f^{-1}\rho_f\boldsymbol{g},\nabla q_h). \tag{26}$$

Step 2: Given $p_h^{n,i}\in Q_h$, $n=1,\ldots,N$, find $\boldsymbol{u}_h^{n,i}\in\boldsymbol{V}_h$, $n=1,\ldots,N$, such that

$$a(\boldsymbol{u}_h^{n,i},\boldsymbol{v}_h)=\alpha(p_h^{n,i},\operatorname{div}\boldsymbol{v}_h)+(\rho\boldsymbol{g},\boldsymbol{v}_h),\quad\forall\,\boldsymbol{v}_h\in\boldsymbol{V}_h. \tag{27}$$

The fully parallel-in-time scheme needs for the numerical examples considered more iterations (for the same tuning parameter) than the partially parallel scheme. A throughout analysis of this second scheme is beyond the aim of this paper.

4.2. Convergence analysis of the partially parallel-in-time scheme

Let $\delta\boldsymbol{u}_h^{n,i}=\boldsymbol{u}_h^{n,i}-\boldsymbol{u}_h^{n,i-1}$ and $\delta p_h^{n,i}=p_h^{n,i}-p_h^{n,i-1}$ denote the difference between two succesive approximations for displacements and for pressure, respectively.

Theorem 2. *The fixed-stress splitting method given in (24)–(25) is convergent for any stabilization parameter* $L\geq\frac{\alpha^2}{2(\frac{2G}{d}+\lambda)}$. *There holds*

$$\sum_{n=1}^{N}\tau\|\bar\partial_t\delta p_h^{n,i}\|^2\leq\frac{L}{(\frac{1}{\beta}+L)}\sum_{n=1}^{N}\tau\|\bar\partial_t\delta p_h^{n,i-1}\|^2. \tag{28}$$

Proof. Similarly to the proof of Theorem 1, we take the difference of two successive iterates of the mechanics equation (25) and the flow equation (24), and test the resulting equations by $\mathbf{v}_h=\bar\partial_t\delta\mathbf{u}_h^{n,i-1}$ and $q_h=\bar\partial_t\delta p_h^{n,i}$ respectively to get for $n=1,2,\ldots,N$,

$$2G(\boldsymbol{\varepsilon}(\bar\partial_t\delta\mathbf{u}_h^{n,i}),\boldsymbol{\varepsilon}(\bar\partial_t\delta\mathbf{u}_h^{n,i-1}))+\lambda(\nabla\cdot\bar\partial_t\delta\mathbf{u}_h^{n,i},\nabla\cdot\bar\partial_t\delta\mathbf{u}_h^{n,i-1})$$
$$-\alpha(\bar\partial_t\delta p_h^{n,i},\nabla\cdot\bar\partial_t\delta\mathbf{u}_h^{n,i-1})=0. \tag{29}$$

$$\frac{1}{\beta}\|\bar\partial_t\delta p_h^{n,i}\|^2+L(\bar\partial_t(\delta p_h^{n,i}-\delta p_h^{n,i-1}),\bar\partial_t\delta p_h^{n,i})+b(\delta p_h^{n,i},\bar\partial_t\delta p_h^{n,i})$$
$$+\alpha(\nabla\cdot\bar\partial_t\delta\mathbf{u}_h^{n,i-1},\bar\partial_t\delta p_h^{n,i})=0. \tag{30}$$

After summing up Eqs. (29) and (30), and using the identities in (18) one has

$$\frac{G}{2}\|\boldsymbol{\varepsilon}(\bar\partial_t\delta\mathbf{u}_h^{n,i}+\bar\partial_t\delta\mathbf{u}_h^{n,i-1})\|^2+\frac{\lambda}{4}\|\nabla\cdot(\bar\partial_t\delta\mathbf{u}_h^{n,i}+\bar\partial_t\delta\mathbf{u}_h^{n,i-1})\|^2+\frac{1}{\beta}\|\bar\partial_t\delta p_h^{n,i}\|^2$$
$$+\frac{L}{2}(\|\bar\partial_t\delta p_h^{n,i}\|^2+\|\bar\partial_t\delta p_h^{n,i}-\bar\partial_t\delta p_h^{n,i-1}\|^2)+\frac{1}{2\tau}(\|\delta p_h^{n,i}\|_B^2+\|\delta p_h^{n,i}-\delta p_h^{n-1,i}\|_B^2)$$
$$=\frac{G}{2}\|\boldsymbol{\varepsilon}(\bar\partial_t\delta\mathbf{u}_h^{n,i}-\bar\partial_t\delta\mathbf{u}_h^{n,i-1})\|^2+\frac{\lambda}{4}\|\nabla\cdot(\bar\partial_t\delta\mathbf{u}_h^{n,i}-\bar\partial_t\delta\mathbf{u}_h^{n,i-1})\|^2$$
$$+\frac{L}{2}\|\bar\partial_t\delta p_h^{n,i-1}\|^2+\frac{1}{2\tau}\|\delta p_h^{n-1,i}\|_B^2. \tag{31}$$

Next, we consider the difference of two successive iterates of the mechanics equation (25) and test by $\mathbf{v}_h = \bar{\partial}_t \delta \mathbf{u}_h^{n,i} - \bar{\partial}_t \delta \mathbf{u}_h^{n,i-1}$ to get

$$\begin{aligned} 2G\|\boldsymbol{\varepsilon}(\bar{\partial}_t \delta \mathbf{u}_h^{n,i} - \bar{\partial}_t \delta \mathbf{u}_h^{n,i-1})\|^2 + \lambda \|\nabla \cdot (\bar{\partial}_t \delta \mathbf{u}_h^{n,i} - \bar{\partial}_t \delta \mathbf{u}_h^{n,i})\|^2 \\ = \alpha(\bar{\partial}_t \delta p_h^{n,i} - \bar{\partial}_t \delta p_h^{n,i-1}, \nabla \cdot (\bar{\partial}_t \delta \mathbf{u}_h^{n,i} - \bar{\partial}_t \delta \mathbf{u}_h^{n,i-1})). \end{aligned} \tag{32}$$

From this equality, by applying Cauchy–Schwarz inequality, it is easy to see

$$\|\nabla \cdot (\bar{\partial}_t \delta \mathbf{u}_h^{n,i} - \bar{\partial}_t \delta \mathbf{u}_h^{n,i-1})\| \leq \frac{\alpha}{\frac{2G}{d} + \lambda} \|\bar{\partial}_t \delta p_h^{n,i} - \bar{\partial}_t \delta p_h^{n,i-1}\|. \tag{33}$$

Inserting equality (32) into Eq. (31) and by applying Cauchy–Schwarz inequality and (33), we obtain

$$\begin{aligned} &\frac{G}{2}\|\boldsymbol{\varepsilon}(\bar{\partial}_t \delta \mathbf{u}_h^{n,i} + \bar{\partial}_t \delta \mathbf{u}_h^{n,i-1})\|^2 + \frac{\lambda}{4}\|\nabla \cdot (\bar{\partial}_t \delta \mathbf{u}_h^{n,i} + \bar{\partial}_t \delta \mathbf{u}_h^{n,i-1})\|^2 + \frac{1}{\beta}\|\bar{\partial}_t \delta p_h^{n,i}\|^2 \\ &+ \frac{L}{2}(\|\bar{\partial}_t \delta p_h^{n,i}\|^2 + \|\bar{\partial}_t \delta p_h^{n,i} - \bar{\partial}_t \delta p_h^{n,i-1}\|^2) + \frac{1}{2\tau}(\|\delta p_h^{n,i}\|_B^2 + \|\delta p_h^{n,i} - \delta p_h^{n-1,i}\|_B^2) \\ &\quad \leq \frac{L}{2}\|\bar{\partial}_t \delta p_h^{n,i-1}\|^2 + \frac{1}{2\tau}\|\delta p_h^{n-1,i}\|_B^2 + \frac{\alpha^2}{4(\frac{2G}{d} + \lambda)}\|\bar{\partial}_t \delta p_h^{n,i} - \bar{\partial}_t \delta p_h^{n,i-1}\|^2. \end{aligned}$$

Discarding positive terms, taking $L \geq \frac{\alpha^2}{2(\frac{2G}{d}+\lambda)}$, and summing up from $n = 1$ to N, we finally obtain (28). This implies that the scheme is a contraction and therefore convergent. This completes the proof. □

Remark 5. Notice that the values of parameter L turn out to be the same as in the classical fixed-stress splitting scheme.

5. Numerical experiments

In this section, we present two numerical experiments with the purpose of illustrating the performance of the partially parallel-in-time fixed-stress splitting (PFS) method described in Section 4. We compare the PFS method with the classical fixed-stress splitting (FS), see e.g. [14]. As first test problem, we use Mandel's problem, which is a well-established 2D benchmark problem with a known analytical solution [34,35]. This problem is very often used in the community for verifying the implementation and the performance of the numerical schemes, see e.g. [5,10,30,36]. As a second test, we use a three-dimensional problem on a L-shaped domain with time dependent boundary conditions, see e.g. [16,37]. For both numerical experiments, a stabilized P1–P1 scheme has been used here for spatial discretization. However, we would like to mention that any stable pair could be considered instead.

The performance of both methods, FS and PFS, is similar if they are running sequentially. One of the main differences between the two methods, however, is the memory consumption. While FS uses a fixed memory amount independent to the time step, the PFS uses a memory amount proportional to the number of time steps. This is because PFS requires to store each variable for all time levels. However, to have access to the variables at every time step allows that several tasks of the implementation can run in parallel, mainly the solution of the mechanics problem at Eq. (25) for each time level and the assembly of the right hand sides at each time step.

The schemes were implemented in the open-source software package deal.II [38] configured for multithreading. The number of threads running in parallel simultaneously can be specified between 1 and 32 in a system of 4×8 cores Intel Xeon 2.7 GHz. In this regard, PFS is set to use one thread to solve the flow problem and up to 32 threads to assemble the right hand side, impose the boundary conditions, solve the mechanics problem and write the output results at each time step, while FS is set to use only one thread for the same tasks. In both numerical experiments, we report the absolute wall time of each method. We would like to mention that all the linear systems are solved by using a direct solver for simplicity in the implementation. However, a preconditioned conjugate gradient would be a good alternative for the efficient solution of such systems.

5.1. Test case 1: Mandel's problem

Mandel's problem consists of a poroelastic slab of extent $2a$ in the x-direction, $2b$ in the y-direction, and infinitely long in the z-direction, and is sandwiched between two rigid impermeable plates (see Fig. 1a). At time $t = 0$, a uniform vertical load of magnitude $2F$ is applied and an equal, but upward force is applied to the bottom plate. This load is supposed to remain constant. The domain is free to drain and stress-free at $x = \pm a$. Gravity is neglected.

For the numerical solution, the symmetry of the problem allows us to use a quarter of the physical domain as computational domain (see Fig. 1b). Moreover, the rigid plate condition is enforced by adding constrained equations so that vertical displacement $u_y(b, t)$ on the top is equal to a known constant value.

The application of a load ($2F$) causes an instantaneous and uniform pressure increase throughout the domain [39]; this is predicted theoretically [34] and it can be used as an initial condition

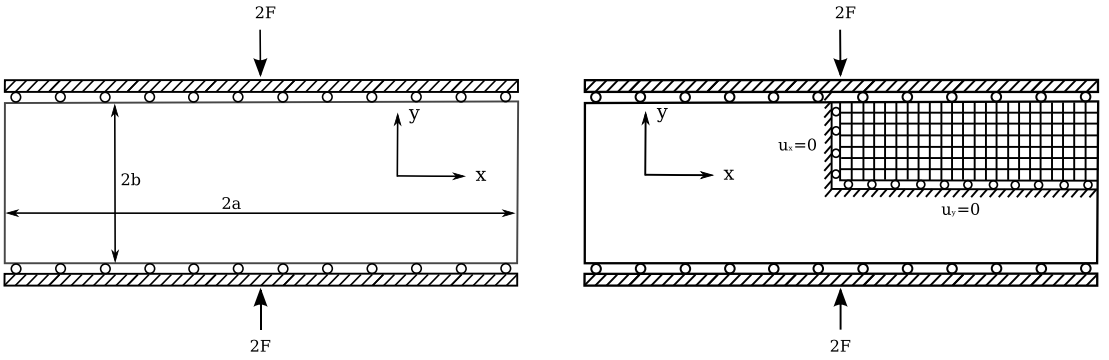

(a) Mandel's problem physical domain.

(b) Mandel's problem quarter domain.

Fig. 1. Mandel's problem.

Table 1
Boundary conditions for Mandel's problem.

Boundary	Flow	Mechanics
$x = 0$	$\boldsymbol{q} \cdot \mathbf{n} = 0$	$\boldsymbol{u} \cdot \mathbf{n} = 0$
$y = 0$	$\boldsymbol{q} \cdot \mathbf{n} = 0$	$\boldsymbol{u} \cdot \mathbf{n} = 0$
$x = a$	$p = 0$	$\sigma \cdot \mathbf{n} = 0$
$y = b$	$\boldsymbol{q} \cdot \mathbf{n} = 0$	$\sigma_{12} = 0; \boldsymbol{u} \cdot \mathbf{n} = u_y(b, t)$

Table 2
Input parameter for Mandel's problem.

Symbol	Quantity	Value	Symbol	Quantity	Value
a	Dimension in x	100 m	b	Dimension in y	10 m
K	Permeability	100 D	μ_f	Dynamic viscosity	10 cp
α	Biot's constant	1.0	β	Biot's modulus	1.65×10^{10} Pa
ν	Poisson's ratio	0.4	E	Young's modulus	5.94×10^{9} Pa
B	Skempton coefficient	0.83333	ν_u	Undrained Poisson's ratio	0.44
c	Diffusivity coefficient	46.526 m^2/s	F	Force intensity	6.8×10^{8} N/m
h_x	Grid spacing in x	2.5 m	h_y	Grid spacing in y	$h_x/10$
τ	Time step	1 s	T	Total simulation time	32 s

$$p(x, y, 0) = \frac{FB(1+\nu_u)}{3a},$$
$$\boldsymbol{u}(x, y, 0) = \left(\tfrac{F\nu_u x}{2G}, \quad \tfrac{-Fb(1-\nu_u)y}{2Ga}\right)^{\top},$$

where B is the Skempton coefficient and $\nu_u = \frac{3\nu+B(1-2\nu)}{3-B(1-2\nu)}$ is the undrained Poisson ratio.

The boundary conditions are specified in Table 1 and the input parameters for Mandel's problem are listed in Table 2. For all cases, the following stopping criterion is used $\|\delta p^{n,i}\| + \|\delta \boldsymbol{u}^{n,i}\| \leq 10^{-8}$.

In Fig. 2, the numerical and the analytical solutions of Mandel's problem are depicted for different values of time. There is a very good match between both solutions for all cases. Moreover, the results demonstrate the Mandel–Cryer effect, first showing a pressure raise during the first 20 s and then, a sudden dissipation throughout the domain.

The number of iterations for PFS and FS are reported in Fig. 3 for different values of parameter L and various values of ν. We remark a very similar behaviour of the two methods, with the optimal stabilization parameter L being in this case the physical one $L_{phy} := \alpha^2/\left(\frac{2G}{d} + \lambda\right)$, see e.g. [10,13,14].

We remark that the mesh size and the time step τ do not influence the number of iterations. This can be seen in Table 3, where we provide the number of iterations for both algorithms, varying the space and time discretization parameters.

Further, Fig. 4 shows the wall time for PFS reported for different mesh sizes and time steps (see Figs. 4a and 4b, respectively). The figure shows how the wall time decreases proportionally to the number of threads being used. However, the wall time does not decrease substantially when using more than 16 threads because of the sequential tasks that the code still has to perform (for instance solving the flow problem).

Table 4 shows the wall time for both FS and PFS. Since FS is running sequentially, it is set to use one thread. As expected, we clearly observe that PFS consumes around 20% of the wall time of FS. Furthermore, the more time steps are considered, the more this time reduction increases.

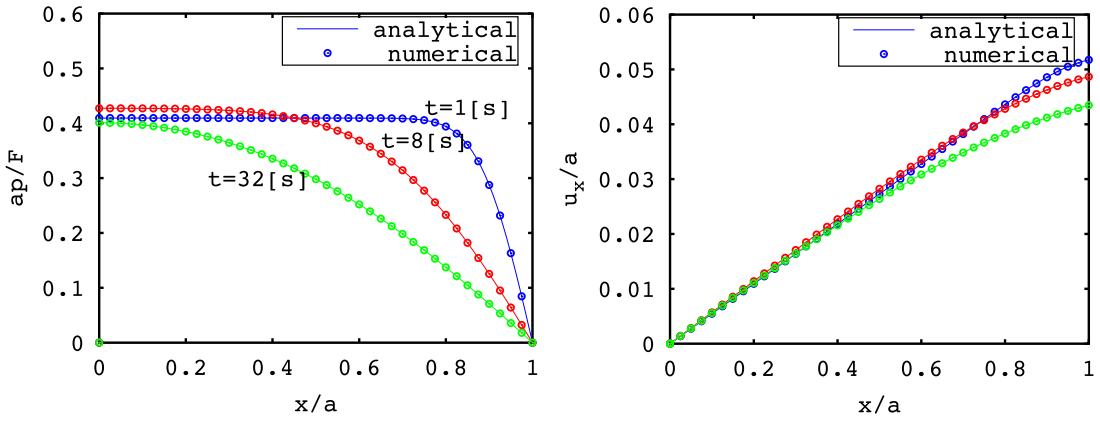

(a) Pressure solutions. (b) Displacement solutions.

Fig. 2. Comparison of numerical and analytical solutions of the (a) pore pressure and (b) displacements for Mandel's problem in different times with $\nu = 0.2$.

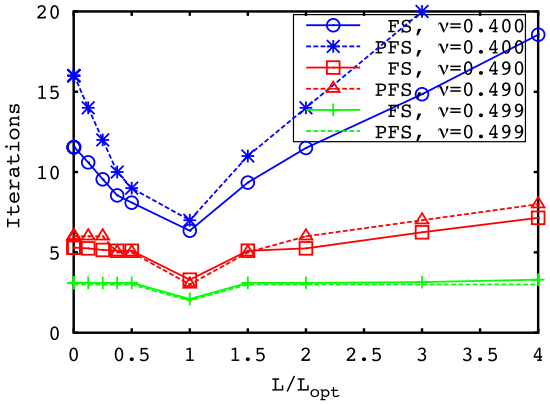

Fig. 3. Performance of the splitting schemes PFS and FS for different values of L, $\tau = 1[s]$, $h_x = 2.5$ [m]. Both schemes have the same optimum value $L_{opt} = L_{phy}$.

Table 3
Number of iterations for different values of τ, h_x, ν.

$\nu = 0.49999$, $h_x = 6.25$ [m].			$\nu = 0.499$, $\tau = 0.5$ [s].		
τ [s]	PFS	FS	h_x [m]	PFS	FS
1.000	2	2.10	12.5000	3	3.20
0.500	2	2.03	6.2500	3	3.20
0.250	2	2.02	3.1250	3	3.19
0.125	2	2.01	1.5625	3	3.19

5.2. Test case 2: Poroelastic L-shaped problem

The second numerical example is taken from [16,37]. It consists of a poroelastic L-shaped domain $\Omega \subset \mathbb{R}^3$ (see Fig. 5), with the long and short edges in the x and y-direction being 1 [m] and 0.5 [m] respectively and an extrusion of 0.5 [m] in the z-direction. The boundary conditions, numerical solution and input parameters are shown in Figs. 5–6 and Table 5. Gravity is neglected.

The number of iterations for the PFS method and the classical FS method are reported in Fig. 7 for different values of parameters L and ν. The methods show again a very similar behaviour.

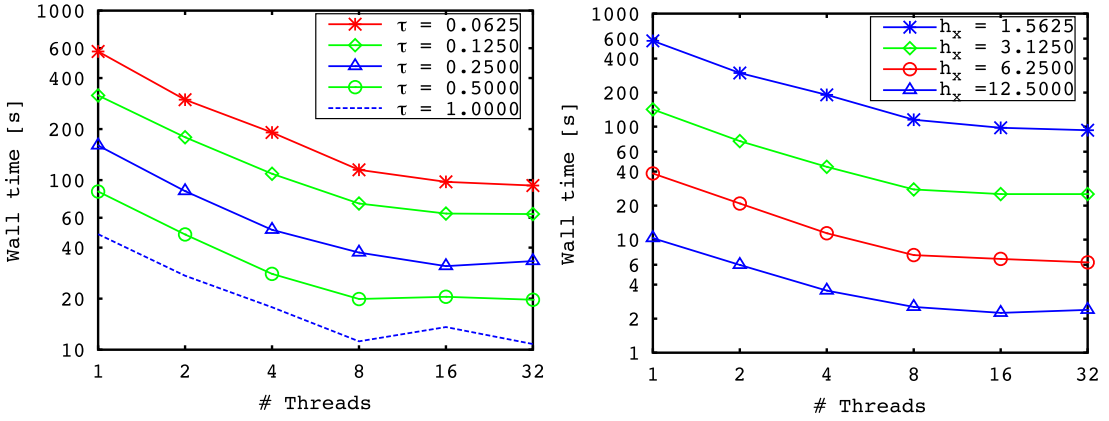

(a) Wall time for different time step sizes; $h_x = 1.5625[m]$.

(b) Wall time for different mesh sizes; $\tau = 0.0625[s]$.

Fig. 4. Wall time for different discretization parameters in space and time (first test).

Table 4
Wall time of FS/PFS for different time step sizes; $h_x = 6.25$ [m].

	τ [s]	1.0	0.5	0.25	0.125	0.0625
Method	# Threads	Wall time [s]				
FS	1	43.3	78.6	146.0	281.0	499.0
PFS	1	48.0	85.7	160.0	316.0	574.0
	2	27.3	47.8	86.1	179.0	298.0
	4	17.8	28.0	50.9	109.0	191.0
	8	11.2	19.9	37.4	72.8	115.0
	16	13.6	20.5	31.1	63.5	97.7
	32	10.8	19.7	33.3	63.1	92.9

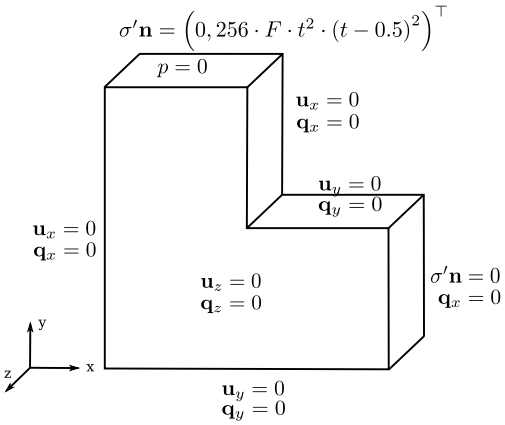

Fig. 5. L-shaped domain and boundary conditions (symmetric in the z-direction).

We remark again that the mesh size and the time step do not influence the number of iterations. This can be seen in Table 6, where we provide the number of iterations for both algorithms, varying the space and time discretization parameters.

Fig. 8 shows the wall time of PFS for different time steps and mesh sizes. Again, we observe that as the number of time steps increases the more threads are used the more the PFS reduces the wall time. In Table 7 we report the wall time of FS vs. PFS, observing a similar behaviour as in the first experiment.

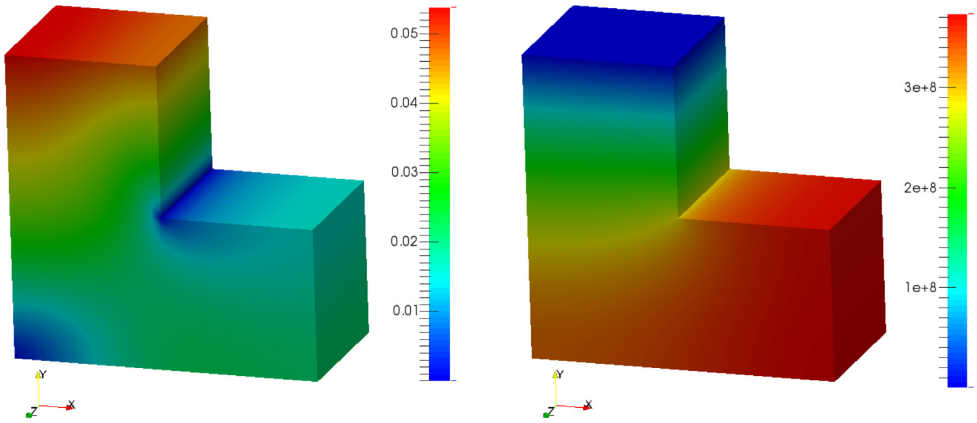

(a) Displacement's magnitude [m]. (b) Pressure [Pa].

Fig. 6. Numerical solutions at $t = 0.26$ and $\nu = 0.4$, $L = L_{phy}$.

Table 5
Input parameters for L-shaped problem.

Symbol	Quantity	Value	Symbol	Quantity	Value
K	Permeability	1000 mD	μ_f	Dynamic viscosity	10 cp
α	Biot's constant	0.9	β	Biot's modulus	100×10^9 Pa
ν	Poisson's ratio	0.4	E	Young's modulus	100×10^9 Pa
h	Grid spacing	$1/2^5$ m	F	Traction force constant	10×10^9 Pa
τ	Time step	0.01 s	T	Total simulation time	0.5 s

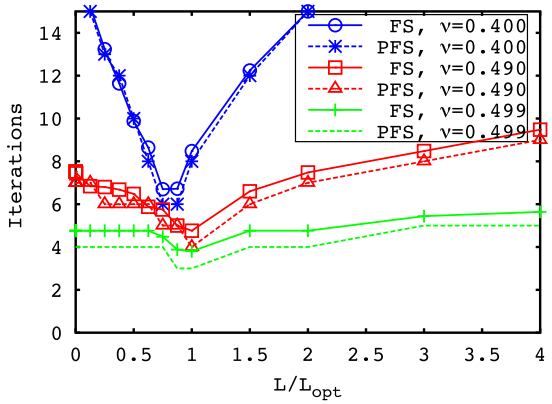

Fig. 7. Performance of the splitting schemes PFS and FS for different values of L, $\tau = 0.02$ [s], $h = 0.03125$ [m], $L_{opt} = \frac{L_{phy}}{2}$.

Table 6
Number of iterations for different values of τ, h, ν.

$\nu = 0.49999$, $h = 0.125$ [m].			$\nu = 0.499$, $\tau = 0.02$ [s].		
τ [s]	PFS	FS	h [m]	PFS	FS
0.050	2	2.80	0.25000	3	3.82
0.020	2	2.84	0.12500	3	3.80
0.010	2	2.94	0.06250	3	3.78
0.005	2	2.97	0.03125	3	3.78

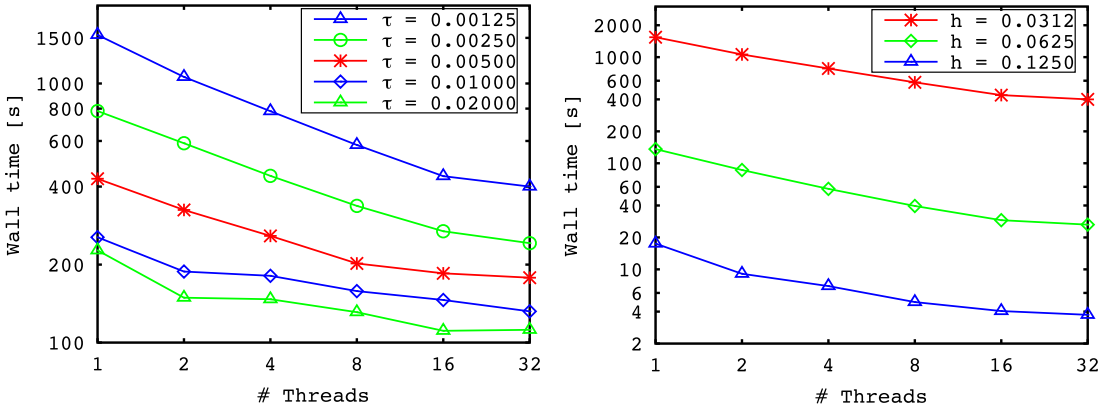

(a) Wall time for different time step sizes; $h = 0.03125[m]$.

(b) Wall time for different time step sizes; $\tau = 0.00125[m]$.

Fig. 8. Wall time for different discretization parameters in space and time (second test).

Table 7
Wall time in seconds of FS/PFS for different time step sizes; $h = 0.0625$ [m].

	τ [s]	0.02	0.01	0.005	0.0025	0.00125
Method	# Trheats	Wall time [s]				
FS	1	10.6	17.1	31.2	63.6	115.0
PFS	1	11.5	19.2	35.5	68.7	136.0
	2	8.5	12.1	22.3	44.1	86.4
	4	7.2	11.7	17.9	30.2	57.4
	8	7.1	8.7	14.7	21.6	39.6
	16	5.7	7.6	11.9	19.3	29.1
	32	6.5	6.2	11.0	16.3	26.4

6. Conclusions

We considered the quasi-static Biot model in the two-field formulation and presented a new fixed-stress type splitting method for solving it. The main benefit of the new method is that the mechanics can be solved in a parallel-in-time manner. We have rigorously analysed the convergence of the proposed method. If the stabilization term L is chosen big enough, the method is shown to be convergent. The theoretical results are indicating a similar behaviour with the classical fixed-stress splitting method (in terms of convergence rate and stabilization parameter size). We further performed numerical tests by using two well-known benchmark problems. The numerical results confirm the theoretical findings. We observe that the new scheme PFS is very efficient (around 20% of the wall time of FS). Nevertheless, the parallel implementation has still to be optimized. A combination of the new scheme with a parallel algorithm for solving the flow (like e.g. PFASST, parareal, WRMG, MGRIT, or STMG) would substantially increase the efficiency.

Acknowledgments

The work of F.A. Radu and K. Kumar was partially supported by the NFR - Toppforsk project TheMSES, Norway, #250223 and Norwegian Academy of Science and Equinor, Norway, through VISTA AdaSim no. 6367. The work of F.J. Gaspar is supported by the European Union's Horizon 2020 research and innovation programme, Spain, under the Marie Sklodowska-Curie grant agreement NO 705402, POROSOS. The research of C. Rodrigo is supported in part by the Spanish project FEDER /MCYT MTM2016-75139-R and the DGA, Spain (Grupo de Referencia APEDIF, ref. E24_17R). We also want to thank the anonymous reviewers for helping us to substantially improve the paper and Dr. Uwe Köcher for his help concerning parallel computing and deal.II.

References

[1] K. Terzaghi, Theoretical Soil Mechanics, Wiley, New York, 1943, http://dx.doi.org/10.1002/9780470172766.
[2] M.A. Biot, General theory of three-dimensional consolidation, J. Appl. Phys. 12 (2) (1941) 155–164, http://dx.doi.org/10.1063/1.1712886.

[3] M.A. Biot, Theory of elasticity and consolidation for a porous anisotropic solid, J. Appl. Phys. 26 (2) (1955) 182–185, http://dx.doi.org/10.1063/1.1721956.
[4] R. Showalter, Diffusion in poro-elastic media, J. Math. Anal. Appl. 251 (1) (2000) 310–340, http://dx.doi.org/10.1006/jmaa.2000.7048.
[5] P. Phillips, M. Wheeler, A coupling of mixed and continuous Galerkin finite element methods for poroelasticity I: the continuous in time case, Comput. Geosci. 11 (2) (2007) 131–144, http://dx.doi.org/10.1007/s10596-007-9045-y.
[6] L. Bergamaschi, M. Ferronato, G. Gambolati, Novel preconditioners for the iterative solution to FE-discretized coupled consolidation equations, Comput. Methods Appl. Mech. Eng. 196 (25) (2007) 2647–2656, http://dx.doi.org/10.1016/j.cma.2007.01.013.
[7] M. Ferronato, L. Bergamaschi, G. Gambolati, Performance and robustness of block constraint preconditioners in finite element coupled consolidation problems, Internat. J. Numer. Methods Engrg. 81 (2010) 381–402, http://dx.doi.org/10.1002/nla.372.
[8] F.J. Gaspar, F.J. Lisbona, C. Oosterlee, R. Wienands, A systematic comparison of coupled and distributive smoothing in multigrid for the poroelasticity system, Numer. Linear Algebra Appl. 11 (2004) 93–113, http://dx.doi.org/10.1002/nla.372.
[9] P. Luo, C. Rodrigo, F.J. Gaspar, C.W. Oosterlee, On an Uzawa smoother in multigrid for poroelasticity equations, Numer. Linear Algebra Appl. 24 (1) (2017) http://dx.doi.org/10.1002/nla.2074.
[10] J. Kim, H.A. Tchelepi, R. Juanes, Stability, accuracy and efficiency of sequential methods for coupled flow and geomechanics, in: The SPE Reservoir Simulation Symposium, Houston, Texas, 2009 SPE 119084. http://dx.doi.org/10.2118/119084-PA.
[11] J. Kim, H.A. Tchelepi, R. Juanes, Stability and convergence of sequential methods for coupled flow and geomechanics: fixed-stress and fixed-strain splits, Comput. Methods Appl. Mech. Eng. 200 (13–16) (2011) 1591–1606, http://dx.doi.org/10.1016/j.cma.2011.02.011.
[12] J. Kim, H.A. Tchelepi, R. Juanes, Stability and convergence of sequential methods for coupled flow and geomechanics: Drained and undrained splits, Comput. Methods Appl. Mech. Eng. 200 (23–24) (2011) 2094–2116, http://dx.doi.org/10.1016/j.cma.2010.12.022.
[13] A. Mikelić, M.F. Wheeler, Convergence of iterative coupling for coupled flow and geomechanics, Comput. Geosci. (17) (2013) 455–461, http://dx.doi.org/10.1007/s10596-012-9318-y.
[14] J.W. Both, M. Borregales, J.M. Nordbotten, K. Kumar, F.A. Radu, Robust fixed stress splitting for Biot's equations in heterogeneous media, Appl. Math. Lett. 68 (2017) 101–108, http://dx.doi.org/10.1016/j.aml.2016.12.019.
[15] T. Almani, K. Kumar, A. Dogru, G. Singh, M.F. Wheeler, Convergence analysis of multirate fixed-stress split iterative schemes for coupling flow with geomechanics, Comput. Methods Appl. Mech. Eng. 311 (1) (2016) 180–207, http://dx.doi.org/10.1016/j.cma.2016.07.036.
[16] M. Bause, F.A. Radu, U. Köcher, Space-time finite element approximation of the Biot poroelasticity system with iterative coupling, Comput. Methods Appl. Mech. Eng. 320 (2017) 745–768, http://dx.doi.org/10.1016/j.cma.2017.03.017.
[17] N. Castelleto, J.A. White, H.A. Tchelepi, Accuracy and convergence properties of the fixed-stress iterative solution of two-way coupled poromechanics, Int. J. Numer. Anal. Methods Geomech. 39 (2015) 1593–1618, http://dx.doi.org/10.1002/nag.2400.
[18] F.J. Gaspar, C. Rodrigo, On the fixed-stress split scheme as smoother in multigrid methods for coupling flow and geomechanics, Comput. Methods Appl. Mech. Eng. 326 (2017) 526–540, http://dx.doi.org/10.1016/j.cma.2017.08.025.
[19] M. Borregales, F.A. Radu, K. Kumar, J.M. Nordbotten, Robust iterative schemes for non-linear poromechanics, Comput. Geosci. 22 (2018) 1021–1038, http://dx.doi.org/10.1007/s10596-018-9736-6.
[20] J.W. Both, J.M. Nordbotten, K. Kumar, F.A. Radu, Anderson accelerated fixed-stress splitting schemes for consolidation of unsaturated porous media, Comput. Math. Appl. (2018) 1–24, http://dx.doi.org/10.1016/j.camwa.2018.07.033.
[21] M.J. Gander, 50 Years of Time Parallel Time Integration, Springer International Publishing, Cham, 2015, pp. 69–113, http://dx.doi.org/10.1007/978-3-319-23321-5_3.
[22] M. Emmett, M.L. Minion, Toward an efficient parallel in time method for partial differential equations, Commun. Appl. Math. Comput. Sci. 7 (2012) 105–132, http://dx.doi.org/10.2140/camcos.2012.7.105.
[23] J. Lions, Y. Maday, G.A. Turinici, A "parareal" in time discretization of PDE's, C.R. Math. Acad. Sci. Ser. I Math., 332, 661–668. http://dx.doi.org/10.1016/S0764-4442(00)01793-6.
[24] R.D. Falgout, S. Friedhoff, T.V. Kolev, S.P. MacLachlan, J.B. Schroder, Parallel time integration with multigrid, SIAM J. Sci. Comput. 16 (2014) 635–661, http://dx.doi.org/10.1137/130944230.
[25] G. Horton, S. Vandewalle, A space-time multigrid method for parabolic partial differential equations, SIAM J. Sci. Comput. 16 (4) (1995) 848–864, http://dx.doi.org/10.1137/0916050.
[26] C. Lubich, A. Ostermann, Multi-grid dynamic iteration for parabolic equations, BIT Numer. Math. 27 (2) (1987) 216–234, http://dx.doi.org/10.1007/BF01934186.
[27] G. Horton, S. Vandewalle, P. Worley, An algorithm with polylog parallel complexity for solving parabolic partial differential equations, SIAM J. Sci. Comput. 16 (3) (1995) 531–541, http://dx.doi.org/10.1137/0916034.
[28] A. Ženíšek, The existence and uniqueness theorem in Biot's consolidation theory, Apl. Mat. 29 (3) (1984) 194–211.
[29] G. Aguilar, F. Gaspar, F. Lisbona, C. Rodrigo, Numerical stabilization of Biot's consolidation model by a perturbation on the flow equation, Int. J. Numer. Methods Eng. 75 (11) (2008) 1282–1300, http://dx.doi.org/10.1002/nme.2295.
[30] C. Rodrigo, F. Gaspar, X. Hu, L. Zikatanov, Stability and monotonicity for some discretizations of the Biot's consolidation model, Comput. Methods Appl. Mech. Eng. 298 (2016) 183–204, http://dx.doi.org/10.1016/j.cma.2015.09.019.
[31] M.A. Murad, A.F.D. Loula, Improved accuracy in finite element analysis of Biot's consolidation problem, Comput. Methods Appl. Mech. Engrg. 95 (3) (1992) 359–382, http://dx.doi.org/10.1016/0045-7825(92)90193-N.
[32] M.A. Murad, A.F.D. Loula, On stability and convergence of finite element approximations of Biot's consolidation problem, Internat. J. Numer. Methods Engrg. 37 (4) (1994) 645–667, http://dx.doi.org/10.1002/nme.1620370407.
[33] M.A. Murad, V. Thomée, A.F.D. Loula, Asymptotic behavior of semidiscrete finite-element approximations of Biot's consolidation problem, SIAM J. Numer. Anal. 33 (3) (1996) 1065–1083, http://dx.doi.org/10.1137/0733052.
[34] Y. Abousleiman, A.-D. Cheng, L. Cui, E. Detournay, J.-C. Roegiers, Mandel's problem revisited, Geotechnique 46 (2) (1996) 187–195, http://dx.doi.org/10.1680/geot.1996.46.2.187.
[35] J. Mandel, Consolidation Des Sols (étude de mathématique), Géotechnique 3 (1953) 287–299, http://dx.doi.org/10.1680/geot.1953.3.7.287.
[36] A. Mikelić, B. Wang, M.F. Wheeler, Numerical convergence study of iterative coupling for coupled flow and geomechanics, Comput. Geosci. 18 (3–4) (2014) 325–341, http://dx.doi.org/10.1007/s10596-013-9393-8.
[37] J.W. Both, U. Köcher, Numerical investigation on the fixed-stress split- ting scheme for Biots equations: Optimality of the tuning parameter, arXivPreprint arXiv:1801.08352.
[38] W. Bangerth, G. Kanschat, T. Heister, L. Heltai, G. Kanschat, The deal.II library version 8.4, J. Numer. Math. 24 (2016) 135–141, http://dx.doi.org/10.1515/jnma-2016-1045.
[39] X. Gai, R.H. Dean, M.F. Wheeler, R. Liu, Coupled geomechanical and reservoir modeling on parallel computers, in: The SPE Reservoir Simulation Symposium, Houston, Texas, Feb. 3-5, 2003. http://dx.doi.org/10.2118/79700-MS.

Paper E

Robust fixed stress splitting for Biots equations in heterogeneous media

J.W. Both, M. Borregales, J.M. Nordbotten, K.Kumar and F.A. Radu

Applied Mathematics Letters (2017). Elsevier.

doi: 10.1016/j.aml.2016.12.019

Applied Mathematics Letters 68 (2017) 101–108

Contents lists available at ScienceDirect

Applied Mathematics Letters

www.elsevier.com/locate/aml

Robust fixed stress splitting for Biot's equations in heterogeneous media

Jakub Wiktor Both[a,*], Manuel Borregales[a], Jan Martin Nordbotten[a,b], Kundan Kumar[a], Florin Adrian Radu[a]

[a] Department of Mathematics, University of Bergen, Bergen, Norway
[b] Department of Civil and Environmental Engineering, Princeton University, Princeton, NJ, USA

ARTICLE INFO

Article history:
Received 31 October 2016
Received in revised form 30 December 2016
Accepted 30 December 2016
Available online 12 January 2017

Keywords:
Linear poroelasticity
Biot's equations
Iterative coupling
Heterogeneous porous media

ABSTRACT

We study the iterative solution of coupled flow and geomechanics in heterogeneous porous media, modeled by a three-field formulation of the linearized Biot's equations. We propose and analyze a variant of the widely used Fixed Stress Splitting method applied to heterogeneous media. As spatial discretization, we employ linear Galerkin finite elements for mechanics and mixed finite elements (lowest order Raviart–Thomas elements) for flow. Additionally, we use implicit Euler time discretization. The proposed scheme is shown to be globally convergent with optimal theoretical convergence rates. The convergence is rigorously shown in energy norms employing a new technique. Furthermore, numerical results demonstrate robust iteration counts with respect to the full range of Lamé parameters for homogeneous and heterogeneous media. Being in accordance with the theoretical results, the iteration count is hardly influenced by the degree of heterogeneities.

1. Introduction

The coupling of mechanics and flow in porous media is relevant for many applications ranging from environmental engineering to biomedical engineering. The simplest model of real applied importance is the quasi-static linearized Biot system, applicable for infinitesimally deforming, fully saturated porous media. Existence, uniqueness and regularity for Biot's equations have been investigated first by Showalter [1].

There are two approaches currently employed for solving Biot's equations. They are referred to as fully-implicit and iterative coupling [2]. The fully-implicit approach involves solving the fully coupled system of governing equations simultaneously, providing the benefit of unconditional stability. It requires advanced and efficient preconditioners. For this purpose, (Schur complement based) block preconditioners appear to be a sound choice [3–6]. The iterative coupling approach involves the sequential-implicit solution of flow and

* Corresponding author.
E-mail addresses: jakub.both@uib.no (J.W. Both), manuel.borregales@uib.no (M. Borregales), jan.nordbotten@uib.no (J.M. Nordbotten), kundan.kumar@uib.no (K. Kumar), florin.radu@uib.no (F.A. Radu).

http://dx.doi.org/10.1016/j.aml.2016.12.019
0893-9659/

mechanics using the latest solution information, iterating the procedure at each time step until convergence. The sequential-implicit approach offers greater flexibility in code design than the fully-implicit approach. On the other hand, being equivalent to a preconditioned Richardson method [7], sequential-implicit approaches also provide a basis to design efficient block preconditioners for the fully-implicit approach [8,9]. Among iterative coupling schemes, the widely used Fixed Stress Splitting method has been rigorously shown to be unconditionally stable in the sense of a Von Neumann analysis [10] and globally convergent [11], when considering slightly compressible flow in a homogeneous porous medium.

The new contributions of this work are:

- We prove global, linear convergence in energy norms of the Fixed Stress Splitting method applied to the fully discretized three-field formulation of Biot's equations for heterogeneous media, where linear finite elements are employed for mechanics, mixed finite elements (lowest order Raviart–Thomas elements) are employed for flow, and backward Euler time discretization is applied.
- We propose a new, optimized tuning parameter for heterogeneous media.

In the case of homogeneous media, the results are in consistency with previous numerical studies, cf., e.g., [12]. To the best of our knowledge, this is the first time the convergence of the Fixed Stress Splitting method is rigorously shown for energy norms and considering heterogeneous media.

2. Mathematical model — Biot's equations

We consider the quasi-static Biot's equations [13,14], modeling a linearly elastic porous medium $\Omega \subset \mathbb{R}^d$, $d \in \{2, 3\}$, saturated with a slightly compressible fluid. On the space–time domain $\Omega \times (0, T)$, the governing equations read

$$-\boldsymbol{\nabla} \cdot [2\mu\boldsymbol{\varepsilon}(\boldsymbol{u}) + \lambda\boldsymbol{\nabla} \cdot \boldsymbol{u}] + \alpha\boldsymbol{\nabla} p = \boldsymbol{f}, \qquad \partial_t \left(\frac{p}{M} + \alpha\boldsymbol{\nabla} \cdot \boldsymbol{u}\right) + \boldsymbol{\nabla} \cdot \boldsymbol{w} = S_f, \qquad \boldsymbol{K}^{-1}\boldsymbol{w} + \boldsymbol{\nabla} p = \rho_f \boldsymbol{g}. \quad (1)$$

Here, $\boldsymbol{u}$ is the displacement, p is the fluid pressure, $\boldsymbol{w}$ is the Darcy flux, $\boldsymbol{\varepsilon}(\boldsymbol{u}) = 0.5(\boldsymbol{\nabla}\boldsymbol{u} + \boldsymbol{\nabla}\boldsymbol{u}^\top)$ is the linearized strain tensor, μ, λ are the Lamé parameters, α is the Biot coefficient, M is the Biot modulus, ρ_f is the fluid density, $\boldsymbol{K}$ is the permeability tensor divided by fluid viscosity, $\boldsymbol{g}$ is the gravity vector, and S_f is a volume source term. For simplicity, we assume homogeneous boundary $\boldsymbol{u} = \boldsymbol{0}$, $p = 0$ on $\partial\Omega \times [0, T]$ and initial conditions $\boldsymbol{u} = \boldsymbol{u}_0$, $p = p_0$ in $\Omega \times \{0\}$. We make the following assumptions on the effective coefficients:

(A1) Let $\rho_f \in \mathbb{R}$, $\boldsymbol{g} \in \mathbb{R}^d$ be constant.
(A2) Let $M, \alpha, \mu, \lambda \in L^\infty(\Omega)$ be positive, uniformly bounded, with the lower bound strictly positive.
(A3) Let $\boldsymbol{K} \in L^\infty(\Omega)^{d\times d}$ be a symmetric matrix, which is constant in time and has uniformly bounded eigenvalues, i.e., there exist constants $k_m, k_M \in \mathbb{R}$, satisfying for all $\boldsymbol{x} \in \Omega$ and for all $\boldsymbol{z} \in \mathbb{R}^d \setminus \{\boldsymbol{0}\}$

$$0 < k_m \boldsymbol{z}^\top \boldsymbol{z} \leq \boldsymbol{z}^\top \boldsymbol{K}(x)\boldsymbol{z} \leq k_M \boldsymbol{z}^\top \boldsymbol{z} < \infty.$$

Below, we consider a numerical approximation of the weak solution of Biot's equations as described above.

3. Fixed stress splitting for the fully discretized system

Let $\mathcal{T}_h$ be a regular decomposition of mesh size h of the domain Ω. Furthermore, let $0 = t_0 < t_1 < \cdots < t_N = T$, $N \in \mathbb{N}$, define a partition of the time interval $(0, T)$ with constant time step size $\tau = t_{k+1} - t_k$, $k \geq 0$. In order to discretize Biot's equations in space, we use linear, constant and lowest order Raviart–Thomas

elements to approximate the displacement, pressure and flux, respectively. The corresponding discrete spaces are given by

$$\boldsymbol{V}_h = \left\{ \boldsymbol{v}_h \in [H_0^1(\Omega)]^d \,\middle|\, \forall T \in \mathcal{T}_h, \boldsymbol{v}_h|_T \in [\mathbb{P}_1]^d \right\}, \qquad Q_h = \left\{ q_h \in L^2(\Omega) \,\middle|\, \forall T \in \mathcal{T}_h, q_h|_T \in \mathbb{P}_0 \right\},$$
$$\boldsymbol{Z}_h = \left\{ \boldsymbol{z}_h \in H(\mathrm{div};\Omega) \,\middle|\, \forall T \in \mathcal{T}_h, \boldsymbol{z}_h|_T(\boldsymbol{x}) = \boldsymbol{a} + b\boldsymbol{x}, \boldsymbol{a} \in \mathbb{R}^d, b \in \mathbb{R} \right\},$$

where $\mathbb{P}_0$ and $\mathbb{P}_1$ denote the spaces of scalar piecewise constant and piecewise linear functions, respectively. Additionally, we use backward Euler time discretization in order to discretize Biot's equations in time.

Let $\langle \cdot, \cdot \rangle$ denote the standard $L^2(\Omega)$ scalar product. Then for given initial values $(\boldsymbol{u}_h^0, \boldsymbol{v}_h^0, \boldsymbol{w}_h^0) \in \boldsymbol{V}_h \times Q_h \times \boldsymbol{Z}_h$, the fully-implicit discretization reads: For all $n \in \mathbb{N}$, $n \geq 1$, given $(\boldsymbol{u}_h^{n-1}, p_h^{n-1}, \boldsymbol{w}_h^{n-1}) \in \boldsymbol{V}_h \times Q_h \times \boldsymbol{Z}_h$, find the current displacement, pressure and flux fields $(\boldsymbol{u}_h^n, p_h^n, \boldsymbol{w}_h^n) \in \boldsymbol{V}_h \times Q_h \times \boldsymbol{Z}_h$, satisfying for all $(\boldsymbol{v}_h, q_h, \boldsymbol{z}_h) \in \boldsymbol{V}_h \times Q_h \times \boldsymbol{Z}_h$

$$\langle 2\mu\boldsymbol{\varepsilon}(\boldsymbol{u}_h^n), \boldsymbol{\varepsilon}(\boldsymbol{v}_h) \rangle + \langle \lambda \boldsymbol{\nabla} \cdot \boldsymbol{u}_h^n, \boldsymbol{\nabla} \cdot \boldsymbol{v}_h \rangle - \langle \alpha p_h^n, \boldsymbol{\nabla} \cdot \boldsymbol{v}_h \rangle = \langle \boldsymbol{f}, \boldsymbol{v}_h \rangle, \tag{2}$$

$$\left\langle \frac{1}{M} p_h^n, q_h \right\rangle + \langle \alpha \boldsymbol{\nabla} \cdot \boldsymbol{u}_h^n, q_h \rangle + \tau \langle \boldsymbol{\nabla} \cdot \boldsymbol{w}_h^n, q_h \rangle = \tau \langle S_f, q_h \rangle + \left\langle \frac{1}{M} p_h^{n-1}, q_h \right\rangle + \langle \alpha \boldsymbol{\nabla} \cdot \boldsymbol{u}_h^{n-1}, q_h \rangle, \tag{3}$$

$$\langle \boldsymbol{K}^{-1} \boldsymbol{w}_h^n, \boldsymbol{z}_h \rangle - \langle p_h^n, \boldsymbol{\nabla} \cdot \boldsymbol{z}_h \rangle = \langle \rho_f \boldsymbol{g}, \boldsymbol{z}_h \rangle. \tag{4}$$

Instead of solving system (2)–(4) in a fully coupled manner, a popular alternative is to use iterative methods, which decouple mechanics and flow problems and allow for an efficient solution of the separate subproblems. Here, we limit our considerations to the widely used Fixed Stress Splitting method and adapt the idea by Mikelić and Wheeler [11], which considers keeping an artificial volumetric stress constant. Nevertheless, the same ideas can be also used to prove the convergence of the optimized Undrained Splitting scheme.

The iterative scheme defines a sequence $(\boldsymbol{u}_h^{n,i}, p_h^{n,i}, \boldsymbol{w}_h^{n,i})$, $i \geq 0$. After initialization $\boldsymbol{u}_h^{n,0} = \boldsymbol{u}_h^{n-1}$, $p_h^{n,0} = p_h^{n-1}$, and $\boldsymbol{w}_h^{n,0} = \boldsymbol{w}_h^{n-1}$, each iterate is defined in two steps. First, the flow problem is solved independently, keeping the artificial volumetric stress $\sigma_\beta = \sigma_0 + K_{dr} \boldsymbol{\nabla} \cdot \boldsymbol{u} - \alpha p$ constant, which introduces a tuning parameter $K_{dr} \in L^\infty(\Omega)$ (classically the drained bulk modulus). Equivalently, we consider the tuning parameter $\beta_{FS} = \alpha^2 / K_{dr}$. Second, the mechanics problem is solved using updated pressure and flux. For fixed $n, i \in \mathbb{N}$, the detailed splitting scheme reads as follows:

Step 1: Given $(\boldsymbol{u}_h^{n,i-1}, p_h^{n,i-1}, \boldsymbol{w}_h^{n,i-1}) \in \boldsymbol{V}_h \times Q_h \times \boldsymbol{Z}_h$, find $(p_h^{n,i}, \boldsymbol{w}_h^{n,i}) \in Q_h \times \boldsymbol{Z}_h$ s.t. for all $(q_h, \boldsymbol{z}_h) \in Q_h \times \boldsymbol{Z}_h$ it holds

$$\left\langle \left(\frac{1}{M} + \beta_{FS} \right) p_h^{n,i}, q_h \right\rangle + \tau \langle \boldsymbol{\nabla} \cdot \boldsymbol{w}_h^{n,i}, q_h \rangle = \tau \langle S_f, q_h \rangle + \left\langle \frac{1}{M} p_h^{n-1}, q_h \right\rangle + \langle \alpha \boldsymbol{\nabla} \cdot \boldsymbol{u}_h^{n-1}, q_h \rangle$$
$$+ \langle \beta_{FS} p_h^{n,i-1}, q_h \rangle - \langle \alpha \boldsymbol{\nabla} \cdot \boldsymbol{u}_h^{n,i-1}, q_h \rangle, \tag{5}$$

$$\langle \boldsymbol{K}^{-1} \boldsymbol{w}_h^{n,i}, \boldsymbol{z}_h \rangle - \langle p_h^{n,i}, \boldsymbol{\nabla} \cdot \boldsymbol{z}_h \rangle = \langle \rho_f \boldsymbol{g}, \boldsymbol{z}_h \rangle. \tag{6}$$

Step 2: Given $p_h^{n,i} \in Q_h$, find $\boldsymbol{u}_h^{n,i} \in \boldsymbol{V}_h$ such that for all $\boldsymbol{v}_h \in \boldsymbol{V}_h$ it holds

$$\langle 2\mu\boldsymbol{\varepsilon}\left(\boldsymbol{u}_h^{n,i}\right), \boldsymbol{\varepsilon}(\boldsymbol{v}_h) \rangle + \langle \lambda \boldsymbol{\nabla} \cdot \boldsymbol{u}_h^{n,i}, \boldsymbol{\nabla} \cdot \boldsymbol{v}_h \rangle = \langle \boldsymbol{f}, \boldsymbol{v}_h \rangle + \langle \alpha p_h^{n,i}, \boldsymbol{\nabla} \cdot \boldsymbol{v}_h \rangle. \tag{7}$$

In the following, we consider three tuning parameters — the classical, physically motivated choice β_{FS}^{cl}, cf., e.g., [10], and the parameters β_{FS}^{λ}, β_{FS}^{opt}, revealed by the analysis of Mikelić and Wheeler [11,12], which is valid for homogeneous Lamé parameters. The latter parameter is also revealed by the present convergence analysis, valid for heterogeneous Lamé parameters. More precisely, the parameters are given by

$$\beta_{FS}^{cl} = \frac{\alpha^2}{\frac{2\mu}{d} + \lambda}, \qquad \beta_{FS}^{\lambda} = \frac{\alpha^2}{2\lambda}, \qquad \beta_{FS}^{opt} = \frac{\alpha^2}{2\left(\frac{2\mu}{d} + \lambda\right)}. \tag{8}$$

4. Convergence analysis

We prove linear convergence of the Fixed Stress Splitting method, when applied to Biot's equations in heterogeneous media. For this purpose, we show a contraction with respect to energy norms, making use of the following lemma and remark. We refer to the Supplementary material (see Appendix A) for further standard lemmas used in the proof. Furthermore, in the Supplementary material, the proof is repeated for homogeneous media in a simpler, but a more detailed form.

Lemma 1 (*Thomas' Lemma, [15]*)**.** *There exists a constant $C_{\Omega,d} > 0$ not depending on the mesh size h, such that given an arbitrary $q_h \in Q_h$ there exists $\boldsymbol{z}_h \in \boldsymbol{Z}_h$, satisfying $\boldsymbol{\nabla} \cdot \boldsymbol{z}_h = q_h$ and $\|\boldsymbol{z}_h\| \leq C_{\Omega,d}\|q_h\|$.*

Remark 1 (*Weighted $L^2(\Omega)^d$ Norms*)**.** Let $k \in \{1, d\}$. Let further $\boldsymbol{A} \in [L^\infty(\Omega)]^{k\times k}$ be a symmetric, uniformly positive definite matrix and let its eigenvalues be uniformly bounded, i.e., there exist constants $a_m, a_M \in \mathbb{R}$ such that for all eigenvalues $\lambda(\boldsymbol{x})$ of matrix $\boldsymbol{A}(\boldsymbol{x})$, $\boldsymbol{x} \in \Omega$, it holds $0 < a_m \leq \lambda(x) \leq a_M \leq \infty$. Then, we define a weighted scalar product $\langle\cdot,\cdot\rangle_{\boldsymbol{A}}$ on $L^2(\Omega)^d$ by $\langle \boldsymbol{f}, \boldsymbol{g}\rangle_{\boldsymbol{A}} = \langle \boldsymbol{A}\boldsymbol{f}, \boldsymbol{g}\rangle$, $\boldsymbol{f}, \boldsymbol{g} \in L^2(\Omega)^d$. Let $\|\cdot\|_{\boldsymbol{A}}$ denote the corresponding norm. Then it holds $\forall \boldsymbol{f}, \boldsymbol{g} \in L^2(\Omega)^d$

$$a_m\|\boldsymbol{f}\|^2 \leq \|\boldsymbol{f}\|^2_{\boldsymbol{A}} \leq a_M\|\boldsymbol{f}\|^2, \qquad \langle \boldsymbol{f}, \boldsymbol{g}\rangle \leq \|\boldsymbol{f}\|_{\boldsymbol{A}}\|\boldsymbol{g}\|_{\boldsymbol{A}^{-1}}.$$

Theorem 2 (*Linear Convergence for Fixed Stress Splitting*)**.** *Assume* (A1)–(A3). *Let $(\boldsymbol{u}_h^n, p_h^n, \boldsymbol{w}_h^n)$ and $(\boldsymbol{u}_h^{n,i}, p_h^{n,i}, \boldsymbol{w}_h^{n,i})$ be the solutions of Eqs.* (2)–(4) *and Eqs.* (5)–(7)*, respectively. Let $e_{\boldsymbol{u}}^i = \boldsymbol{u}_h^{n,i} - \boldsymbol{u}_h^n$, $e_p^i = p_h^{n,i} - p_h^n$ and $e_{\boldsymbol{w}}^i = \boldsymbol{w}_h^{n,i} - \boldsymbol{w}_h^n$ denote the errors at current iteration. Then for all $\beta_{FS} \in L^\infty(\Omega)$, satisfying*

$$\beta_{FS} \geq \frac{\alpha^2}{2(\frac{2\mu}{d} + \lambda)} \quad \text{on } \Omega, \tag{9}$$

for all $i \geq 1$, it holds

$$\|e_p^i\|^2_{\beta_{FS}} \leq \left\| \frac{\frac{\beta_{FS}}{2}}{\frac{1}{M} + \frac{\beta_{FS}}{2} + \frac{\tau k_m}{C^2_{\Omega,d}}} \right\|_\infty \|e_p^{i-1}\|^2_{\beta_{FS}}, \tag{10}$$

$$\|\boldsymbol{\varepsilon}(e_{\boldsymbol{u}}^i)\|^2_{2\mu} + \|\boldsymbol{\nabla}\cdot e_{\boldsymbol{u}}^i\|^2_\lambda \leq \|e_p^i\|^2_{\frac{\alpha^2}{\frac{2\mu}{d}+\lambda}}. \tag{11}$$

Optimal convergence rates are obtained in case of equality in Eq. (9).

Proof. Due to Assumptions (A1)–(A3), all effective coefficients fulfill the requirements for defining weighted $L^2(\Omega)$-norms, cf. Remark 1. Throughout the proof we make use of weighted norms without further comment.

Step 1*: Flow and mechanics.* By taking the differences of corresponding Eqs. (5)–(7) and Eqs. (2)–(4), testing with $\boldsymbol{v}_h = e_{\boldsymbol{u}}^{i-1} \in \boldsymbol{V}_h$, $q_h = e_p^i \in Q_h$ and $\boldsymbol{z}_h = \tau e_{\boldsymbol{w}}^i \in \boldsymbol{Z}_h$ and adding all together, we obtain

$$\langle \boldsymbol{\varepsilon}(e_{\boldsymbol{u}}^i), \boldsymbol{\varepsilon}(e_{\boldsymbol{u}}^{i-1})\rangle_{2\mu} + \langle \boldsymbol{\nabla}\cdot e_{\boldsymbol{u}}^i, \boldsymbol{\nabla}\cdot e_{\boldsymbol{u}}^{i-1}\rangle_\lambda + \|e_p^i\|^2_{\frac{1}{M}} + \tau\|e_{\boldsymbol{w}}^i\|^2_{\boldsymbol{K}^{-1}} + \langle e_p^i - e_p^{i-1}, e_p^i\rangle_{\beta_{FS}} = 0.$$

Using a polarization and binomial identity yields

$$\begin{aligned}\frac{1}{4}\|\boldsymbol{\varepsilon}(e_{\boldsymbol{u}}^i + e_{\boldsymbol{u}}^{i-1})\|^2_{2\mu} + \frac{1}{4}\|\boldsymbol{\nabla}\cdot(e_{\boldsymbol{u}}^i + e_{\boldsymbol{u}}^{i-1})\|^2_\lambda - \frac{1}{4}\|\boldsymbol{\varepsilon}(e_{\boldsymbol{u}}^i - e_{\boldsymbol{u}}^{i-1})\|^2_{2\mu} - \frac{1}{4}\|\boldsymbol{\nabla}\cdot(e_{\boldsymbol{u}}^i - e_{\boldsymbol{u}}^{i-1})\|^2_\lambda \\ + \|e_p^i\|^2_{\frac{1}{M}} + \tau\|e_{\boldsymbol{w}}^i\|^2_{\boldsymbol{K}^{-1}} + \|e_p^i\|^2_{\frac{\beta_{FS}}{2}} + \|e_p^i - e_p^{i-1}\|^2_{\frac{\beta_{FS}}{2}} - \|e_p^{i-1}\|^2_{\frac{\beta_{FS}}{2}} = 0.\end{aligned} \tag{12}$$

Step 2: Mechanics. Evaluating Eq. (7) at iteration i and $i-1$, taking the difference and testing with $\boldsymbol{v}_h = e^i_{\boldsymbol{u}} - e^{i-1}_{\boldsymbol{u}}$ yields

$$\|\boldsymbol{\varepsilon}\big(e^i_{\boldsymbol{u}} - e^{i-1}_{\boldsymbol{u}}\big)\|^2_{2\mu} + \|\boldsymbol{\nabla}\cdot(e^i_{\boldsymbol{u}} - e^{i-1}_{\boldsymbol{u}})\|^2_{\lambda} = \langle e^i_p - e^{i-1}_p, \boldsymbol{\nabla}\cdot(e^i_{\boldsymbol{u}} - e^{i-1}_{\boldsymbol{u}})\rangle_{\alpha}.$$

Let $\gamma \in L^\infty(\Omega)$ with $\gamma(\Omega) \subset [0,1]$ and $f_\mu, f_\lambda \in L^\infty(\Omega)$, satisfying the assumptions of Remark 1. Then by applying weighted Cauchy–Schwarz inequalities, cf. Remark 1, and an arithmetic mean-root mean square inequality (AM-QM inequality), we obtain

$$\begin{aligned}
&\|\boldsymbol{\varepsilon}\big(e^i_{\boldsymbol{u}} - e^{i-1}_{\boldsymbol{u}}\big)\|^2_{2\mu} + \|\boldsymbol{\nabla}\cdot(e^i_{\boldsymbol{u}} - e^{i-1}_{\boldsymbol{u}})\|^2_{\lambda} \\
&\quad= \langle e^i_p - e^{i-1}_p, \boldsymbol{\nabla}\cdot(e^i_{\boldsymbol{u}} - e^{i-1}_{\boldsymbol{u}})\rangle_{\gamma\alpha} + \langle e^i_p - e^{i-1}_p, \boldsymbol{\nabla}\cdot(e^i_{\boldsymbol{u}} - e^{i-1}_{\boldsymbol{u}})\rangle_{(1-\gamma)\alpha} \\
&\quad\le \|e^i_p - e^{i-1}_p\|_{\gamma\alpha^2 f_\mu^{-1}} \|\boldsymbol{\nabla}\cdot(e^i_{\boldsymbol{u}} - e^{i-1}_{\boldsymbol{u}})\|_{\gamma f_\mu} + \|e^i_p - e^{i-1}_p\|_{(1-\gamma)\alpha^2 f_\lambda^{-1}} \|\boldsymbol{\nabla}\cdot(e^i_{\boldsymbol{u}} - e^{i-1}_{\boldsymbol{u}})\|_{(1-\gamma) f_\lambda} \\
&\quad\le \|e^i_p - e^{i-1}_p\|_{\gamma\alpha^2 f_\mu^{-1}} \|\boldsymbol{\varepsilon}\big(e^i_{\boldsymbol{u}} - e^{i-1}_{\boldsymbol{u}}\big)\|_{\gamma d f_\mu} + \|e^i_p - e^{i-1}_p\|_{(1-\gamma)\alpha^2 f_\lambda^{-1}} \|\boldsymbol{\nabla}\cdot(e^i_{\boldsymbol{u}} - e^{i-1}_{\boldsymbol{u}})\|_{(1-\gamma) f_\lambda}.
\end{aligned}$$

By applying Young's inequality, rearranging terms and scaling, it holds for $c \in (0,\infty)$ and γ, f_μ, f_λ as above

$$\|\boldsymbol{\varepsilon}\big(e^i_{\boldsymbol{u}} - e^{i-1}_{\boldsymbol{u}}\big)\|^2_{c(2\mu - \frac{1}{2}\gamma d f_\mu)} + \|\boldsymbol{\nabla}\cdot(e^i_{\boldsymbol{u}} - e^{i-1}_{\boldsymbol{u}})\|^2_{c(\lambda - \frac{1}{2}(1-\gamma) f_\lambda)} \le \|e^i_p - e^{i-1}_p\|^2_{\frac{\alpha^2}{2} c(\gamma f_\mu^{-1} + (1-\gamma) f_\lambda^{-1})}.$$

By choosing $c, \gamma, f_\mu, f_\lambda$ optimally, we finally obtain

$$\frac{1}{4}\|\boldsymbol{\varepsilon}\big(e^i_{\boldsymbol{u}} - e^{i-1}_{\boldsymbol{u}}\big)\|^2_{2\mu} + \frac{1}{4}\|\boldsymbol{\nabla}\cdot(e^i_{\boldsymbol{u}} - e^{i-1}_{\boldsymbol{u}})\|^2_{\lambda} \le \|e^i_p - e^{i-1}_p\|^2_{\frac{\alpha^2}{4\left(\frac{2\mu}{d} + \lambda\right)}}. \tag{13}$$

Step 3: Darcy. Taking the difference of Eqs. (6) and (4) yields for any $\boldsymbol{z}_h \in \boldsymbol{Z}_h$

$$\langle \boldsymbol{K}^{-1} e^i_{\boldsymbol{w}}, \boldsymbol{z}_h\rangle - \langle e^i_p, \boldsymbol{\nabla}\cdot\boldsymbol{z}_h\rangle = 0. \tag{14}$$

Using Thomas' Lemma, there exists a constant $C_{\Omega,d} > 0$ and a function $\tilde{\boldsymbol{z}}_h \in \boldsymbol{Z}_h$ satisfying $\boldsymbol{\nabla}\cdot\tilde{\boldsymbol{z}}_h = e^i_p$ and $\|\tilde{\boldsymbol{z}}_h\| \le C_{\Omega,d}\|e^i_p\|$. Then, together with Eq. (14) and Assumption (A3), after some rearranging, we obtain

$$\frac{k_m}{C^2_{\Omega,d}}\|e^i_p\|^2 \le \langle \boldsymbol{K}^{-1} e^i_{\boldsymbol{w}}, e^i_{\boldsymbol{w}}\rangle. \tag{15}$$

Step 4: Combining Step 1–3. Discarding the first two terms in Eq. (12), using Assumption (9), Eq. (13) and inserting Eq. (15) yields

$$\|e^i_p\|^2_{\frac{1}{M} + \frac{\beta_{FS}}{2} + \frac{\tau k_m}{C^2_{\Omega,d}}} \le \|e^{i-1}_p\|^2_{\frac{\beta_{FS}}{2}}.$$

By employing Remark 1, we obtain Eq. (10).

Step 5: Mechanics revisited. Taking the difference of Eqs. (7) and (2), tested with $\boldsymbol{v}_h = e^i_{\boldsymbol{u}}$ yields

$$\|\boldsymbol{\varepsilon}\big(e^i_{\boldsymbol{u}}\big)\|^2_{2\mu} + \|\boldsymbol{\nabla}\cdot e^i_{\boldsymbol{u}}\|^2_{\lambda} = \langle e^i_p, \boldsymbol{\nabla}\cdot e^i_{\boldsymbol{u}}\rangle_{\alpha}.$$

We repeat all steps from Step 2. Due to linearity, we obtain Eq. (11) analogously. □

Remark 2 (*Discussion*)**.** The above analysis covers global convergence in energy norms for all considered tuning parameters β^{cl}_{FS}, β^{λ}_{FS} and β^{opt}_{FS}, where the first two only yield sub-optimal convergence rates in the energy norms and the latter yields optimal rates, as shown by our proof. The parameter β^{λ}_{FS} recovers optimality in the limit of $\frac{\mu}{\lambda} \ll 1$. For soft materials, i.e., in the limit of $\frac{\mu}{\lambda} \gg 1$, we expect deteriorating convergence rates due to lack of dependence on μ.

Table 1
Problem parameters, chosen identically to [12].

Symb.	Quantity	Values [Unit]
E	Bulk modulus	0.594 [GPa]
α	Biot's coefficient	1
M	Biot's modulus	1.65e10 [Pa]
$\boldsymbol{K}$	Permeability tensor divided by fluid viscosity	$100\boldsymbol{I}$ [mD/cP]
$\boldsymbol{g}$	Gravity vector	$\mathbf{0}$ [m/s^2]
$\Delta x, \Delta y$	Grid spacing in x and y	0.025 [m]
τ	Time step size	1 [s]
δ_a	Absolute error tolerance	1e−6
δ_r	Relative error tolerance	1e−6

5. Numerical results

We analyze the robustness of the Fixed Stress Splitting scheme with respect to different Lamé parameters and compare the convergence behavior for the tuning parameters β_{FS}^{cl}, β_{FS}^{λ} and β_{FS}^{opt}. For further test cases with $d \in \{2, 3\}$, we refer to the Supplementary material (see Appendix A). Note, that convergence has been already demonstrated by Mikelić et al. [12]. Focusing on the performance of the splitting scheme, we employ direct solvers for all occurring subproblems. Furthermore, let $(\mathbf{u}^i, \mathbf{p}^i, \mathbf{w}^i)$ denote the solution coefficient vector in step i. Then given tolerances $\delta_a, \delta_r > 0$, we employ the stopping criterion $\|(\mathbf{u}^i, \mathbf{p}^i, \mathbf{w}^i) - (\mathbf{u}^{i-1}, \mathbf{p}^{i-1}, \mathbf{w}^{i-1})\| \leq \delta_a + \delta_r \|(\mathbf{u}^i, \mathbf{p}^i, \mathbf{w}^i)\|$. For the implementation we used the Dune libraries [16].

5.1. Two-dimensional homogeneous medium — Constant Poisson's ratio

Let $\Omega = (0, 1) \times (0, 1) \subset \mathbb{R}^2$. For given $\xi \in \mathbb{R}$, we prescribe displacement, pressure and flux fields

$$\boldsymbol{u}(x, y, t) = tx(1 - x)y(1 - y)\begin{bmatrix}1 & 1\end{bmatrix}^\top, \qquad p(x, y, t) = \xi \cdot tx(1 - x)y(1 - y), \qquad \boldsymbol{w} = -\boldsymbol{K}\boldsymbol{\nabla} p \tag{16}$$

and choose source terms, initial and Dirichlet boundary conditions such that Eq. (16) is the solution of problem (1). We choose the same set of physical parameters as [12] apart from varying mechanical parameters (see Table 1). Instead of considering the full range of Lamé parameters, it is equivalent to consider the range $\nu \in (0, 0.5)$ for the Poisson's ratio as $\nu = (2(1 + \mu/\lambda))^{-1}$. For the rather realistic parameters, we choose $\xi = 1e8$ to achieve convergence of the discretization.

The iteration count for different Poisson's ratios and different tuning parameters is illustrated in Fig. 1. Both β_{FS}^{cl} and β_{FS}^{opt} are robust with respect to the full range of Poisson's ratios, whereas the parameter β_{FS}^{λ} shows deteriorating convergence rates for soft materials, demonstrating the general necessity of the dependence of the tuning parameter on both Lamé parameters. As expected, in the limit, i.e., for $\nu \to 0.5$, both parameters β_{FS}^{λ} and β_{FS}^{opt} yield identical iteration counts.

5.2. Three-dimensional heterogeneous medium — Jumping Poisson's ratio

We compare Fixed Stress Splitting iteration counts for three-dimensional, heterogeneous media with constant and non-constant Poisson's ratios. We consider a cube $\Omega = (0, 1) \times (0, 1) \times (0, 1) \subset \mathbb{R}^3$ discretized by $20 \times 20 \times 20$ hexahedra. For given $\xi \in \mathbb{R}$, we prescribe displacement and pressure fields

$$\boldsymbol{u}(x, y, z, t) = tx(1 - x)y(1 - y)z(1 - z)\begin{bmatrix}1 & 1 & 1\end{bmatrix}^\top, \quad p(x, y, z, t) = \xi \cdot tx(1 - x)y(1 - y)z(1 - z) \tag{17}$$

and a corresponding flux field $\boldsymbol{w} = -\boldsymbol{K}\boldsymbol{\nabla} p$. Further, we proceed analogously to Section 5.1, also considering the same physical parameters besides a locally varying Poisson's ratio. For chosen $\Delta\nu \in \{0.0, 0.05, 0.1, 0.2\}$

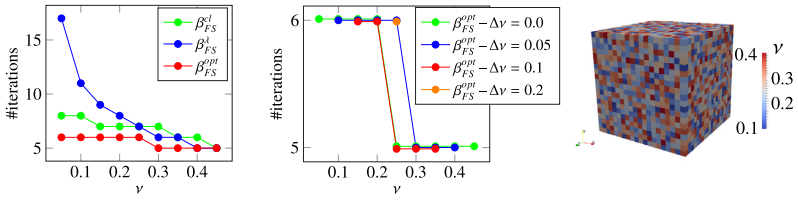

Fig. 1. *Left and Center:* Number of Fixed Stress iterations against Poisson's ratio for the first time step for (*left*) the homogeneous (Section 5.1) and (*center*) the heterogeneous (Section 5.2) test case. *Right:* Example for Poisson's ratio distribution in the interval $[0.1, 0.4]$ (Section 5.2).

and $\nu \in (\Delta\nu, 0.5 - \Delta\nu)$, we consider uniformly distributed Poisson's ratios in the interval $[\nu - \Delta\nu, \nu + \Delta\nu]$. An example distribution is shown in Fig. 1. We note, that for $\Delta\nu = 0$ the medium is homogeneous.

The iteration counts for different values for ν and $\Delta\nu$ are visualized in Fig. 1. We make two observations. For homogeneous media, the iteration count is robust with respect to different Poisson's ratios as it remains almost constant, as already seen for the two-dimensional test case in Section 5.1. Furthermore, we note that for heterogeneous media, the iteration count is bounded by the maximum of numbers of iterations obtained for homogeneous media over all Poisson's ratio values taken in the heterogeneous medium. This is in accordance with the theoretical convergence result, as the theoretical convergence rate includes a infinity norm, evaluating the worst case.

6. Conclusion

We have proposed an optimized Fixed Stress Splitting method for heterogeneous media. Its global convergence has been shown in weighted energy norms. The optimized tuning parameter depends on all mechanical parameters and shows stable iteration counts on the full range of Poisson's ratios. Numerical test cases show no significant increase of iterations when switching from a homogeneous to a heterogeneous medium or from two to three dimensions, demonstrating the robustness of the splitting scheme with respect to heterogeneities.

Acknowledgments

The research was partially supported by the NFR-DAADppp grant 255715 and the NFR-Toppforsk project 250223.

Appendix A. Supplementary material

Supplementary material related to this article can be found online at http://dx.doi.org/10.1016/j.aml.2016.12.019.

References

[1] R. Showalter, Diffusion in poro-elastic media, J. Math. Anal. Appl. 251 (1) (2000) 310–340. http://dx.doi.org/10.1006/jmaa.2000.7048.
[2] A. Settari, F.M. Mourits, A coupled reservoir and geomechanical simulation system, SPE J. 3 (3) (1998) 219–226. http://dx.doi.org/10.2118/50939-PA.

[3] K.K. Phoon, K.C. Toh, S.H. Chan, F.H. Lee, An efficient diagonal preconditioner for finite element solution of Biot's consolidation equations, Int. J. Numer. Methods Eng. 55 (4) (2002) 377–400. http://dx.doi.org/10.1002/nme.500.
[4] J.A. White, R.I. Borja, Block-preconditioned Newton–Krylov solvers for fully coupled flow and geomechanics, Comput. Geosci. 15 (4) (2011) 647. http://dx.doi.org/10.1007/s10596-011-9233-7.
[5] J.B. Haga, H. Osnes, H.P. Langtangen, Efficient block preconditioners for the coupled equations of pressure and deformation in highly discontinuous media, Int. J. Numer. Anal. Methods Geomech. 35 (13) (2011) 1466–1482. http://dx.doi.org/10.1002/nag.973.
[6] J.J. Lee, K.-A. Mardal, R. Winther, Parameter-robust discretization and preconditioning of Biot's consolidation model, 2015. arXiv:1507.03199 [math.NA].
[7] N. Castelletto, J.A. White, H.A. Tchelepi, Accuracy and convergence properties of the fixed-stress iterative solution of two-way coupled poromechanics, Int. J. Numer. Anal. Methods Geomech. 39 (14) (2015) 1593–1618. http://dx.doi.org/10.1002/nag.2400.
[8] N. Castelletto, J.A. White, M. Ferronato, Scalable algorithms for three-field mixed finite element coupled poromechanics, J. Comput. Phys. 327 (2016) 894–918. http://dx.doi.org/10.1016/j.jcp.2016.09.063.
[9] J.A. White, N. Castelletto, H.A. Tchelepi, Block-partitioned solvers for coupled poromechanics: A unified framework, Comput. Methods Appl. Mech. Engrg. 303 (2016) 55–74. http://dx.doi.org/10.1016/j.cma.2016.01.008.
[10] J. Kim, H.A. Tchelepi, R. Juanes, Stability, Accuracy, and Efficiency of Sequential Methods for Coupled Flow and Geomechanics. Society of Petroleum Engineers, 2011. http://dx.doi.org/10.2118/119084-PA.
[11] A. Mikelić, M.F. Wheeler, Convergence of iterative coupling for coupled flow and geomechanics, Comput. Geosci. 17 (3) (2013) 455–461. http://dx.doi.org/10.1007/s10596-012-9318-y.
[12] A. Mikelić, B. Wang, M.F. Wheeler, Numerical convergence study of iterative coupling for coupled flow and geomechanics, Comput. Geosci. 18 (3) (2014) 325–341. http://dx.doi.org/10.1007/s10596-013-9393-8.
[13] M. Biot, General theory of three-dimensional consolidation, J. Appl. Phys. 12 (2) (1941) 155–164.
[14] O. Coussy, Mechanics of Porous Continua, Wiley, 1995.
[15] J. Thomas, Sur l'analyse numérique des méthodes d'éléments finis hybrides et mixtes, Thése d'Etat, Université Pierre & Marie Curie, Paris, 1977.
[16] P. Bastian, M. Blatt, A. Dedner, C. Engwer, R. Klöfkorn, R. Kornhuber, M. Ohlberger, O. Sander, A generic grid interface for parallel and adaptive scientific computing. Part II: Implementation and tests in DUNE, Computing 82 (2–3) (2008) 121–138. http://dx.doi.org/10.1007/s00607-008-0004-9.

Graphic design: Communication Division, UiB / Print: Skipnes Kommunikasjon AS

uib.no

ISBN: 9788230863749 (print)
9788230868331 (PDF)